AN OBJECT-ORIENTED DISTRIBUTION SYSTEM DISTRIBUTED QUASI-DYNAMIC STATE ESTIMATOR

A Dissertation
Presented to
The Academic Faculty

by

Boqi Xie

In Partial Fulfillment
of the Requirements for the Degree
Doctor of Philosophy in the
School of Electrical and Computer Engineering

Georgia Institute of Technology
August 2020

AN OBJECT-ORIENTED DISTRIBUTION SYSTEM DISTRIBUTED QUASI-DYNAMIC STATE ESTIMATOR

Approved by:

Dr. A. P. Meliopoulos, Advisor
School of Electrical and Computer Engineering
Georgia Institute of Technology

Dr. Lukas Graber
School of Electrical and Computer Engineering
Georgia Institute of Technology

Dr. Daniel Molzahn
School of Electrical and Computer Engineering
Georgia Institute of Technology

Dr. Shijie Deng
School of Industrial and Systems Engineering
Georgia Institute of Technology

Dr. Santiago Carlos Grijalva
School of Electrical and Computer Engineering
Georgia Institute of Technology

Date Approved: June 26, 2020

To my beloved parents Ankuan Xie, Peiya Yao, and my wife Yi Cao

ACKNOWLEDGEMENTS

The doctoral study at Georgia Tech is an exciting and rewarding journey. This journey would not have been accomplished without help and support from countless people. This acknowledgment provides me an opportunity to express my heartfelt gratitude to them.

First, I would like to express my sincere appreciation to my advisor Dr. A. P. Sakis Meliopoulos for giving me this opportunity to pursue my Ph.D. degree under his supervision. I am greatly thankful to his guidance and inspiration. Thanks to his patient guidance, I am able to learn something every time I meet with him. Thanks to his inspiration, I am able to get into touch of the beauty of power system study. In addition, his passion and enthusiasm to the academic study set a role model for me. His dedication and wisdom have been a great source for me to continue to aspire to be a better engineer. I would also take this opportunity to express my appreciation to Dr. George Cokkinides, who is an expert in power system, especially in software development and hardware implementation. His professional expertise is always excellent and admirable.

I would also express my appreciation to all the members of my committee from School of Electrical and Computer Engineering and School of Industrial and Systems Engineering at Georgia Institute of Technology: Dr. Daniel Molzahn, Dr. Santiago Carlos Grijalva, Dr. Lukas Graber, and Dr. Shijie Deng for their valuable and constructive suggestions on my work and my dissertation, and for kindly serving as my committee members.

My special thanks to the current and former members of Power Systems Control and Automation Laboratory, including Dr. Georgios K. Stefopoulos, Dr. Evangelos Farantatos, Dr. Renke Huang, Dr. Dongbo Zhao, Dr. Ye Tao, Dr. Evangelos Polymeneas, Dr. Liangyi Sun, Dr. Yu Liu, Dr. Rui Fan, Dr. Zhenyu Tan, Dr. Bai Cui, Dr. Hussain F. Albinali, Dr. Abdullah Alamri, Dr. Chiyang Zhong, Dr. Jiahao Xie, Dr. Yuan Kong, Yi Du, Wenlu Fu, Kaiyu Liu, Orestis Vasios, Maad Al Owaifeer, and Gad Monga Ilunga. I really enjoyed working with them. I will always remember my lab life with them. I also would like to express my appreciation to all my friends I made at Georgia Tech. Among them special thanks to Dr. Jiaming Li, Dr. Huan Yu, Dr. Xiangyu Han, and Dr. Yiren Wu. The friendship I made and the support I gained from them are invaluable.

Finally, I would like to express my gratitude to my parents Ankuan Xie and Peiya Yao, who constantly support me and encourage me. Also, I would like to express my appreciation to my beloved wife Yi Cao, who always accompanies me and helps me go through those difficult times. I will definitely not finish my Ph.D. degree without their support and encouragement.

TABLE OF CONTENTS

LIST OF TABLES

LIST OF FIGURES

SUMMARY

The distribution system is becoming more sophisticated than before with distributed energy resources (DERs) being installed at a rapid pace. The DERs (including solar photovoltaic, wind turbines, energy storage, electric vehicle, etc.) create opportunities for utilities to manage the load/voltage profile, improve power quality and resiliency, and help meet green energy goals. To achieve these objectives, operators need the validated model of the distribution system for operating and controlling the system with model-based approaches to compute controls, maximize the security of the system and in general achieve the operating objectives. Therefore, a state estimator for distribution systems, which is able to constantly monitor the distribution system and provide such necessary information, is required.

However, the increasing penetration level of DERs in the distribution system brings a series of challenges for operators to apply conventional state estimators on distribution systems: (1) In order to incorporate DERs into state estimation, the state estimator needs to employ multi-phase detailed models for each type of DER. Since the conventional state estimator adopts simplified models (such as positive sequence network implying a balanced and symmetric system), it is not applicable to the unbalanced and asymmetric distribution system, especially with DERs. (2) More dynamics are introduced to distribution systems with an increasing penetration level of DERs. As the conventional state estimator employs static state estimation (SSE) considering all the devices in a power system to be static, i.e., frequency domain models, such type of state estimator is not able to reveal more detailed information (i.e., dynamics) in power systems. (3) The operating

states of the DERs are changing fast compared with the execution rate of conventional state estimators. As the conventional state estimator is centralized, i.e., all the data obtained from intelligent electronic devices (IEDs) are processed in a control center, the collected data are tremendous considering a distribution system may contain thousands of devices and a great number of installed IEDs. Such centralized architecture causes heavy data traffic and results in long execution times for the state estimator. As a result, conventional state estimators are not able to accurately and timely provide the operating state of the distribution system with large numbers of DERs. Because of these challenges, it is not realistic to apply a conventional centralized state estimator to distribution systems, and a state estimator for distribution systems with following characteristics is needed: (1) It employs multi-phase detailed modeling for each device in distribution systems, (2) it considers dynamics introduced by power components in distribution systems, and (3) it is able to execute at a rate that is fast enough to track the dynamics in the system caused by DERs. With these characteristics, the state estimator is able to constantly provide the operating state and the validated model of the distribution system to distribution management system (DMS) for further applications (e.g., voltage regulation, distribution system optimal control, etc.).

Thus, the objective of this dissertation is to develop an object-oriented distributed quasi-dynamic state estimator (considers slow dynamics such as electromechanical transients while neglects fast electromagnetic transients) that constantly monitors the states of the distribution system and provides the validated data to DMS, i.e., an object-oriented distribution system distributed quasi-dynamic state estimator (DS-DQDSE). The objective has been achieved by the development of such an approach which is based on the following

contributions: (1) development of an object-oriented quasi-dynamic domain multi-phase detailed device modeling approach so that all the devices in the distribution system are expressed in a unified syntax; (2) development of an object-oriented network-level measurement model creation procedure, given the device models and measurements in this network; (3) development of an object-oriented quasi-dynamic state estimation, given the network-level measurement model.

In particular, the dissertation first proposes a distributed and seamless infrastructure starting from measurement data from sensors installed across distribution systems to estimated states and system model output from the state estimator. Specifically, as shown in Figure 1.1.1, a distribution system is partitioned into several sections; at each section a local state estimator is installed. Each local state estimator performs quasi-dynamic state estimation (QDSE) using only section-wise measurements from this local section. QDSE incorporates slow dynamics (e.g., electromechanical transients of rotating electrical machines, controls of power electronics, etc.) while neglecting fast electromagnetic transients. The estimated states and validated section model are streamed to the DMS, where estimated states and validated model for the whole distribution system are synthesized for further real-time applications. Such a procedure requires at least one GPS-synchronized IED in each section, accelerates the speed of state estimation, and dramatically reduces the data traffic between the IEDs and the control center.

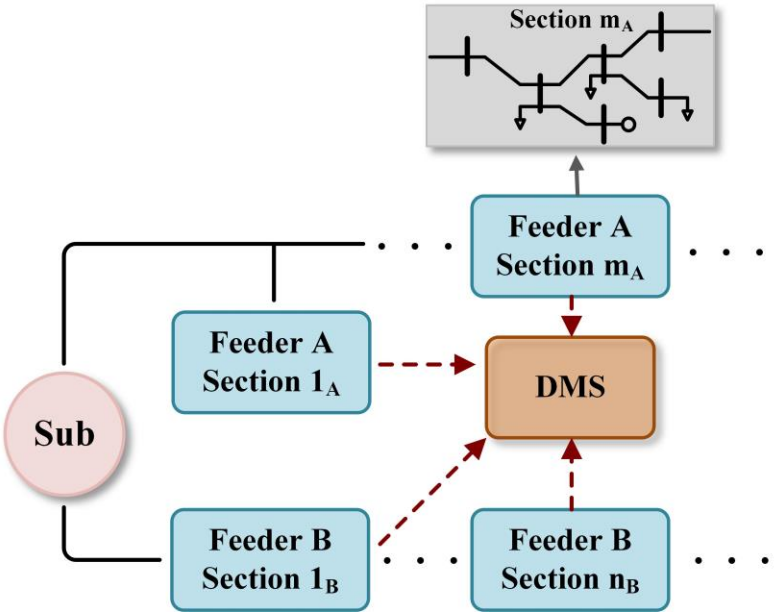

Figure 1.1.1: The Distributed Architecture of DS-DQDSE

To automate the whole procedure as well as to guarantee the accuracy of the output results from the state estimator, an object-oriented physically based high-fidelity device modeling approach is proposed. Such modeling approach enables all the devices in distribution systems to be expressed in a unified syntax referred to as state and control algebraic quadratic companion form, which is seamlessly incorporated into the proposed state estimator. Given measurements and device models from a selected feeder section, a network-level measurement model is created. To achieve observability and increase redundancy, the network-level measurement model is augmented with derived measurements (type I derived and type II derived), pseudo, and virtual measurements. By combing all these measurement models, the network-level measurement model is constructed and processed directly by the QDSE state estimator. QDSE provides the best estimates of the monitored feeder section and the confidence level that evaluates if the measurements are consistent with the feeder section model. If an inconsistency occurs, a

bad date detection and identification process is performed. The bad data are then removed and QDSE is rerun using the remaining measurements. The output of the state estimator including estimated states, estimated measurements, and validated model of the monitored system are then transmitted to DMS where the states and the model of the whole feeder are synthesized.

Since the designed DS-DQDSE adopts QDSE for state estimation while conventional state estimator adopts static state estimation (SSE), a comparison study between QDSE and SSE is presented. The study illustrates a better performance of QDSE over SSE. Furthermore, two use cases are presented to demonstrate DS-DQDSE. The performance of DS-DQDSE on a reduced feeder model is first presented, and then the application of DS-DQDSE on a full feeder model follows. The proposed DS-DQDSE is proved to be applicable to the distribution systems with DER penetration.

CHAPTER 1. INTRODUCTION

1.1 Problem Statement

Distribution systems are transforming from passive systems to active ones as distributed energy resources (DERs) are being installed at a rapid pace. For instance, in 2016, distributed solar photovoltaic installations account for over 12% of new capacity additions in the U.S., and California has over 7000 MW of installed DER capacity in 2015 [1]. The DERs (small, geographically dispersed generation resources connected to the distribution system, such as solar photovoltaic, wind turbines, energy storage, electric vehicle, etc.) create opportunities for utilities to manage the load/voltage profile, improve power quality and resiliency, and help meet green energy goals [2]–[4]. To achieve these objectives, operators need operating points and the validated model of the distribution system. Therefore, a state estimator for distribution systems, which is able to constantly monitor the distribution system and provide such necessary information, is required.

However, the increasing penetration level of DERs in the distribution system brings a series of challenges [5], [6] for operators to apply conventional state estimators on distribution systems: (1) In order to incorporate DERs into state estimation, the state estimator needs to employ multi-phase detailed models for each type of DER. Since the conventional state estimator adopts simplified models (such as positive sequence network implying a balanced and symmetric system) [7], it is not applicable to the unbalanced and asymmetric distribution system, especially with DERs. (2) More dynamics are introduced to distribution systems with an increasing penetration level of DERs. As the conventional state estimator employs static state estimation (SSE) [8], [9], which considers all the

devices in a power system to be static, i.e., frequency domain models, such type of state estimator is not able to reveal more detailed information (i.e., dynamics) in power systems. (3) The operating states of the DERs are changing fast compared with the execution rate of conventional state estimators. As the conventional state estimator is in a centralized manner, i.e., all the data obtained from intelligent electronic devices (IEDs) are processed in a control center, the collected data are tremendous considering a distribution system may contain thousands of devices and a great number of installed IEDs. Such centralized architecture causes heavy data traffic and results in a long time for the state estimator to respond. As a result, conventional state estimators are not able to accurately reflect the operating states of the distribution system after incorporating DERs. Because of these challenges, it is not realistic to apply a conventional centralized state estimator to distribution systems, and a state estimator for distribution systems with following characteristics is needed: (1) It employs multi-phase detailed modeling for each device in distribution systems, (2) it considers dynamics introduced by power components in distribution systems, especially those DERs, and (3) it is able to execute in a rate that is fast enough to track the dynamics in the system caused by DERs. With these characteristics, the state estimator is able to constantly provide the operating states and the validated model of the distribution system to distribution management system (DMS) for further applications (e.g., voltage regulation, distribution system optimal control, etc.).

The high-sampling rate GPS-synchronized measurements enable new approaches to power system state estimation [10]–[14]. One of the approaches is that GPS-synchronized measurements enable the transition from a centralized state estimator to distributed quasi-dynamic state estimators (DQDSE). DQDSE, a combination of previous

work in [15]–[19], performs substation level quasi-dynamic state estimation (QDSE) using phasor measurements. QDSE incorporates slow dynamics (e.g., electromechanical transients of rotating electrical machines [20], controls of power electronics [21], [22], etc.) while neglecting fast electromagnetic transients. Compared with the conventional state estimator, DQDSE has the following advantages: (1) With the adoption of multi-phase detailed models, DQDSE processes unbalanced systems and outputs reliable and accurate results. (2) By employing quasi-dynamic domain models that incorporate slow dynamics, the state estimator is able to provide more accurate information of the monitored power system. (3) By dividing a transmission system into several sections, DQDSE performs QDSE in each section in parallel and transmits estimated states and validated models to a master data management center. Such a procedure accelerates the speed of state estimation and dramatically reduces data traffic between local sections and the data center. These advantages lay a sound foundation for the development of a state estimator applicable to distribution systems.

1.2 Research Objectives

The objective of this dissertation is to develop an object-oriented distributed quasi-dynamic state estimator that constantly monitors the states of the distribution system and provides the validated data to DMS. The objective has been achieved by the development of such an approach which is based on the following contributions: (1) development of an object-oriented quasi-dynamic domain multi-phase detailed device modeling approach so that all the devices in the distribution system are expressed in a precise and unified syntax; (2) development of an object-oriented network-level measurement model creation procedure, given the device models and measurements in this network; (3) development of

an object-oriented quasi-dynamic state estimation, given the network-level measurement model.

In particular, the dissertation first proposes a distributed and seamless infrastructure starting from measurement data from sensors installed across distribution systems to estimated states and system model output from the state estimator. Specifically, a feeder is partitioned into several sections with each section installed a local state estimator. Each local state estimator performs QDSE using only section-wise measurements from this local section. The estimated states and validated section model are streamed to the data control center, where estimated states and validated model for the whole feeder are synthesized for further real-time applications. Such a procedure requires at least one GPS-synchronized IED in each section, accelerates the speed of state estimation, and dramatically reduces the data traffic between the IEDs and the control center.

In order to accommodate different types of devices, automate the whole procedure, and guarantee the accuracy of the output results from the state estimator, an object-oriented physically based high-fidelity device modeling approach is proposed. Such modeling approach enables all the devices in distribution systems to be expressed in a unified syntax referred to as state and control algebraic quadratic companion form (SCAQCF), which is seamlessly incorporated into the proposed state estimator. Given measurements and device models from a selected feeder section, a network-level measurement model is created. To achieve observability and increase redundancy, the formulated network-level measurement model comprises of proposed different types of measurements, i.e., actual, derived (type I and type II derived measurements), pseudo, and virtual measurements. By combing all these measurement models, the network-level measurement model is constructed and

processed directly by the QDSE state estimator. The QDSE provides the best estimates of the monitored feeder section and the confidence level that evaluates if the measurements are consistent with the feeder section model. If an inconsistency occurs, a bad date detection and identification process is performed. The bad data are then removed and QDSE is rerun using the remaining measurements. The output of the state estimator including estimated states, estimated measurements, and validated model of the monitored system are then transmitted to DMS where the states and the model of the whole feeder are synthesized.

1.3 Thesis Outline

The outline of the remaining parts of this dissertation is as follows.

In Chapter 2, a literature review is provided on the existing technologies related to the proposed distribution system state estimator. Specifically, the evolution of the state estimator from the conventional centralized state estimator to the substation based distributed state estimator is introduced. In addition, different state estimation solution methods, such as weighted least square method, least absolute deviation method, min-max method, extended Kalman filtering method are also reviewed.

Chapter 3 introduces the overall approach of the proposed distribution system distributed quasi-dynamic state estimator that starts from object-oriented devices and measurements from sensors to the estimated states output from the state estimator.

Chapter 4 describes a high-fidelity standardized modeling approach for power devices that enables object-oriented analysis in distribution systems. The modeling

approach is initiated from physically based model of a power device expressed in equations, inequality constraints and other information to a general and unified syntax that is applicable to all the device models in power systems.

Chapter 5 presents an autonomous procedure that creates the network-level measurement model given measurements and device models from selected feeder section. In addition to actual measurements obtained from IEDs, four other measurement types are proposed in this chapter, i.e., type I derived measurement, type II derived measurement, pseudo measurement, and virtual measurement. These measurement types together with actual measurements constitute the network-level measurement model.

Chapter 6 describes the quasi-dynamic state estimation algorithm. Two state estimation methods based on weighted least square method are presented, i.e., unconstrained weighted least square method and constrained weighted least square method. The evaluation of the state estimation (i.e., chi-square test) as well as bad data detection and identification are also introduced in this chapter.

Chapter 7 presents a performance comparison study between static state estimation (SSE) and QDSE. The quasi-dynamic domain model and frequency domain model of a generator with governor, turbine, and exciter are first described. Then, the QDSE and SSE are applied on the generator model. The state estimation results show that the QDSE is able to reveal more accurate information (e.g., dynamics in the rotating rotor).

Chapter 8 shows numerical cases for demonstration of the proposed distributed quasi-dynamic state estimator. The proposed state estimator is first applied on a reduced feeder case with 15 buses. Then, the full feeder model with over 200 buses is used as an

example to validate the effectiveness of the proposed state estimator. The state estimation results of these two use cases are presented in this chapter.

Finally, Chapter 9 summarizes the dissertation, outlines the contribution of the research work, and proposes some future work direction.

In addition, Appendix A describes an object-oriented modeling example, i.e., a quasi-dynamic domain generator with governor, turbine, and exciter model. The compact model of the physical circuit, the quadratized model, and the SCAQCF model are described respectively.

CHAPTER 2. LITERATURE REVIEW

2.1 Overview

State estimation is a computational procedure that uses a redundant set of measurements and a bus-oriented network model to compute a statistical estimate of the system operating state. This chapter provides the background information of existing technologies related to the proposed distribution system state estimator along with a literature review of the research efforts on this topic. Section 2.2 summarizes the evolution of the state estimator from the conventional centralized state estimator to the substation based distributed state estimator. Section 2.3 reviews different state estimation solution methods, such as weighted least square method, least absolute deviation method, min-max method, extended Kalman filtering method, etc. Section 2.4 summaries this literature review.

2.2 Evolution of State Estimator

2.2.1 Legacy State Estimator

The 1960s witnessed the introduction and the application of state estimation in power systems [8], [9] after the great northeast blackout in 1965 [23]. Taking place in a control center, the conventional state estimator collects redundant measurement data from the power system, performs state estimation, and gives the best estimate of the monitored transmission system. The characteristics of the legacy state estimator are: (1) it estimates positive sequence voltage phasors at transmission buses, (2) transmission circuits are the only needed models, and (3) it is in a centralized architecture (i.e., all the measurements

are processed at a central location). The legacy state estimator encounters several challenges because of its characteristics: (1) It employs simplified positive sequence models, which implies it is monitoring a balanced and symmetric system. Because of this practice, the legacy state estimator is not suitable for unbalanced or asymmetric multi-phase power system, especially for distribution systems. (2) It only accommodates transmission circuits, which are not suitable to the various devices (especially various types of DERs) in the distribution system. (3) The centralized architecture causes data latency, which results in a long response time, typically several minutes, for the state estimator.

2.2.2 Three-Phase GPS-Synchronized State Estimator

Many efforts have been done to develop more accurate state estimators [10], [24], [25]. With the introduction of GPS synchronization technology, phasor measurement unit (PMU) and other intelligent electronic devices (IEDs) are developed. These measurement devices provide GPS-synchronized phasor measurements with high accuracy. In addition, three-phase models enable the researchers to alleviate the bias created from the legacy state estimator. However, since such state estimator is still in a centralized architecture, all the data are processed in the control center resulting in a long response time. Moreover, as the state estimator only employs static state transmission circuits, it is not applicable to various types of devices in the distribution system, especially those containing dynamics.

2.2.3 Substation Based State Estimator

GPS-synchronized measurements enable the transition from a centralized state estimator to distributed quasi-dynamic state estimators (DQDSE). DQDSE performs substation level quasi-dynamic state estimation (QDSE), which uses phasor measurements.

QDSE incorporates slow dynamics (such as electromechanical transients of rotating electrical machines from cycles to seconds and controls of power electronics in cycles) while neglecting fast electromagnetic transients. DQDSE adopts three-phase detailed models, so that it is able to process unbalanced systems and output reliable and accurate results. In addition, DQDSE is substation based and in a distributed manner [17]–[19], [26]. To be more specific, a DQDSE is installed in each substation, performs QDSE in parallel using all the device models in this substation as well as the interconnected circuits, and computes the estimated states of this substation and the states of the interconnected circuits [27], [28]. The estimated states and the validated models of this substation are transmitted to the control center for further use. Such a procedure accelerates the speed of state estimation and dramatically reduces the data traffic between the substations and the control center [29], [30]. However, as the DQDSE only employs generation, transmission, and sub-transmission level devices, it is not applicable to various types of devices in distribution systems.

2.3 State Estimation Solution Methods

2.3.1 Weighted Least Square Method

Weighted least square (WLS) method is the most commonly used method in power system state estimation [7], [31]. Given a measurement model $\mathbf{z} = h(\mathbf{x}) + \boldsymbol{\eta}$, the optimization problem is expressed to minimize the sum of the residual squares between measurements and estimated measurements:

$$\textit{Minimize} \quad J = \left(\mathbf{z}(t) - h(\mathbf{x})\right)^{\mathrm{T}} W \left(\mathbf{z}(t) - h(\mathbf{x})\right) \tag{2.3.1}$$

where **z** is the measurement vector, $h(\mathbf{x})$ is the measurement model, **η** is the measurement error vector, W is the weight matrix with the weights defined as the inverse of the squared standard deviations: $W = \mathrm{diag}\left\{1/\delta_1^2, 1/\delta_2^2, \cdots, 1/\delta_n^2\right\}$, δ_i is the standard deviation of measurement i. Unknown state vector **x** is obtained by the optimal condition:

$$dJ/d\mathbf{x} = 0 \tag{2.3.2}$$

If the measurement model is linear (i.e., $h(\mathbf{x}) = H\mathbf{x} - \mathbf{b}$, where H is the linear coefficient matrix, and **b** is the constant vector), the solution is obtained directly as shown in (2.3.3) and (2.3.4):

$$0 = dJ/d\mathbf{x} = 2H^T W\left(H\mathbf{x} - \mathbf{b} - \mathbf{z}\right) \tag{2.3.3}$$

$$\mathbf{x} = \left(H^T W H\right)^{-1} H^T W\left(\mathbf{z} + \mathbf{b}\right) \tag{2.3.4}$$

If the measurement model is nonlinear, we first linearize the nonlinear equations at point $\mathbf{x}^{\nu}$ by assuming an initial guess $\mathbf{x}^{\nu}$ is very close to the optimal solution yielding:

$$\mathbf{r} = h(\mathbf{x}^{\nu}) + \partial h(\mathbf{x})/\partial\mathbf{x}\Big|_{\mathbf{x}=\mathbf{x}^{\nu}}\left(\mathbf{x} - \mathbf{x}^{\nu}\right) - \mathbf{z} \tag{2.3.5}$$

After we set $H = \partial h(\mathbf{x})/\partial\mathbf{x}\Big|_{\mathbf{x}=\mathbf{x}^{\nu}}$, and $\mathbf{z}' = -h(\mathbf{x}^{\nu}) + H\mathbf{x}^{\nu} + \mathbf{z}$, the residual vector is expressed as: $\mathbf{r} = H\mathbf{x} - \mathbf{z}'$. The optimization problem is now expressed as a linear form:

$$\textit{Minimize} \quad J = \left(H\mathbf{x} - \mathbf{z}'\right)^{\mathbf{T}} W\left(H\mathbf{x} - \mathbf{z}'\right) \tag{2.3.6}$$

Thus, we generalize the solution as an iterative equation shown in (2.3.7), and the solution is obtained once the algorithm converges.

$$\mathbf{x}^{\nu+1} = \left(H^T W H\right)^{-1} H^T W\mathbf{z}' = \mathbf{x}^{\nu} - \left(H^T W H\right)^{-1} H^T W\left(h\left(\mathbf{x}^{\nu}\right) - \mathbf{z}\right) \tag{2.3.7}$$

The WLS method described above is also referred to as unconstrained WLS, since the optimization problem (2.3.1) does not contain any constraints. By adding constraints into the optimization problem, the constrained WLS problem is formulated [32]:

$$\begin{aligned} &\textit{Minimize} \quad J = \left(\mathbf{z}(t) - h(\mathbf{x})\right)^{\mathbf{T}} W \left(\mathbf{z}(t) - h(\mathbf{x})\right) \\ &\textit{subject to}: \; 0 = g(\mathbf{x}) \end{aligned} \tag{2.3.8}$$

To solve this optimization problem, a Lagrangian function is constructed by introducing a Lagrangian multiplier vector $\boldsymbol{\lambda}$ with a scalar two, which is:

$$L(\mathbf{x}, \boldsymbol{\lambda}) = J + 2\boldsymbol{\lambda}^T g(\mathbf{x}) \tag{2.3.9}$$

If the measurement model is linear (i.e., $h(\mathbf{x}) = H\mathbf{x} - \mathbf{b}_1$, $g(\mathbf{x}) = G\mathbf{x} - \mathbf{b}_2$), the solution is computed directly via the optimal condition of the Lagrangian function as:

$$\begin{aligned} 0 &= \frac{\partial L(\mathbf{x}, \boldsymbol{\lambda})}{\partial \mathbf{x}} = 2H^T W \left(H\mathbf{x} - \mathbf{z} - \mathbf{b}_1\right) + 2G^T \boldsymbol{\lambda} \\ 0 &= \frac{\partial L(\mathbf{x}, \boldsymbol{\lambda})}{\partial \boldsymbol{\lambda}} = 2G\mathbf{x} - 2\mathbf{b}_2 \end{aligned} \tag{2.3.10}$$

And the solution is solved as:

$$\begin{bmatrix} \mathbf{x} \\ \boldsymbol{\lambda} \end{bmatrix} = \begin{bmatrix} H^T W H & G^T \\ G & 0 \end{bmatrix}^{-1} \begin{bmatrix} H^T W \left(\mathbf{z} + \mathbf{b}_1\right) \\ \mathbf{b}_2 \end{bmatrix} \tag{2.3.11}$$

If the measurement model is nonlinear, linearization is applied to $h(\mathbf{x})$ and $g(\mathbf{x})$ separately with an initial guess $\mathbf{x}^{\nu}$ and $\boldsymbol{\lambda}^{\nu}$, i.e.,

$$\begin{aligned} h\left(\mathbf{x}^{\nu} + \Delta\mathbf{x}\right) &= h\left(\mathbf{x}^{\nu}\right) + H\Delta\mathbf{x} \\ g\left(\mathbf{x}^{\nu} + \Delta\mathbf{x}\right) &= g\left(\mathbf{x}^{\nu}\right) + G\Delta\mathbf{x} \end{aligned} \tag{2.3.12}$$

where H and G are the Jacobian matrices of $h(\mathbf{x})$ and $g(\mathbf{x})$. And the update is given by:

$$\begin{aligned}\mathbf{x}^{\nu+1} &= \mathbf{x}^{\nu} + \Delta\mathbf{x} \\ \boldsymbol{\lambda}^{\nu+1} &= \boldsymbol{\lambda}^{\nu} + \Delta\boldsymbol{\lambda}\end{aligned} \tag{2.3.13}$$

Now the Lagrangian function becomes (2.3.14), and the solution is computed via the optimal condition of the Lagrangian function as shown in (2.3.15):

$$L(\mathbf{x},\boldsymbol{\lambda}) = \left(h\left(\mathbf{x}^{\nu}\right) + H\Delta\mathbf{x} - \mathbf{z}\right)^{T} W\left(h\left(\mathbf{x}^{\nu}\right) + H\Delta\mathbf{x} - \mathbf{z}\right) + 2\left(\boldsymbol{\lambda}^{\nu} + \Delta\boldsymbol{\lambda}\right)^{T}\left(g\left(\mathbf{x}^{\nu}\right) + G\Delta\mathbf{x}\right) \tag{2.3.14}$$

$$\begin{aligned}0 &= \frac{\partial L(\mathbf{x},\boldsymbol{\lambda})}{\partial \mathbf{x}} = 2H^{T}WH\Delta\mathbf{x} + 2H^{T}W\left(h\left(\mathbf{x}^{\nu}\right) - \mathbf{z}\right) + 2G^{T}\left(\boldsymbol{\lambda}^{\nu} + \Delta\boldsymbol{\lambda}\right) \\ 0 &= \frac{\partial L(\mathbf{x},\boldsymbol{\lambda})}{\partial \boldsymbol{\lambda}} = 2G\Delta\mathbf{x} + 2g\left(\mathbf{x}^{\nu}\right)\end{aligned} \tag{2.3.15}$$

Therefore, the solution is obtained by the iterative equation:

$$\begin{bmatrix}\Delta\mathbf{x} \\ \Delta\boldsymbol{\lambda}\end{bmatrix} = -\begin{bmatrix}H^{T}WH & G^{T} \\ G & 0\end{bmatrix}^{-1}\begin{bmatrix}H^{T}W\left(h\left(\mathbf{x}^{\nu}\right) - \mathbf{z}\right) + G^{T}\boldsymbol{\lambda}^{\nu} \\ g\left(\mathbf{x}^{\nu}\right)\end{bmatrix} \tag{2.3.16}$$

or

$$\begin{bmatrix}\mathbf{x}^{\nu+1} \\ \boldsymbol{\lambda}^{\nu+1}\end{bmatrix} = \begin{bmatrix}\mathbf{x}^{\nu} \\ \boldsymbol{\lambda}^{\nu}\end{bmatrix} - \begin{bmatrix}H^{T}WH & G^{T} \\ G & 0\end{bmatrix}^{-1}\begin{bmatrix}H^{T}W\left(h\left(\mathbf{x}^{\nu}\right) - \mathbf{z}\right) + G^{T}\boldsymbol{\lambda}^{\nu} \\ g\left(\mathbf{x}^{\nu}\right)\end{bmatrix} \tag{2.3.17}$$

2.3.2 Least Absolute Deviation Method

The least absolute deviation method [7] aims to minimize the weighted sum of the absolute deviations of the components of the residual vector **r** as follows:

$$\begin{aligned}&\textit{Minimize} \quad J = \mathbf{c}^{T}|\mathbf{r}| \\ &\textit{subject to}: \ \mathbf{r} = h(\mathbf{x}) - \mathbf{z}\end{aligned} \tag{2.3.18}$$

Such optimization problem can be easily translated into a linear programming problem, and the solution is obtained after several iterative linear programming. To be more specific, the problem is linearized around $\mathbf{x}^\nu$ at iteration ν:

$$\begin{aligned} &\textit{Minimize} \quad J = \mathbf{c}^T |\mathbf{r}| \\ &\textit{subject to}: \ \mathbf{r} = H\Delta\mathbf{x} - \mathbf{z}' \end{aligned} \tag{2.3.19}$$

where $H = \partial h(\mathbf{x}) / \partial \mathbf{x}\big|_{\mathbf{x}=\mathbf{x}^\nu}$, $\mathbf{z}' = \mathbf{z} - h(\mathbf{x}^\nu)$. Then the problem is transformed into an optimization problem of the linear programming variety, by replacing the variables $\mathbf{r}$ and $\Delta\mathbf{x}$ with a pair of nonnegative variables: $\mathbf{r} = \mathbf{r}_+ - \mathbf{r}_-$, $\Delta\mathbf{x} = \mathbf{x}_+^\nu - \mathbf{x}_-^\nu$. The solution is obtained by the linear programming formulation:

$$\begin{aligned} &\textit{Minimize} \quad J = \mathbf{c}^T \left(\mathbf{r}_+ + \mathbf{r}_-\right) \\ &\textit{subject to}: \ \mathbf{r}_+ - \mathbf{r}_- - H\left(\mathbf{x}_+^\nu - \mathbf{x}_-^\nu\right) = -\mathbf{z}' \\ &\qquad\qquad \mathbf{r}_+, \mathbf{r}_-, \mathbf{x}_+^\nu, \mathbf{x}_-^\nu \geq 0 \end{aligned} \tag{2.3.20}$$

2.3.3 Min-Max Method

The min-max method [33] aims to minimize the absolutely largest (maximum) component of the residual vector $\mathbf{r}$. Its mathematical expression is expressed as follows:

$$\begin{aligned} &\textit{Minimize} \quad J = r^* \\ &\textit{subject to}: \ w_i \left|h_i\left(\mathbf{x}\right) - z_i\right| \leq r^*, \ i = 1, 2, ..., m \end{aligned} \tag{2.3.21}$$

Upon linearization of the residuals around $\mathbf{x}^\nu$ at iteration ν, the stated problem is:

$$\begin{aligned} &\textit{Minimize} \quad J = r^* \\ &\textit{subject to}: \ W\left(H\Delta\mathbf{x} - \mathbf{R}^*\right) \leq \mathbf{z}' \\ &\qquad\qquad W\left(H\Delta\mathbf{x} + \mathbf{R}^*\right) \geq \mathbf{z}' \end{aligned} \tag{2.3.22}$$

where $\mathbf{R}^* = \begin{bmatrix} r^* & r^* & \cdots & r^* \end{bmatrix}^T$, H is the Jacobian matrix of $h(\mathbf{x})$ at $\mathbf{x}^v$, $\mathbf{z}' = \mathbf{z} - h(\mathbf{x}^v)$. The linearized optimization problem is translated into a standard linear programming problem, and the solution is obtained by a standard linear programming solver.

$$\begin{aligned} &\textit{Minimize} \quad r^* \\ &\textit{subject to:} \quad W\left(H\mathbf{x}_+ - H\mathbf{x}_- - \mathbf{R}^*\right) + \mathbf{p} = \mathbf{z}' \\ &\qquad\qquad\quad W\left(H\mathbf{x}_+ - H\mathbf{x}_- + \mathbf{R}^*\right) - \mathbf{q} = \mathbf{z}' \\ &\qquad\qquad\quad \mathbf{x}_+, \mathbf{x}_-, r^*, \mathbf{p}, \mathbf{q} \geq 0 \end{aligned} \tag{2.3.23}$$

where $\Delta\mathbf{x} = \mathbf{x}_+ - \mathbf{x}_-$, $\mathbf{x}_+$, $\mathbf{x}_-$, $\mathbf{p}$, and $\mathbf{q}$ are nonnegative vectors.

2.3.4 Extended Kalman Filtering

Extended Kalman filtering (EKF) is another widely adopted method in dynamic state estimation [34]–[39]. For a nonlinear dynamic system described by differential equations in (2.3.24) and further in discrete form in (2.3.25), the purpose of EKF is to minimize the covariance of the mismatch between estimated states and states.

$$\begin{aligned} d\mathbf{x}/dt &= f_c\left(\mathbf{x}, \mathbf{y}, \mathbf{u}, \mathbf{w}\right) \\ 0 &= g_c\left(\mathbf{x}, \mathbf{y}, \mathbf{u}, \mathbf{v}\right) \end{aligned} \tag{2.3.24}$$

$$\begin{aligned} &\mathbf{x}_k = \mathbf{x}_{k-1} + f_c\left(\mathbf{x}_{k-1}, \mathbf{y}_{k-1}, \mathbf{u}_{k-1}, \mathbf{w}_{k-1}\right)\Delta t \equiv f\left(\mathbf{x}_{k-1}, \mathbf{y}_{k-1}, \mathbf{u}_{k-1}, \mathbf{w}_{k-1}\right) \\ &0 = g_c\left(\mathbf{x}_k, \mathbf{y}_k, \mathbf{u}_k, \mathbf{v}_k\right) \Rightarrow \mathbf{y}_k = h\left(\mathbf{x}_k, \mathbf{u}_k, \mathbf{v}_k\right) \end{aligned} \tag{2.3.25}$$

where **x** represents the dynamic state variables, **y** represents the static state variables, **u** is the vector of input variables, **w** and **v** are processing noise and measurement noise, respectively, subscript *c* denotes the continuous form.

The EKF problem is solved in a two-step process, i.e., prediction and correction:

$$\text{Prediction}: \begin{cases} \hat{\mathbf{x}}_k^- = f\left(\hat{\mathbf{x}}_{k-1}, h\left(\hat{\mathbf{x}}_{k-1}, \mathbf{u}_{k-1}\right), \mathbf{u}_{k-1}, 0\right) \\ P_k^- = A_k P_{k-1} A_k^T + W_k Q_{k-1} W_k^T \end{cases} \tag{2.3.26}$$

$$\text{Correction}: \begin{cases} K_k = P_k^- H_{z,k}^T \left(H_{z,k} P_k^- H_{z,k}^T + V_k R_k V_k^T\right)^{-1} \\ \hat{\mathbf{x}}_k = \hat{\mathbf{x}}_k^- + K_k \left(\mathbf{z}_k - h\left(\hat{\mathbf{x}}_k^-, \mathbf{u}_k, 0\right)\right) \\ P_k = \left(I - K_k H_{z,k}\right) P_k^- \end{cases} \tag{2.3.27}$$

where the superscript – denotes a priori state, A_k and W_k are the process Jacobians at step k, P_k is the covariance matrix of the state estimation error and is also called gain factor matrix, Q_k is the process noise covariance at step k. $H_{z,k}$ and V_k are the measurement Jacobians at step k, and R_k is the measurement noise covariance at step k. $A = \partial f / \partial \mathbf{x}$, $H_z = \partial h / \partial \mathbf{x}$, $W = \partial f / \partial \mathbf{w}$, $V = \partial h / \partial \mathbf{v}$.

2.3.5 Artificial Intelligence Based Techniques

Other methods such as artificial neural network (ANN) [40]–[42] and machine learning technique are also attempted in power system state estimation. An ANN is a mathematical model that is based on the architecture and functionality of biological neural networks. The elemental building unit of an ANN is the neuron. The neuron receives a number of inputs X, process them, and generates a response Y. The ANN is formulated by organizing a number of neurons in several layers as shown in Figure 2.3.1. ANN technique is applied in different ways in state estimation. Ramesh et al. [43] uses ANN as a filter to receive raw measurements and provide their estimated values. Manitsas et al. [44] creates pseudo measurements using ANN to achieve observability of the state estimation. Note that an ANN has to be first trained off-line since a large amount of patterns are needed for training, and these patterns may not cover all the cases that occur in a distribution system,

which is a disadvantage of this method. Machine learning technique acts a similar role as ANN in power system state estimation. In [45], machine learning technique is applied as a filter that receives raw data, provides reliable pseudo measurements, and fills the gap of the streaming measurement data whenever a time delay or a communication failure in an IED occurs.

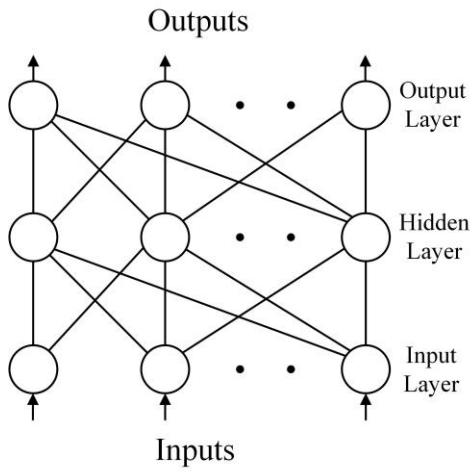

Figure 2.3.1: Architecture of the Neural Network

2.4 Summary

This literature review introduces the evolvement of the state estimator and different state estimation methods. According to the literature review, most of the state estimators are static, i.e., they are not able to capture the quasi-dynamics in the system. Besides, these state estimators do not employ detailed device modeling, especially the devices in the distribution system. For the state estimation methods, although many methods are introduced and applied, the weighted least square method is still the most commonly used method in the state estimator. In this dissertation, an object-oriented distributed quasi-

dynamic state estimator, which employs detailed device modeling that incorporates quasi-dynamics, is introduced for the distribution system.

CHAPTER 3. THE OVERALL APPROACH

3.1 Overview

This chapter introduces the overall approach for the proposed research. The objective of the proposed research is to develop a state estimator especially designed for the distribution system named as distribution system distributed quasi-dynamic state estimator (DS-DQDSE) that constantly estimates the states of the selected feeder (or part of the feeder) and streams the estimated states to the distribution management system (DMS). The objective has been achieved based on the following contributions: (1) Development of an object-oriented physically based, interoperable and unified syntax for devices in the distribution system, so that the proposed state estimator is able to perform in an object-oriented manner, (2) development of an object-oriented network measurement model formulation process that automatically forms the network measurement model of the distribution system based on the devices and measurements in this distribution system, and (3) development of an object-oriented quasi-dynamic state estimation process that seamlessly adopts the formulated network measurement model and estimates the states across the distribution system.

3.2 The Proposed Architecture

The DS-DQDSE is designed in a distributed manner. As shown in Figure 3.2.1, a distribution system is arbitrarily partitioned into several sections, each having a local distributed state estimator, which performs quasi-dynamic state estimation (QDSE) by using the measurements collected only in the corresponding section. Each local state

estimator streams the data to the data control center, where estimated states and validated model for the whole feeder are synthesized for further real-time applications. Such a procedure requires at least one GPS-synchronized intelligent electronic device (IED) in each section [46], accelerates the speed of state estimation, and dramatically reduces the data traffic between the IEDs and the control center.

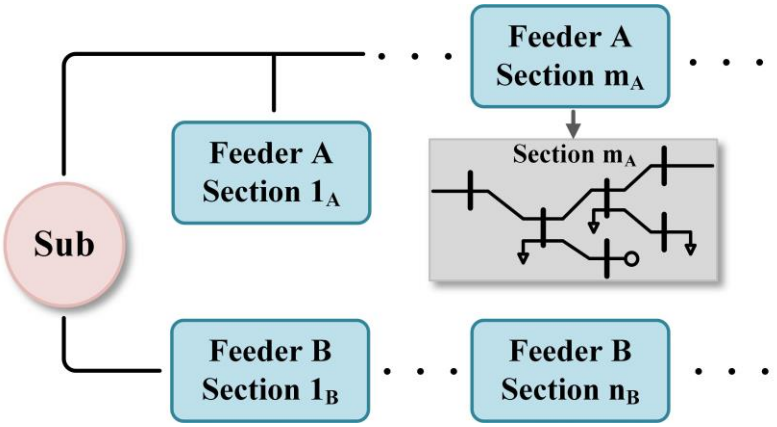

Figure 3.2.1: Partitioned Sections in a Distribution System

The infrastructure of the DS-DQDSE is a high-fidelity device modeling approach for power devices that enables object-oriented analysis in distribution systems [47]–[49]. The modeling approach starts from a physically based model, which is a set of equations describing the physical characteristics of a device. Any existing model can be expressed as a compact device model, and it is in terms of states and control variables. Then, a quadratization procedure is applied so that the highest order in the model equations is less than or equal to two. This procedure is achieved by introducing additional variables to reduce higher order terms to nonlinear terms of highest order two. Since the physically based model may contain differential terms that reflect the dynamics, the quadratic integration method is applied to transform the differential equations to algebraic equations

[50]. The final result of this procedure is an object-oriented interoperable syntax called State and Control Algebraic Quadratic Companion Form (SCAQCF), which in general is also in terms of states and controls with other device information (connectivity, etc.). The network measurement model formulation process and QDSE algorithm introduced in the following paragraphs are all based on the models in such standard without any other inputs.

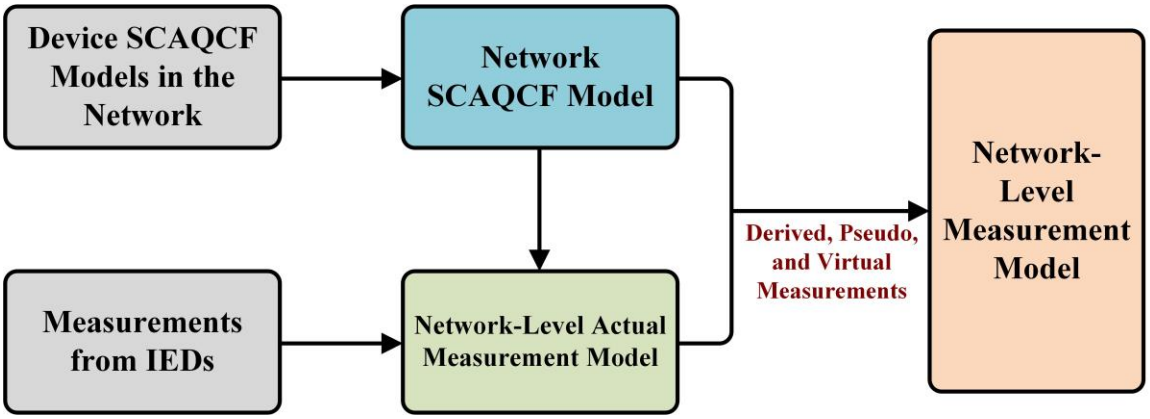

Figure 3.2.2: Network-Level Measurement Model Formulation

The DS-DQDSE requires measurements obtained from the distribution system to perform the QDSE. Any measurements, irrespectively of the source of the measurements, i.e., actual, type I derived, type II derived, virtual, or pseudo measurements (described in Chapter 5), can be expressed as functions of the states in the SCAQCF syntax and in this form are utilized by the DS-DQDSE to perform QDSE. Specifically, given all the measurements from IEDs and all the SCAQCF device models from a partitioned section, the measurement models are first developed at the device-level, i.e., they are expressed as functions of the state and control variables of individual devices. Subsequently, the mapping between devices and the network is developed and the measurement models are converted from device-level to network-level by the mapping. During this procedure, type

I derived, type II derived, virtual, and pseudo measurement models are also developed based on the network topology as shown in Figure 3.2.2. These additional measurements together with actual measurements achieve the observability of the monitored system and increase redundancy as well.

The QDSE algorithm works directly on the measurement mathematical models at the network-level. Weighted least square method is applied in QDSE [51], and the DS-DQDSE provides a quantitative probabilistic consistency between the network measurement model and the network model. Specifically, The DS-DQDSE works in a real-time fast execution rate that accommodates the high-sampling rate streaming data from IEDs (e.g., 60 samples per second). The DS-DQDSE constantly provides the best estimate of the states, the differences (residuals) between measurements and estimated measurements, and the expected standard deviation of these quantities. Note that the output information is GPS-synchronized. As a consequence, the output of each DS-DQDSE for each section is directly sent to the DMS where the states and model of the entire distribution system is constructed from the states and model of each section at a specific time stamp, which is referred to as real-time operating conditions and model [52], [53].

3.3 Summary

A distribution system distributed quasi-dynamic state estimator is proposed in this chapter. The advantage of the proposed state estimator include: (1) It adopts physically based multi-phase detailed modeling approach for each device in the distribution system, (2) slow dynamic such as electromechanical transients are considered and incorporated into the device modeling approach, and (3) the distributed architecture enables the state

estimator to execute in a rate that is fast enough to track the dynamics in the system caused by DERs and other power components. With these advantages, the state estimator is able to constantly provide accurate operating states and the validated model of the distribution system to DMS for further applications (e.g., voltage regulation, distribution system optimal control [54]–[57], etc.).

CHAPTER 4. OBJECT-ORIENTED DEVICE MODELING

4.1 Overview

This chapter describes a high-fidelity standardized modeling approach for power devices that enables object-oriented analysis in the distribution system. As shown in Figure 4.1.1, the modeling approach starts from physically based model of a power device referred to as compact device model, which is a set of equations and inequalities describing the physical and mathematical properties of the device. Any existing model can be expressed as a compact device model, and it is in terms of states and control variables. A quadratization procedure is then applied to the compact model. The procedure consists of introducing additional variables to reduce higher order terms to nonlinear terms of highest order two [58]–[60]. In case the compact model is linear or quadratic, this procedure is not needed. The end result is a quadratized device model which in general is also in terms of states and controls with other device information (e.g., connectivity, etc.). The quadratized device model is integrated for the purpose of converting it into an algebraic model. We have selected the quadratic integration method for the integration. The reason for this selection is that the quadratic integration method has better properties [50] than the popular trapezoidal integration method and it is also reasonably manageable (from the complexity point of view). The integration process transforms the state and control quadratized device model (SCQDM) into a state and control algebraic quadratic companion form (SCAQCF). It is also important to note that the models are in quasi-dynamic domain, where the compact models typically ignore fast electromagnetic transients, but include differential terms for only slow dynamics such as those arising from electromechanical oscillations or controller

actions [61]. An example of this modeling approach (i.e., generator with turbine, governor, and exciter) is illustrated in Appendix A.

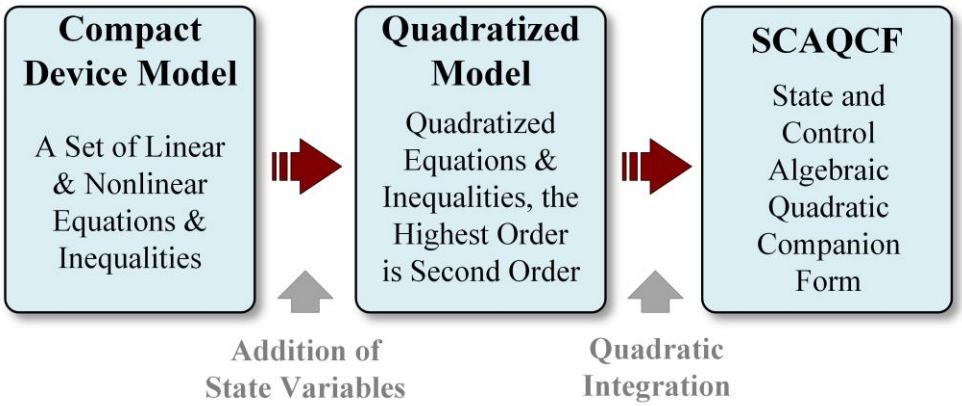

Figure 4.1.1: Object-Oriented Device Modeling Approach

The rest of this chapter is organized as follows. The quasi-dynamic domain SCQDM is described in Section 4.2, the quadratic integration method is described in Section 4.3, and the quasi-dynamic domain SCAQCF device model is described in Section 4.4.

4.2 Quasi-Dynamic Domain State and Control Quadratized Device Model

The quasi-dynamic domain state and control quadratized device model (SCQDM) is used to represent the physical model and it is a preliminary step to obtain the quasi-dynamic SCAQCF device model. All the terms in SCQDM are at most second order. The specific syntax of the model is provided below with the following selections and requirements: (a) List all the linear equations for through variables first; (b) list all the remaining linear equations; (c) all differential terms only appear in the linear equations; (d) list all the remaining algebraic quadratic equations; (e) the equations containing through

variables must be listed first; (f) the highest order of the model is second order. The requirements are always easily met by introduction of additional state variables. Note that the phasors are divided into real and imaginary parts in quadratized device model and that all the elements in the matrices are real values. Equation set one and two are linear, and equation set three is quadratic. Other device information (such as connectivity, normalization factors, etc.) is also with SCQDM. The general expression for SCQDM is:

Model Description: *Type, Code, ID, Title*

$$\mathbf{i}(t) = Y_{eqx1}\mathbf{x}(t) + Y_{equ1}\mathbf{u}(t) + D_{eqxd1}\frac{d\mathbf{x}(t)}{dt} + C_{eqc1}$$

$$0 = Y_{eqx2}\mathbf{x}(t) + Y_{equ2}\mathbf{u}(t) + D_{eqxd2}\frac{d\mathbf{x}(t)}{dt} + C_{eqc2}$$

$$0 = Y_{eqx3}\mathbf{x}(t) + Y_{equ3}\mathbf{u}(t) + \left\{\begin{matrix}\vdots\\ \mathbf{x}(t)^T\left\langle F^i_{eqxx3}\right\rangle\mathbf{x}(t)\\ \vdots\end{matrix}\right\} + \left\{\begin{matrix}\vdots\\ \mathbf{u}(t)^T\left\langle F^i_{equu3}\right\rangle\mathbf{u}(t)\\ \vdots\end{matrix}\right\} + \left\{\begin{matrix}\vdots\\ \mathbf{u}(t)^T\left\langle F^i_{equx3}\right\rangle\mathbf{x}(t)\\ \vdots\end{matrix}\right\} + C_{eqc3}$$

$$\mathbf{h}(\mathbf{x},\mathbf{u}) = Y_{hfeqx}\mathbf{x}(t) + Y_{hfequ}\mathbf{u}(t) + \left\{\begin{matrix}\vdots\\ \mathbf{x}(t)^T F^i_{hfeqxx}\mathbf{x}(t)\\ \vdots\end{matrix}\right\} + \left\{\begin{matrix}\vdots\\ \mathbf{u}(t)^T F^i_{hfequu}\mathbf{u}(t)\\ \vdots\end{matrix}\right\} + \left\{\begin{matrix}\vdots\\ \mathbf{u}(t)^T F^i_{hfequx}\mathbf{x}(t)\\ \vdots\end{matrix}\right\} + C_{hfeqc}$$

Constraints : $\mathbf{h}(\mathbf{x},\mathbf{u}) \le \mathbf{0},\ \mathbf{u_{hmin}} \le \mathbf{u} \le \mathbf{u_{hmax}},\ \left|\mathbf{du}\right| \le \mathbf{u_{hllim}}$

Model Dimensions : $\mathrm{n}_{equ1}, n_{equ2}, n_{equ3}, n_{state}, n_{control}, n_{Feqxx}, n_{Fequu}, n_{Fequx}, n_{fconst}, n_{Ffeqxx}, n_{Ffequu}, n_{Ffequx}$

Connectivity : $nn_t, ivn, inn, onn, S_{st}$

Normalization Factors: $x_{NF}, e_{NF}, u_{NF}, h_{NF}$

Units: $xUnit, eUnit, uUnit, hUnit$

where: **i**(*t*) is the terminal through variable vector, **x**(*t*) is the state variable vector, Y_{eqx1}, Y_{eqx2}, Y_{eqx3}, Y_{hfeqx} are linear coefficient matrices for state variables in equation set one, two, three, and constraint function, respectively, Y_{equ1}, Y_{equ2}, Y_{equ3}, Y_{hfequ} are linear coefficient matrices for control variables in equation set one, two, three, and constraint function, respectively, D_{eqxd1} and D_{eqxd2} are differential coefficient matrices for state variables in equation set one and two, C_{eqc1}, C_{eqc2}, C_{eqc3}, C_{hfeqc} are constant vectors, F_{eqxx3}, F_{equu3}, F_{equx3},

F_{hfeqxx}, F_{hfequu}, F_{hfequx} are coefficients of quadratic terms, **h** denotes functional constraints, $\mathbf{u}_{hmin}$, $\mathbf{u}_{hmax}$ are lower and upper bounds for control variables, $\mathbf{u}_{hlim}$ denotes the maximum permissible control variable excursions to maintain linearization error below a threshold. Besides, the SCQDM also provides additional information for this model including model type, model ID, model title, model dimensions, connectivity information, normalization factors, and units.

Note that SCQDM must satisfy the following requirements: (1) The equations are in terms of the state vector $\mathbf{x}(t)$, control vector $\mathbf{u}(t)$, and through variable vector $\mathbf{i}(t)$. The number of states and equations have to be even, since quasi-dynamic domain works with phasor values with real and imaginary parts. (2) The device terminal across variables must appear at the top of the state vector (e.g., the terminal voltages of a purely electrical device). Any additional states (referred to as internal states) are added below the terminal across variables as necessary. (3) The through variable vector $\mathbf{i}(t)$ consists of the device terminal through variables (e.g., the terminal currents of a purely electrical device). The positive direction of through variables is always defined into the device terminal. (4) All variables are in metric system.

4.3 Quadratic Integration Method and Derivation from SCQDM to SCAQCF

This section introduces the quadratic integration method and the derivation from SCQDM to SCAQCF. The quadratic integration method assumes that a function $x(t)$ varies quadratically within the integration time step $[t\text{-}h, t]$ as shown in Figure 4.3.1. Assuming $y(\tau) = a + b\tau + c\tau^2 \approx x(t)$, where $\tau \in [0, h]$, we have:

$$\begin{cases} y(0) = a = x(t-h) \\ y\left(\frac{h}{2}\right) = a + \frac{h}{2}b + \frac{h^2}{4}c = x_m \\ y(h) = a + bh + ch^2 = x(t) \end{cases} \Rightarrow \begin{cases} a = x(t-h) \\ b = \frac{1}{h}\left[-3x(t-h) + 4x_m - x(t)\right] \\ c = \frac{2}{h^2}\left[x(t-h) - 2x_m + x(t)\right] \end{cases} \quad (4.3.1)$$

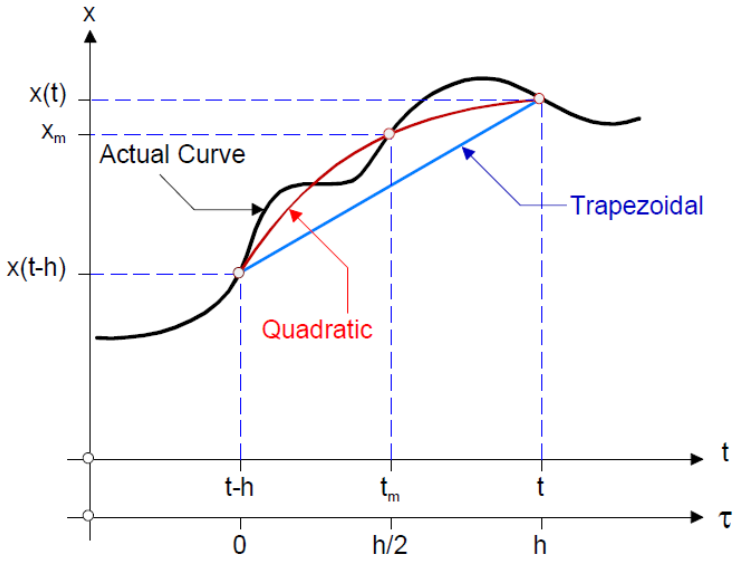

Figure 4.3.1: Illustration of Quadratic Integration Method

The integration of function $x(t)$ in the time interval $[t\text{-}h, t]$ and $[t\text{-}h, t_m]$ are listed in (4.3.2). Given (4.3.2), we are able to integrate SCQDM and obtain SCAQCF.

$$\begin{aligned} \int_{t-h}^{t} x(T)\,dT &= \int_0^h y(\tau)d\tau = \frac{h}{6}x(t-h) + \frac{2h}{3}x_m + \frac{h}{6}x(t) \\ \int_{t-h}^{t_m} x(T)dT &= \int_0^{h/2} y(\tau)d\tau = \frac{5h}{24}x(t-h) + \frac{h}{3}x_m - \frac{h}{24}x(t) \end{aligned} \quad (4.3.2)$$

Derivation of Equation Set 1 in SCQDM

From equation set 1 in SCQDM, we have:

$$D_{eqxd1}\frac{d\mathbf{x}(t)}{dt} = -Y_{eqx1}\mathbf{x}(t) - Y_{equ1}\mathbf{u}(t) + \mathbf{i}(t) - C_{eqc1} \tag{4.3.3}$$

The integration of (4.3.3) over time interval [*t*-*h*, *t*] yields:

$$\begin{aligned}\begin{bmatrix}\frac{h}{6}I & \frac{2h}{3}I\end{bmatrix}\begin{bmatrix}\mathbf{i}(t)\\ \mathbf{i}_m\end{bmatrix} &= \begin{bmatrix}\frac{h}{6}Y_{eqx1}+D_{eqxd1} & \frac{2h}{3}Y_{eqx1}\end{bmatrix}\begin{bmatrix}\mathbf{x}(t)\\ \mathbf{x}_m\end{bmatrix}+\begin{bmatrix}\frac{h}{6}Y_{equ1} & \frac{2h}{3}Y_{equ1}\end{bmatrix}\begin{bmatrix}\mathbf{u}(t)\\ \mathbf{u}_m\end{bmatrix}\\ &+\left(\frac{h}{6}Y_{eqx1}-D_{eqxd1}\right)\mathbf{x}(t-h)+\frac{h}{6}Y_{equ1}\mathbf{u}(t-h)-\frac{h}{6}\mathbf{i}(t-h)+hC_{eqc1}\end{aligned} \tag{4.3.4}$$

The integration of (4.3.3) over time interval [*t*-*h*, t_m] yields:

$$\begin{aligned}\begin{bmatrix}-\frac{h}{24}I & \frac{h}{3}I\end{bmatrix}\begin{bmatrix}\mathbf{i}(t)\\ \mathbf{i}_m\end{bmatrix} &= \begin{bmatrix}-\frac{h}{24}Y_{eqx1} & \frac{h}{3}Y_{eqx1}+D_{eqxd1}\end{bmatrix}\begin{bmatrix}\mathbf{x}(t)\\ \mathbf{x}_m\end{bmatrix}+\begin{bmatrix}-\frac{h}{24}Y_{equ1} & \frac{h}{3}Y_{equ1}\end{bmatrix}\begin{bmatrix}\mathbf{u}(t)\\ \mathbf{u}_m\end{bmatrix}\\ &+\left(\frac{5h}{24}Y_{eqx1}-D_{eqxd1}\right)\mathbf{x}(t-h)+\frac{5h}{24}Y_{equ1}\mathbf{u}(t-h)-\frac{5h}{24}\mathbf{i}(t-h)+\frac{h}{2}C_{eqc1}\end{aligned} \tag{4.3.5}$$

From (4.3.4) and (4.3.5), we have:

$$\begin{aligned}\begin{bmatrix}\frac{h}{6}I & \frac{2h}{3}I\\ -\frac{h}{24}I & \frac{h}{3}I\end{bmatrix}\begin{bmatrix}\mathbf{i}(t)\\ \mathbf{i}_m\end{bmatrix} &= \begin{bmatrix}\frac{h}{6}Y_{eqx1}+D_{eqxd1} & \frac{2h}{3}Y_{eqx1}\\ -\frac{h}{24}Y_{eqx1} & \frac{h}{3}Y_{eqx1}+D_{eqxd1}\end{bmatrix}\begin{bmatrix}\mathbf{x}(t)\\ \mathbf{x}_m\end{bmatrix}+\begin{bmatrix}\frac{h}{6}Y_{equ1} & \frac{2h}{3}Y_{equ1}\\ -\frac{h}{24}Y_{equ1} & \frac{h}{3}Y_{equ1}\end{bmatrix}\begin{bmatrix}\mathbf{u}(t)\\ \mathbf{u}_m\end{bmatrix}\\ &+\begin{bmatrix}\frac{h}{6}Y_{eqx1}-D_{eqxd1}\\ \frac{5h}{24}Y_{eqx1}-D_{eqxd1}\end{bmatrix}\mathbf{x}(t-h)+\begin{bmatrix}\frac{h}{6}Y_{equ1}\\ \frac{5h}{24}Y_{equ1}\end{bmatrix}\mathbf{u}(t-h)+\begin{bmatrix}\frac{h}{6}I\\ -\frac{5h}{24}I\end{bmatrix}\mathbf{i}(t-h)+\begin{bmatrix}hC_{eqc1}\\ \frac{h}{2}C_{eqc1}\end{bmatrix}\end{aligned}$$

$\Rightarrow$

$$\begin{bmatrix}\mathbf{i}(t)\\ \mathbf{i}_m\end{bmatrix}=\begin{bmatrix}Y_{eqx1}+\frac{4}{h}D_{eqxd1} & -\frac{8}{h}D_{eqxd1}\\ \frac{1}{2h}D_{eqxd1} & Y_{eqx1}+\frac{2}{h}D_{eqxd1}\end{bmatrix}\begin{bmatrix}\mathbf{x}(t)\\ \mathbf{x}_m\end{bmatrix}+\begin{bmatrix}Y_{equ1} & 0\\ 0 & Y_{equ1}\end{bmatrix}\begin{bmatrix}\mathbf{u}(t)\\ \mathbf{u}_m\end{bmatrix}$$
$$+\begin{bmatrix}-Y_{eqx1}+\frac{4}{h}D_{eqxd1}\\ \frac{1}{2}Y_{eqx1}-\frac{5}{2h}D_{eqxd1}\end{bmatrix}\mathbf{x}(t-h)+\begin{bmatrix}-Y_{equ1}\\ \frac{1}{2}Y_{equ1}\end{bmatrix}\mathbf{u}(t-h)+\begin{bmatrix}I\\ -\frac{1}{2}I\end{bmatrix}\mathbf{i}(t-h)+\begin{bmatrix}0\\ \frac{3}{2}C_{eqc1}\end{bmatrix} \tag{4.3.6}$$

Derivation of Equation Set 2 in SCQDM

From equation set 2 in SCQDM, we have:

$$D_{eqxd2}\frac{d\mathbf{x}(t)}{dt}=-Y_{eqx2}\mathbf{x}(t)-Y_{equ2}\mathbf{u}(t)-C_{eqc2} \tag{4.3.7}$$

The integration of (4.3.7) over time interval [*t*-*h*, *t*] yields:

$$0=\begin{bmatrix}\frac{h}{6}Y_{eqx2}+D_{eqxd2} & \frac{2h}{3}Y_{eqx2}\end{bmatrix}\begin{bmatrix}\mathbf{x}(t)\\ \mathbf{x}_m\end{bmatrix}+\begin{bmatrix}\frac{h}{6}Y_{equ2} & \frac{2h}{3}Y_{equ2}\end{bmatrix}\begin{bmatrix}\mathbf{u}(t)\\ \mathbf{u}_m\end{bmatrix}+\left(\frac{h}{6}Y_{eqx2}-D_{eqxd2}\right)\mathbf{x}(t-h)$$
$$+\frac{h}{6}Y_{equ2}\mathbf{u}(t-h)+hC_{eqc2} \tag{4.3.8}$$

The integration of (4.3.7) over time interval [*t*-*h*, t_m] yields:

$$0=\begin{bmatrix}-\frac{h}{24}Y_{eqx2} & \frac{h}{3}Y_{eqx2}+D_{eqxd2}\end{bmatrix}\begin{bmatrix}\mathbf{x}(t)\\ \mathbf{x}_m\end{bmatrix}+\begin{bmatrix}-\frac{h}{24}Y_{equ2} & \frac{h}{3}Y_{equ2}\end{bmatrix}\begin{bmatrix}\mathbf{u}(t)\\ \mathbf{u}_m\end{bmatrix}$$
$$+\left(\frac{5h}{24}Y_{eqx2}-D_{eqxd2}\right)\mathbf{x}(t-h)+\frac{5h}{24}Y_{equ2}\mathbf{u}(t-h)+\frac{h}{2}C_{eqc2} \tag{4.3.9}$$

From (4.3.8) and (4.3.9), we have:

$$\begin{bmatrix} \frac{h}{6}I & \frac{2h}{3}I \\ -\frac{h}{24}I & \frac{h}{3}I \end{bmatrix}\cdot 0 = \begin{bmatrix} \frac{h}{6}Y_{eqx2}+D_{eqxd2} & \frac{2h}{3}Y_{eqx2} \\ -\frac{h}{24}Y_{eqx2} & \frac{h}{3}Y_{eqx2}+D_{eqxd2} \end{bmatrix}\begin{bmatrix} \mathbf{x}(t) \\ \mathbf{x}_m \end{bmatrix}+\begin{bmatrix} \frac{h}{6}Y_{equ2} & \frac{2h}{3}Y_{equ2} \\ -\frac{h}{24}Y_{equ2} & \frac{h}{3}Y_{equ2} \end{bmatrix}\begin{bmatrix} \mathbf{u}(t) \\ \mathbf{u}_m \end{bmatrix}$$
$$+\begin{bmatrix} \frac{h}{6}Y_{eqx2}-D_{eqxd2} \\ \frac{5h}{24}Y_{eqx2}-D_{eqxd2} \end{bmatrix}\mathbf{x}(t-h)+\begin{bmatrix} \frac{h}{6}Y_{equ2} \\ \frac{5h}{24}Y_{equ2} \end{bmatrix}\mathbf{u}(t-h)+\begin{bmatrix} hC_{eqc2} \\ \frac{h}{2}C_{eqc2} \end{bmatrix}$$

$\Rightarrow$

$$\begin{bmatrix} 0 \\ 0 \end{bmatrix}=\begin{bmatrix} Y_{eqx2}+\frac{4}{h}D_{eqxd2} & -\frac{8}{h}D_{eqxd2} \\ \frac{1}{2h}D_{eqxd2} & Y_{eqx2}+\frac{2}{h}D_{eqxd2} \end{bmatrix}\begin{bmatrix} \mathbf{x}(t) \\ \mathbf{x}_m \end{bmatrix}+\begin{bmatrix} Y_{equ2} & 0 \\ 0 & Y_{equ2} \end{bmatrix}\begin{bmatrix} \mathbf{u}(t) \\ \mathbf{u}_m \end{bmatrix}$$
$$+\begin{bmatrix} -Y_{eqx2}+\frac{4}{h}D_{eqxd2} \\ \frac{1}{2}Y_{eqx2}-\frac{5}{2h}D_{eqxd2} \end{bmatrix}\mathbf{x}(t-h)+\begin{bmatrix} -Y_{equ2} \\ \frac{1}{2}Y_{equ2} \end{bmatrix}\mathbf{u}(t-h)+\begin{bmatrix} 0 \\ \frac{3}{2}C_{eqc2} \end{bmatrix} \quad (4.3.10)$$

Derivation of Equation Set 3 in SCQDM

Since no differential terms exist in equation set 3, the quadratic integration method is not applied on equation set 3. Considering equation set 3 at both time t and t_m, we have the following equation:

$$\begin{bmatrix} 0 \\ 0 \end{bmatrix}=\begin{bmatrix} Y_{eqx3} & 0 \\ 0 & Y_{eqx3} \end{bmatrix}\begin{bmatrix} \mathbf{x}(t) \\ \mathbf{x}_m \end{bmatrix}+\begin{bmatrix} Y_{equ3} & 0 \\ 0 & Y_{equ3} \end{bmatrix}\begin{bmatrix} \mathbf{u}(t) \\ \mathbf{u}_m \end{bmatrix}+\begin{bmatrix} C_{eqc3} \\ C_{eqc3} \end{bmatrix}$$
$$+\begin{bmatrix} \vdots \\ \mathbf{x}(t)^T\left\langle F^i_{eqxx3}\right\rangle\mathbf{x}(t) \\ \vdots \\ \vdots \\ \mathbf{x}(t_m)^T\left\langle F^i_{eqxx3}\right\rangle\mathbf{x}(t_m) \\ \vdots \end{bmatrix}+\begin{bmatrix} \vdots \\ \mathbf{u}(t)^T\left\langle F^i_{equu3}\right\rangle\mathbf{u}(t) \\ \vdots \\ \vdots \\ \mathbf{u}(t_m)^T\left\langle F^i_{equu3}\right\rangle\mathbf{u}(t_m) \\ \vdots \end{bmatrix}+\begin{bmatrix} \vdots \\ \mathbf{u}(t)^T\left\langle F^i_{equx3}\right\rangle\mathbf{x}(t) \\ \vdots \\ \vdots \\ \mathbf{u}(t_m)^T\left\langle F^i_{equx3}\right\rangle\mathbf{x}(t_m) \\ \vdots \end{bmatrix} \quad (4.3.11)$$

Derivation of Constraint Function Set in SCQDM

Since no differential terms exist in constraint function set, the quadratic integration method is not applied on this function set. Considering constraint function set at both time t and t_m, we have the following equation:

$$h(\mathbf{x},\mathbf{u}) = \begin{bmatrix} Y_{feqx} & 0 \\ 0 & Y_{feqx} \end{bmatrix} \begin{bmatrix} \mathbf{x}(t) \\ \mathbf{x}_m \end{bmatrix} + \begin{bmatrix} Y_{fequ} & 0 \\ 0 & Y_{fequ} \end{bmatrix} \begin{bmatrix} \mathbf{u}(t) \\ \mathbf{u}_m \end{bmatrix} + \begin{bmatrix} C_{feqc} \\ C_{feqc} \end{bmatrix} + \begin{bmatrix} \vdots \\ \mathbf{x}(t)^T \left\langle F^i_{feqxx} \right\rangle \mathbf{x}(t) \\ \vdots \\ \vdots \\ \mathbf{x}(t_m)^T \left\langle F^i_{feqxx} \right\rangle \mathbf{x}(t_m) \\ \vdots \end{bmatrix} + \begin{bmatrix} \vdots \\ \mathbf{u}(t)^T \left\langle F^i_{fequu} \right\rangle \mathbf{u}(t) \\ \vdots \\ \vdots \\ \mathbf{u}(t_m)^T \left\langle F^i_{fequu} \right\rangle \mathbf{u}(t_m) \\ \vdots \end{bmatrix} + \begin{bmatrix} \vdots \\ \mathbf{u}(t)^T \left\langle F^i_{fequx} \right\rangle \mathbf{x}(t) \\ \vdots \\ \vdots \\ \mathbf{u}(t_m)^T \left\langle F^i_{fequx} \right\rangle \mathbf{x}(t_m) \\ \vdots \end{bmatrix} \quad (4.3.12)$$

By stacking (4.3.6), (4.3.10), (4.3.11), (4.3.12) together, we are able to construct SCAQCF, which will be detailed described in the next section

4.4 Quasi-Dynamic Domain SCAQCF Syntax

The end result of Section 4.3 is the quasi-dynamic domain SCAQCF. Note that this modeling standard can be applied to any device in the power system. The advantages of the SCAQCF device model are: (a) It does not contain differential terms, and it is algebraic. The dynamics are expressed in terms of past history terms, (b) the highest order is second order, and (c) it is easily cast into a standard syntax so that the utilization of the model can be performed by object-oriented algorithms. The final expression of the quasi-dynamic domain SCAQCF device model is:

Model Description: *Type*, *Code*, *ID*, *Title*

$$\begin{Bmatrix} \mathbf{i}(t) \\ 0 \\ 0 \\ \mathbf{i}(t_m) \\ 0 \\ 0 \end{Bmatrix} = \mathbf{e_{lhs}} = Y_{eqx}\mathbf{x} + \begin{Bmatrix} \vdots \\ \mathbf{x}^T \left\langle F^i_{eqxx} \right\rangle \mathbf{x} \\ \vdots \end{Bmatrix} + Y_{equ}\mathbf{u} + \begin{Bmatrix} \vdots \\ \mathbf{u}^T \left\langle F^i_{equu} \right\rangle \mathbf{u} \\ \vdots \end{Bmatrix} + \begin{Bmatrix} \vdots \\ \mathbf{u}^T \left\langle F^i_{equx} \right\rangle \mathbf{x} \\ \vdots \end{Bmatrix} - B_{eq}$$

$$B_{eq} = -N_{eqx}\mathbf{x}(t-h) - N_{equ}\mathbf{u}(t-h) - M_{eq}\mathbf{i}(t-h) - K_{eq}$$

$$\mathbf{h}(\mathbf{x},\mathbf{u}) = Y_{feqx}\mathbf{x} + Y_{fequ}\mathbf{u} + \begin{Bmatrix} \vdots \\ \mathbf{x}^T \left\langle F^i_{feqxx} \right\rangle \mathbf{x} \\ \vdots \end{Bmatrix} + \begin{Bmatrix} \vdots \\ \mathbf{u}^T \left\langle F^i_{fequu} \right\rangle \mathbf{u} \\ \vdots \end{Bmatrix} + \begin{Bmatrix} \vdots \\ \mathbf{u}^T \left\langle F^i_{fequx} \right\rangle \mathbf{x} \\ \vdots \end{Bmatrix} + C_{feqc}$$

Constraints : $\mathbf{h}(\mathbf{x},\mathbf{u}) \le \mathbf{0}, \mathbf{u_{min}} \le \mathbf{u} \le \mathbf{u_{max}}, \ |\mathbf{du}| \le \mathbf{u_{llim}}$

Model Dimensions: n_{equ}, n_{state}, $n_{control}$, n_{Feqxx}, n_{Fequu}, n_{Fequx}, n_{fconst}, n_{Ffeqxx}, n_{Ffequu}, n_{Ffequx}

Connectivity: nn_t, *ivn*, *inn*, *onn*, S_{st}

Normalization Factor: x_{NF}, e_{NF}, u_{NF}, h_{NF}

Units: *xUnit*, *eUnit*, *uUnit*, *hUnit*

where: $\mathbf{i}(t)$ and $\mathbf{i}(t_m)$ are the terminal through variable vectors at time t and t_m, $\mathbf{x}$ is the state variable vector, Y matrices are linear coefficients, F matrices are nonlinear coefficients, B vector is the past history vector containing dynamics, N matrices denote coefficients associated with state variables in past history, M denotes coefficients associated with through variables in past history, K and C vectors are the constant vectors, $\mathbf{h}$ denotes functional constraints, $\mathbf{u}_{\min}$, $\mathbf{u}_{\max}$ are lower and upper bounds for control variables, $\mathbf{u}_{\text{hlim}}$ denotes the maximum permissible control variable excursions to maintain linearization error below a threshold. Besides, the SCAQCF also provides additional information for this model including model type, model ID, model title, model dimensions, connectivity information, normalization factors, and units. All the matrices constructed from SCQDM are shown below:

$$Y_{eqx}=\begin{bmatrix} \frac{4}{t_h}D_{eqxd1}+Y_{eqx1} & -\frac{8}{t_h}D_{eqxd1} \\ \frac{4}{t_h}D_{eqxd2}+Y_{eqx2} & -\frac{8}{t_h}D_{eqxd2} \\ Y_{eqx3} & 0 \\ \frac{1}{2t_h}D_{eqxd1} & \frac{2}{t_h}D_{eqxd1}+Y_{eqx1} \\ \frac{1}{2t_h}D_{eqxd2} & \frac{2}{t_h}D_{eqxd1}+Y_{eqx2} \\ 0 & Y_{eqx3} \end{bmatrix}, Y_{equ}=\begin{bmatrix} Y_{equ1} & 0 \\ Y_{equ2} & 0 \\ Y_{equ3} & 0 \\ 0 & Y_{equ1} \\ 0 & Y_{equ2} \\ 0 & Y_{equ3} \end{bmatrix}, F_{eqx}=\begin{bmatrix} 0 & 0 \\ 0 & 0 \\ F_{eqxx3} & 0 \\ 0 & 0 \\ 0 & 0 \\ 0 & F_{eqxx3} \end{bmatrix},$$

$$F_{equ}=\begin{bmatrix} 0 & 0 \\ 0 & 0 \\ F_{equu3} & 0 \\ 0 & 0 \\ 0 & 0 \\ 0 & F_{equu3} \end{bmatrix}, F_{equx}=\begin{bmatrix} 0 & 0 \\ 0 & 0 \\ F_{equx3} & 0 \\ 0 & 0 \\ 0 & 0 \\ 0 & F_{equx3} \end{bmatrix}, N_{eqx}=\begin{bmatrix} -Y_{eqx1}+\frac{4}{t_h}D_{eqxd1} \\ -Y_{eqx2}+\frac{4}{t_h}D_{eqxd2} \\ 0 \\ \frac{1}{2}Y_{eqx1}-\frac{5}{2t_h}D_{eqxd1} \\ \frac{1}{2}Y_{eqx2}-\frac{5}{2t_h}D_{eqxd2} \\ 0 \end{bmatrix},$$

$$N_{equ}=\begin{bmatrix} -Y_{equ1} \\ -Y_{equ2} \\ 0 \\ \frac{1}{2}Y_{equ1} \\ \frac{1}{2}Y_{equ2} \\ 0 \end{bmatrix}, M_{eq}=\begin{bmatrix} I_{size(i(t))} \\ 0 \\ 0 \\ -\frac{1}{2}I_{size(i(t))} \\ 0 \\ 0 \end{bmatrix}, K_{eq}=\begin{bmatrix} 0 \\ 0 \\ C_{eqc3} \\ \frac{3}{2}C_{eqc1} \\ \frac{3}{2}C_{eqc2} \\ C_{eqc3} \end{bmatrix}$$

$$Y_{feqx}=\begin{bmatrix} Y_{hfeqx} & 0 \\ 0 & Y_{hfeqx} \end{bmatrix} \qquad Y_{fequ}=\begin{bmatrix} Y_{hfequ} & 0 \\ 0 & Y_{hfeqx} \end{bmatrix} \qquad C_{feqc}=\begin{bmatrix} C_{hfeqc} \\ C_{hfeqc} \end{bmatrix}$$

$$F_{feqxx} = \begin{bmatrix} F_{hfeqxx} & 0 \\ 0 & F_{hfeqxx} \end{bmatrix} \qquad F_{fequu} = \begin{bmatrix} F_{hfequu} & 0 \\ 0 & F_{hfequu} \end{bmatrix} \qquad F_{fequx} = \begin{bmatrix} F_{hfequx} & 0 \\ 0 & F_{hfequx} \end{bmatrix}$$

$$\mathbf{u}_{min} = \begin{bmatrix} \mathbf{u}_{hmin} \\ \mathbf{u}_{hmin} \end{bmatrix} \qquad \mathbf{u}_{max} = \begin{bmatrix} \mathbf{u}_{hmax} \\ \mathbf{u}_{hmax} \end{bmatrix} \qquad \mathbf{u}_{llim} = \begin{bmatrix} \mathbf{u}_{hllim} \\ \mathbf{u}_{hllim} \end{bmatrix}$$

4.5 Summary

This chapter presents an object-oriented device modeling approach that is applicable to all power devices in distribution systems. The detailed derivation from physically based compact device model to SCAQCF model is described. This unified syntax lays a sound foundation for the state estimator so that it is able to operate in an object-oriented way. An example of this modeling approach (i.e., generator with turbine, governor, and exciter) is illustrated in Appendix A.

CHAPTER 5. NETWORK-LEVEL MEASUREMENT MODEL FORMULATION

5.1 Overview

This chapter introduces the procedure that formulates the network-level measurement model given SCAQCF devices and measurements from a partitioned section. With increasing deployment of smart meters and other grid sensors in the distribution system, the amount of available measurement is growing. These measurements as well as other measurements proposed in this section construct the network-level measurement model that improves the observability of the distribution system and increases the accuracy of the state estimation results. To construct the network-level measurement model, three tasks are performed: (1) Construct the network-level SCAQCF model and form the mapping lists (states, controls, equations) from devices to the network [62]–[65], (2) create the network-level actual measurement model based on the given measurements from all IEDs and mapping lists, and (3) create the network-level derived, pseudo, and virtual measurement models.

This chapter is organized as follows. Section 5.2 introduces the procedure of constructing the network-level SCAQCF model and forming the mapping lists from devices to the network. Section 5.3 introduces the measurement definitions in the proposed state estimator and the creation of the network-level measurement model. Section 5.4 summarizes this chapter.

5.2 Construction of the Network SCAQCF Model

Given *n* device SCAQCF models in a selected section, the first task is to create the network-level model in SCAQCF syntax as shown in Figure 5.2.1. In general, a device SCAQCF model consists of three types of equations: (a) Equations corresponding to the network interface nodes, (b) equations corresponding to the network common nodes, and (c) device internal equations. To formulate network SCAQCF model, we keep types a and c equations and replace the states and controls in terms of the corresponding devices by the states and controls in terms of the network. For type b equations from different devices but corresponding to a same common node, we apply Kirchhoff's current law (KCL) at each node which provides one equation for each node and which eliminates the through variables. These equations are in terms of the states and controls of the network. During this task, we first create the mapping lists (states, controls, equations) from devices to the network based on the device connectivity. Then, the network SCAQCF model is automatically created by the device SCAQCF models in this network and the mapping lists.

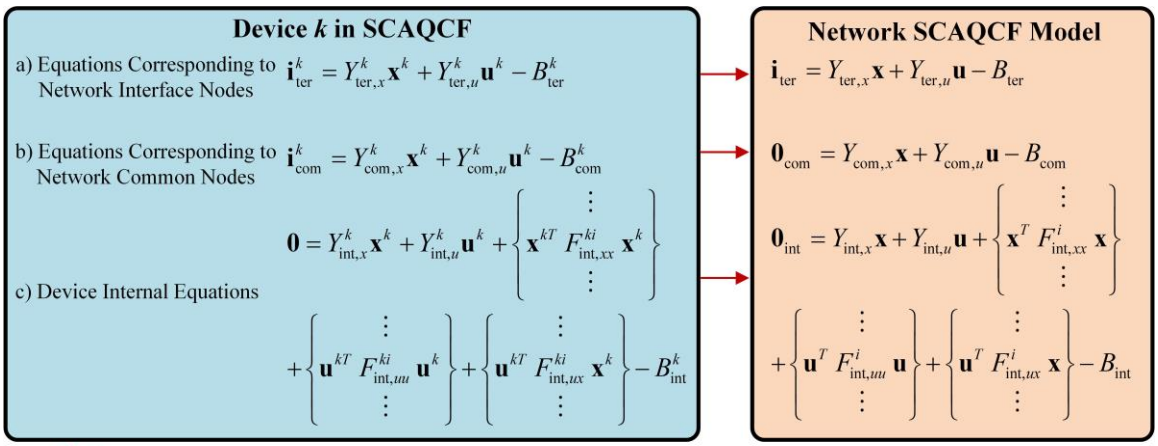

Figure 5.2.1: Network SCAQCF Model Formulation

The output of this step is the network SCAQCF model as listed in Figure 5.2.1. Note that in the network SCAQCF model, the equations with the current **i** on the left-hand side denote the through variables flowing into the network through the interface nodes, and all the other equations with zero values on the left-hand side are the device internal equations as well as the zero sum of equations at the common nodes derived from KCL.

5.3 Network-Level Measurement Model Formulation

The second task is to form the network-level measurement model. For the measurements that are actually collected from IEDs, we name them as actual measurements. These actual measurements can be further classified into across measurements and through measurements. Across measurements (e.g., voltage measurement) are those that the measured quantity is a state or a combination of states and therefore they are not associated with a specific device. Through measurements (e.g., current measurement) are those that can be expressed as a function of state variables of a

specific device. Given the measurements from all IEDs and all device SCAQCF models, we first construct the device-level measurement model. For a GPS-synchronized across measurement, its measurement model is simply a linear combination of the states of the measured device plus a measurement error from this IED, i.e.,

$$z_{VS}(t) = A\mathbf{x}(t) + \eta = x_i(t) - x_j(t) + \eta \tag{5.3.1}$$

where $z_{VS}(t)$ is the measurement, A is the linear coefficient matrix, and η is the noise introduced by this IED.

If an IED does not have a GPS clock, the phasor measurements are not synchronized to the global time reference that the GPS clock offers. As a consequence, data from this IED that are not GPS synchronized are referenced to the phase A voltage. The measured phase angle of phase A voltage is 0, while the "actual" phase angle of the phase A voltage is introduced as an additional state (estimated by the state estimation) as follows:

$$z_{VNS}(t) = A\mathbf{x}(t)e^{j\alpha} + \eta = \left(x_i(t) - x_j(t)\right)e^{j\alpha} + \eta \tag{5.3.2}$$

where $e^{j\alpha} = \cos(\alpha) + j\sin(\alpha) = x_{NS,r} + jx_{NS,i}$, $z_{VNS}(t)$ is the non-synchronized measurement. The introduced state is a complex variable with the restriction that its magnitude is 1 and its phase angle is α. As a result, the following virtual measurement can be added:

$$0 = x_{NS,r}^2 + x_{NS,i}^2 - 1.0 + \eta \tag{5.3.3}$$

where the subscript r and i denote real and imaginary parts. The model of this type of measurement is then expressed as:

$$z_{VNS,r}(t) = x_{i,r}x_{NS,r} - x_{j,r}x_{NS,r} - x_{i,i}x_{NS,i} + x_{j,i}x_{NS,i} + \eta_r$$
$$z_{VNS,i}(t) = x_{i,r}x_{NS,i} - x_{j,r}x_{NS,i} + x_{i,i}x_{NS,r} - x_{j,i}x_{NS,r} + \eta_i \quad (5.3.4)$$

where $z_{VNS,r}(t)$ and $z_{VNS,i}(t)$ are the real and imaginary part of the measurement value, $x_{i,r}$, $x_{j,r}$, $x_{i,i}$, $x_{j,i}$ are the states related to this measurement, and $x_{NS,r}$, $x_{NS,i}$ are the real and imaginary parts of the additional state introduced for the synchronization.

For a voltage magnitude measurement, the model of this measurement type is:

$$z_{Vmag}(t) = \sqrt{\left(x_{i,r} - x_{j,r}\right)^2 + \left(x_{i,i} - x_{j,i}\right)^2} + \eta \quad (5.3.5)$$

where $z_{Vmag}(t)$ is the voltage magnitude value at time t. Then the quadratized measurement model of this measurement type is:

$$z'_{Vmag}(t) = z^2_{Vmag}(t) = x^2_{i,r} + x^2_{i,i} + x^2_{j,r} + x^2_{j,i} - 2x_{i,r}x_{j,r} - 2x_{i,i}x_{j,i} + \eta \quad (5.3.6)$$

For a GPS-synchronized through measurement, its measurement model is obtained directly from the corresponding equations of the device SCAQCF model, i.e.,

$$z_{IS}(t) = Y_{zx}\mathbf{x} + Y_{zu}\mathbf{u} - B_z + \eta$$
$$B_z = -N_{zx}\mathbf{x}(t-h) - N_{zu}\mathbf{u}(t-h) - M_z\mathbf{i}(t-h) - K_z \quad (5.3.7)$$

where $z_{IS}(t)$ is the through measurement, Y_{zx} and Y_{zu} are linear coefficient matrices, N_{zx}, N_{zu}, M_z are linear coefficient matrices with respect to past-history terms, and K_z is the constant term.

For a through measurement from an IED without a GPS clock, similar as the process for the non-synchronized across measurement, an additional state that denotes the

phase angle between the measured phase angle of phase A voltage and the "actual" phase angle of the phase A voltage is introduced as (5.3.8), which can also be described in SCAQCF syntax:

$$z_{INS}(t) = z_{IS}(t)\left(x_{NS,r} + jx_{NS,i}\right) \tag{5.3.8}$$

where $z_{INS}(t)$ is the non-synchronized through measurement. The final expression of this type of measurement is:

$$\begin{aligned} z_{INS,r}(t) &= \sum_i Y_{zx,i}^{k_1} x_i x_{NS,r} + \sum_i Y_{zu,i}^{k_1} u_i x_{NS,r} - B_z^{k_1} x_{NS,r} - \sum_i Y_{zx,i}^{k_2} x_i x_{NS,i} - \sum_i Y_{zu,i}^{k_2} u_i x_{NS,i} + B_z^{k_2} x_{NS,i} + \eta_r \\ z_{INS,i}(t) &= \sum_i Y_{zx,i}^{k_1} x_i x_{NS,i} + \sum_i Y_{zu,i}^{k_1} u_i x_{NS,i} - B_z^{k_1} x_{NS,i} + \sum_i Y_{zx,i}^{k_2} x_i x_{NS,r} + \sum_i Y_{zu,i}^{k_2} u_i x_{NS,r} - B_z^{k_2} x_{NS,r} + \eta_i \end{aligned} \tag{5.3.9}$$

where $z_{INS,r}(t)$ and $z_{INS,i}(t)$ are the real and imaginary part of the measurement value, $Y_{zx,i}^{k_1}$, $Y_{zx,i}^{k_2}$ denote the element of Y_{zx} at k_1-th row and i-th column and at k_2-th row and i-th column, respectively, $Y_{zu,i}^{k_1}$, $Y_{zu,i}^{k_2}$ denote the element of Y_{zu} at k_1-th row and i-th column and at k_2-th row and i-th column, respectively, $B_z^{k_1}$ and $B_z^{k_2}$ denote the element of B_z at k_1-th row and k_2-th row, respectively.

For a current magnitude measurement, the model of this measurement type is:

$$z_{Imag}(t) = \sqrt{z_{Imag,r}^2 + z_{Imag,i}^2} + \eta \tag{5.3.10}$$

where $z_{Imag}(t)$ is the current magnitude value at time t. Then the quadratized measurement model of this measurement type is:

$$
\begin{aligned}
z'_{Imag}(t) &= z^2_{Imag}(t) \\
&= \sum_{i=1}^{n}\left(\left(Y^{k_1}_{zx,i}\right)^2+\left(Y^{k_2}_{zx,i}\right)^2\right)x_i^2+2\sum_{i=1}^{n-1}\sum_{j=i+1}^{n}\left(Y^{k_1}_{zx,i}\cdot Y^{k_1}_{zx,j}+Y^{k_2}_{zx,i}\cdot Y^{k_2}_{zx,j}\right)x_i x_j \\
&+\sum_{i=1}^{n}\left(\left(Y^{k_1}_{zu,i}\right)^2+\left(Y^{k_2}_{zu,i}\right)^2\right)u_i^2+2\sum_{i=1}^{n-1}\sum_{j=i+1}^{n}\left(Y^{k_1}_{zu,i}\cdot Y^{k_1}_{zu,j}+Y^{k_2}_{zu,i}\cdot Y^{k_2}_{zu,j}\right)u_i u_j \\
&+\left(B^{k_1}_{z}\right)^2+\left(B^{k_2}_{z}\right)^2+2\sum_{i=1}^{n}\sum_{j=1}^{n}\left(Y^{k_1}_{zx,i}\cdot Y^{k_1}_{zu,j}+Y^{k_2}_{zx,i}\cdot Y^{k_2}_{zu,j}\right)x_i u_j \\
&-2\sum_{i=1}^{n}\left(B^{k_1}_{z}Y^{k_1}_{zx,i}+B^{k_2}_{z}Y^{k_2}_{zx,i}\right)x_i-2\sum_{i=1}^{n}\left(B^{k_1}_{z}Y^{k_1}_{zu,i}+B^{k_2}_{z}Y^{k_2}_{zu,i}\right)u_i+\eta
\end{aligned}
\tag{5.3.11}
$$

where n is the total number of states of the measured device.

Once the device-level actual measurement model is formed, the network-level actual measurement model is easily obtained by using the formulated mapping lists that map the states, controls, and equations from the device-level actual measurement model to those in the network-level actual measurement model.

To realize the observability and increase the redundancy, four other types of measurements are introduced and their measurement models are constructed: (1) Type I derived measurement: Derived from actual measurements based on the system topology, (2) type II derived measurement: Generated for missing through variable measurements in any multi-terminal device, (3) pseudo measurement: Quantities that are approximately known (e.g., zero value of neutral phase voltage under normal operation, etc.), and (4) virtual measurements: Equations with zero value defined by physical or mathematical laws (e.g., KCL, device internal equations, etc.).

Type I derived measurement is created by derivation from actual measurement based on the network topology. For instance, as shown in Figure 5.3.1, device *i* and *j* are

connected at node *O* with available current phasor measurement $\tilde{I}_i$. Since no other devices are connected at this point *O*, the current flowing into device *j* is simply derived as $z = \tilde{I}_j + \eta = -\tilde{I}_i + \eta$, which is a type I derived measurement. Type I derived measurement can also be created based on the device topology. For example, as a distribution line is usually short, and its shunt capacitance is quite small. Therefore, if we have current measurements at one terminal of this line, we can derive current measurements that have same magnitudes but are with opposite phase angles at the other terminal of this line. Such measurements are also considered as type I derived measurements. By using formulated mapping lists, type I derived measurement model is expressed in terms of variables at network-level as listed in (5.3.12),

$$\begin{aligned} z_{dI}(t) &= Y_{dI,x}\mathbf{x} + Y_{dI,u}\mathbf{u} + \left\{ \begin{array}{c} \vdots \\ \mathbf{x}^T F_{dI,x}^i \mathbf{x} \\ \vdots \end{array} \right\} + \left\{ \begin{array}{c} \vdots \\ \mathbf{u}^T F_{dI,u}^i \mathbf{u} \\ \vdots \end{array} \right\} + \left\{ \begin{array}{c} \vdots \\ \mathbf{u}^T F_{dI,ux}^i \mathbf{x} \\ \vdots \end{array} \right\} - B_{dI} + \eta \\ B_{dI} &= -N_{dI,x}\mathbf{x}(t-h) - N_{dI,u}\mathbf{u}(t-h) - M_{dI}\mathbf{i}(t-h) - K_{dI} \end{aligned} \tag{5.3.12}$$

where subscript *dI* denotes type I derived measurement.

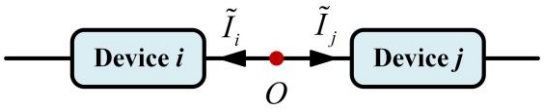

Figure 5.3.1: Illustration of Type I Derived Measurement

Type II derived measurement is generated for missing through variable measurements in any multi-terminal device that has at least one through quantity actual measurement. Specifically, for an *n*-terminal device with *m* terminals having through

measurements, the state estimator creates type II derived measurements for the other *n*-*m* terminals. Similar as type I derived measurement model, type II derived measurement model is also directly obtained from the device SCAQCF model. However, its measurement value is computed from the device SCAQCF model using the estimated states from the last time step. Since the measurement value is not obtained from the current time step, the state estimator assigns a relatively higher measurement error to type II derived measurement compared with the actual measurements from this device (e.g., five times larger than the actual measurement error of this device). By using the formulated link lists between devices and network, type II derived measurement model is expressed in terms of variables at network level in (5.3.13), where subscript *dII* denotes type II derived measurement.

$$\begin{aligned} z_{dII}(t) &= Y_{dII,x}\mathbf{x} + Y_{dII,u}\mathbf{u} + \left\{\begin{array}{c}\vdots\\ \mathbf{x}^T F^i_{dII,x}\mathbf{x}\\ \vdots\end{array}\right\} + \left\{\begin{array}{c}\vdots\\ \mathbf{u}^T F^i_{dII,u}\mathbf{u}\\ \vdots\end{array}\right\} + \left\{\begin{array}{c}\vdots\\ \mathbf{u}^T F^i_{dII,ux}\mathbf{x}\\ \vdots\end{array}\right\} - B_{dII} + \eta \\ B_{dII} &= -N_{dII,x}\mathbf{x}(t-h) - N_{dII,u}\mathbf{u}(t-h) - M_{dII}\mathbf{i}(t-h) - K_{dII} \end{aligned} \tag{5.3.13}$$

Pseudo measurement models are not directly measured but are quantities for which we know their approximate values. For example, the voltage at a neutral is around zero during normal operations. This voltage can be introduced as a pseudo measurement. Since we do not know the exact value of pseudo measurements, a relatively higher measurement error compared with actual measurement model is introduced. The pseudo measurement model could also be expressed in terms of variables at network level as listed in (5.3.14), where subscript *p* denotes pseudo measurement.

$$z_p(t) = Y_{p,x}\mathbf{x} + Y_{p,u}\mathbf{u} + \begin{Bmatrix} \vdots \\ \mathbf{x}^T F_{p,x}^i \mathbf{x} \\ \vdots \end{Bmatrix} + \begin{Bmatrix} \vdots \\ \mathbf{u}^T F_{p,u}^i \mathbf{u} \\ \vdots \end{Bmatrix} + \begin{Bmatrix} \vdots \\ \mathbf{u}^T F_{p,ux}^i \mathbf{x} \\ \vdots \end{Bmatrix} - B_p + \eta$$
$$B_p = -N_{p,x}\mathbf{x}(t-h) - N_{p,u}\mathbf{u}(t-h) - M_p\mathbf{i}(t-h) + K_p \tag{5.3.14}$$

Virtual measurement models are provided by the network internal equations reflecting the physical property (e.g., KCL, etc.) of the network. These are directly obtained from the equations with zero value on the left-hand side in the network-level SCAQCF model with a relatively small measurement error compared with actual measurement models as shown in (5.3.15), where subscript *v* refers to virtual measurement model.

$$z_v(t) = Y_{v,x}\mathbf{x} + Y_{v,u}\mathbf{u} + \begin{Bmatrix} \vdots \\ \mathbf{x}^T F_{v,x}^i \mathbf{x} \\ \vdots \end{Bmatrix} + \begin{Bmatrix} \vdots \\ \mathbf{u}^T F_{v,u}^i \mathbf{u} \\ \vdots \end{Bmatrix} + \begin{Bmatrix} \vdots \\ \mathbf{u}^T F_{v,ux}^i \mathbf{x} \\ \vdots \end{Bmatrix} - B_v + \eta$$
$$B_v = -N_{v,x}\mathbf{x}(t-h) - N_{v,u}\mathbf{u}(t-h) - M_v\mathbf{i}(t-h) + K_v \tag{5.3.15}$$

By following all these tasks and combining network-level actual, type I derived, type II derived, pseudo, and virtual measurement models, the final expression of the network measurement model with a similar syntax as the network SCAQCF model is obtained:

$$\mathbf{z}(t) = h(\mathbf{x}) + \boldsymbol{\eta} = Y_{zx}\mathbf{x} + Y_{zu}\mathbf{u} + \begin{Bmatrix} \vdots \\ \mathbf{x}^T F_{zx}^i \mathbf{x} \\ \vdots \end{Bmatrix} + \begin{Bmatrix} \vdots \\ \mathbf{u}^T F_{zu}^i \mathbf{u} \\ \vdots \end{Bmatrix} + \begin{Bmatrix} \vdots \\ \mathbf{u}^T F_{zux}^i \mathbf{x} \\ \vdots \end{Bmatrix} - B_z + \boldsymbol{\eta}$$
$$B_z = -N_{zx}\mathbf{x}(t-h) - N_{zu}\mathbf{u}(t-h) - M_z\mathbf{i}(t-h) - K_z \tag{5.3.16}$$

5.4 Summary

This chapter introduces the construction of the network-level measurement model. Given all the devices in SCAQCF syntax and measurements from the monitored partitioned section, the process starts from building the network SCAQCF model from those device SCAQCF models. Then, the network-level actual measurement model is created based on the given measurements from all IEDs and the constructed network SCAQCF model. To realize the observability and increase the redundancy, four other types of measurements (type I derived, type II derived, pseudo, and virtual measurements) are introduced and their measurement models are constructed. By stacking actual, type I derived, type II derived, pseudo, and virtual measurement models together, the network-level measurement model is obtained, and it is seamlessly adopted by the QDSE introduced in the next chapter.

CHAPTER 6. QUASI-DYNAMIC STATE ESTIMATION

6.1 Overview

This chapter introduces the QDSE method given the formulated network-level measurement model described in Chapter 5. The QDSE adopts the devices with slow dynamics such as electromechanical transients in the rotor and control action of converters, gives the best estimates of the monitored system, and checks the consistency between the measurements and the system model at each time step. The evaluation of the consistency is reflected by a metric called confidence level. A high consistency indicates the estimated states are trustworthy and a low consistency indicates some bad data or inaccurate models exist in the monitored system. This chapter is organized as follows. Section 6.2 introduces the QDSE using unconstrained weighted least square method. Section 6.3 introduces the QDSE using constrained weighted least square method. Section 6.4 introduces bad data detection and identification procedure in case a low consistency occurs. Section 6.5 summaries this chapter.

6.2 Unconstrained Weighted Least Square Method

For the unconstrained weighted least square method, the optimization problem is expressed to minimize the sum of the residual squares between measurements and estimated measurements as follows [66]–[70]:

$$\textit{Minimize} \quad J = \left(h(\mathbf{x},\mathbf{u}) - \mathbf{z}\right)^T W \left(h(\mathbf{x},\mathbf{u}) - \mathbf{z}\right) \tag{6.2.1}$$

where **z** is the measurement value vector, $h(\mathbf{x},\mathbf{u})$ is the measurement model, W is the weight matrix with the weights defined as the inverse of the squared standard deviation δ_i (i.e., measurement error) for each measurement: $W = diag\left\{1/\delta_1^2, 1/\delta_2^2, ..., 1/\delta_n^2\right\}$.

Then we substitute the control vector **u** in $h(\mathbf{x},\mathbf{u})$ with actual values from DMS, yielding $h(\mathbf{x})$ as shown in (6.2.2). The unknown state vector **x** is obtained by the necessary condition as listed in (6.2.3):

$$h(\mathbf{x}) = Y\mathbf{x} + \begin{Bmatrix} \vdots \\ \mathbf{x}^T F^i \mathbf{x} \\ \vdots \end{Bmatrix} - B = Y\mathbf{x} + \begin{Bmatrix} \vdots \\ \mathbf{x}^T F^i \mathbf{x} \\ \vdots \end{Bmatrix} + N\mathbf{x}(t-h) + M\mathbf{i}(t-h) + K \tag{6.2.2}$$

$$\frac{dJ}{d\mathbf{x}} = 0 \tag{6.2.3}$$

If the measurement model is linear (i.e., F matrices are zero), the solution can be obtained directly as shown in (6.2.4) and (6.2.5):

$$\begin{aligned} 0 = \frac{dJ}{d\mathbf{x}} &= \frac{d}{d\mathbf{x}}\left(\left(Y\mathbf{x} - B - \mathbf{z}\right)^T W \left(Y\mathbf{x} - B - \mathbf{z}\right)\right) \\ &= \frac{d}{d\mathbf{x}}\left(\left(H\mathbf{x} - B - \mathbf{z}\right)^T W \left(H\mathbf{x} - B - \mathbf{z}\right)\right) \\ &= 2H^T W \left(H\mathbf{x} - B - \mathbf{z}\right) \end{aligned} \tag{6.2.4}$$

$$\begin{aligned} \mathbf{x} &= \left(H^T W H\right)^{-1} H^T W \left(\mathbf{z} + B\right) \\ &= \left(H^T W H\right)^{-1} H^T W \left(\mathbf{z} - N\mathbf{x}\left(t-h\right) - M\mathbf{i}\left(t-h\right) - K\right) \end{aligned} \tag{6.2.5}$$

where H is the Jacobian matrix of the measurement model, and in this linear case, H equals to Y.

If the measurement model is nonlinear, to obtain the solution of this nonlinear optimization problem, we first linearize the nonlinear equations by assuming an initial guess $\mathbf{x}^{\nu}$, and the residual between the measurements and the linearized measurement model is:

$$\mathbf{r} = h\left(\mathbf{x}^{\nu}\right) + H\left(\mathbf{x}^{\nu}\right)\left(\mathbf{x} - \mathbf{x}^{\nu}\right) - \mathbf{z} = H\left(\mathbf{x}^{\nu}\right)\mathbf{x} - \mathbf{z}' \tag{6.2.6}$$

where $\mathbf{z}' = -h(\mathbf{x}^{\nu}) + H(\mathbf{x}^{\nu})\mathbf{x}^{\nu} + \mathbf{z}$, $H(\mathbf{x}^{\nu})$ is the Jacobian matrix of $h(\mathbf{x})$ at $\mathbf{x}^{\nu}$, and it is denoted as H for simplicity in the following paragraphs:

$$H = \frac{\partial h(\mathbf{x})}{\partial \mathbf{x}} = Y + \begin{Bmatrix} \vdots \\ \mathbf{x}^T F^i + \mathbf{x}^T \left(F^i\right)^T \\ \vdots \end{Bmatrix} \tag{6.2.7}$$

Now the objective function is in a linear form:

$$Minimize \quad J = \left(H\mathbf{x} - \mathbf{z}'\right)^T W \left(H\mathbf{x} - \mathbf{z}'\right) \tag{6.2.8}$$

where the optimal solution is obtained when $dJ/d\mathbf{x} = 0$. Therefore, the solution is achieved by the iterative equation:

$$\mathbf{x}^{\nu+1} = (H^T W H)^{-1} H^T W \mathbf{z}' = \mathbf{x}^{\nu} - (H^T W H)^{-1} H^T W (\mathbf{h}\left(\mathbf{x}^{\nu}\right) - \mathbf{z}) \tag{6.2.9}$$

Notice that the algorithm performs state estimation using two consecutive measurements (time t and t_m). In addition, the past history terms $\mathbf{x}(t\text{-}h)$ and $\mathbf{i}(t\text{-}h)$ are updated by $\mathbf{x}(t)$ and $\mathbf{i}(t)$ at each time step, i.e., these past history terms constantly correct state estimation results at each time step.

After the solution is obtained, a parameterized chi-square test is performed immediately. The chi-square test is a mathematical method to check if the errors between measurements and estimated measurements are in an acceptable region, i.e., the consistency between the measurements and the network model. The procedure is as follows. First, the chi-square value is obtained by computing the objective function with parameter *k*:

$$\xi = \sum_i \left(\frac{h_i(\mathbf{x}) - z_i}{k\delta_i} \right)^2 \tag{6.2.10}$$

Next, the confidence level is obtained:

$$\mathrm{P} = 1 - \Pr(\xi, n) \tag{6.2.11}$$

where ξ is the chi-square, n is the degree of freedom (the difference between the number of measurements and states), parameter k denotes that we set the standard deviation of each measurement equal to the accuracy of the measurement error times k, Pr() is the probability function, P is the confidence level evaluating the consistency between the measurements and the system model. Setting k equals to one means that we set the standard deviation of each measurement the same as the actual measurement error from IEDs. A high confidence level (e.g., 100%) indicates the measurements matching the system model. Thus, the estimated states and measurements are trustworthy, and the monitored system model is validated. A low confidence level (e.g., 0%) implies the occurrence of some bad data, hidden failures, or incorrect device models in the system.

6.3 Constrained Weighted Least Square Method

Since the virtual measurements are those exactly obey the physical rules of the monitored system, they can be considered as constraints instead of measurements with small errors in state estimation [71]. Therefore, in the constrained weighted least square method, after substituting the control vector **u** in $h(\mathbf{x},\mathbf{u})$ with actual values from DMS, we first separate the network-level measurement model into non-virtual measurement part and virtual measurement part as shown in (6.3.1) and (6.3.2):

$$\begin{aligned}\mathbf{z}(t) &= h_1(\mathbf{x}) + \boldsymbol{\eta} \\ &= Y_1\mathbf{x} + \begin{Bmatrix} \vdots \\ \mathbf{x}^T F_1^i \mathbf{x} \\ \vdots \end{Bmatrix} - B_1 = Y_1\mathbf{x} + \begin{Bmatrix} \vdots \\ \mathbf{x}^T F_1^i \mathbf{x} \\ \vdots \end{Bmatrix} + N_1\mathbf{x}(t-h) + M_1\mathbf{i}(t-h) + K_1\end{aligned} \tag{6.3.1}$$

$$\begin{aligned}0 &= g(\mathbf{x}) \\ &= Y_2\mathbf{x} + \begin{Bmatrix} \vdots \\ \mathbf{x}^T F_2^i \mathbf{x} \\ \vdots \end{Bmatrix} - B_2 = Y_2\mathbf{x} + \begin{Bmatrix} \vdots \\ \mathbf{x}^T F_2^i \mathbf{x} \\ \vdots \end{Bmatrix} + N_2\mathbf{x}(t-h) + M_2\mathbf{i}(t-h) + K_2\end{aligned} \tag{6.3.2}$$

where subscript 1 denotes non-virtual measurements, and subscript 2 denotes virtual measurements.

The objective of the constrained weighted least square method is to minimize the sum of the weighted squares of the difference between non-virtual measurements and their estimated measurements at each time step under the constraints of those virtual measurements, i.e.,

$$\begin{aligned} &\textit{Minimize} \quad J = \left(h_1(\mathbf{x}) - \mathbf{z}\right)^T W \left(h_1(\mathbf{x}) - \mathbf{z}\right) \\ &\textit{s.t.} \qquad\quad 0 = g(\mathbf{x}) \end{aligned} \tag{6.3.3}$$

To solve this optimization problem, a Lagrangian function is constructed by introducing a Lagrangian multiplier vector $\boldsymbol{\lambda}$ with a scalar two, which is:

$$L\left(\mathbf{x},\boldsymbol{\lambda}\right)=J+2\boldsymbol{\lambda}^{T}g\left(\mathbf{x}\right) \tag{6.3.4}$$

If the measurement model is linear (i.e., F matrices in $h_1(\mathbf{x})$ and $g(\mathbf{x})$ are zero), the solution is obtained directly via the necessary condition of this Lagrangian function as shown in (6.3.5) and (6.3.6):

$$0=\frac{\partial L\left(\mathbf{x},\boldsymbol{\lambda}\right)}{\partial\mathbf{x}}=2H^{T}W\left(H\mathbf{x}-B_{1}-\mathbf{z}\right)+2G^{T}\boldsymbol{\lambda} \tag{6.3.5}$$

$$0=\frac{\partial L\left(\mathbf{x},\boldsymbol{\lambda}\right)}{\partial\boldsymbol{\lambda}}=2G\mathbf{x}-2B_{2} \tag{6.3.6}$$

where H is the Jacobian matrix of $h_1(\mathbf{x})$, and G is the Jacobian matrix of $g(\mathbf{x})$. In this linear case, $H = Y_1$, $G = Y_2$. Since the measurement model is linear, the solution is directly solved as:

$$\begin{bmatrix}\mathbf{x}\\ \boldsymbol{\lambda}\end{bmatrix}=\begin{bmatrix}H^{T}WH & G^{T}\\ G & 0\end{bmatrix}^{-1}\begin{bmatrix}H^{T}W\left(\mathbf{z}-N_{1}\mathbf{x}\left(t-h\right)-M_{1}\mathbf{i}\left(t-h\right)-K_{1}\right)\\ -N_{2}\mathbf{x}\left(t-h\right)-M_{2}\mathbf{i}\left(t-h\right)-K_{2}\end{bmatrix} \tag{6.3.7}$$

If the measurement model is nonlinear, linearization is applied to non-virtual measurement model and virtual measurement model separately with an initial guess $\mathbf{x}^{\nu}$ and $\boldsymbol{\lambda}^{\nu}$, i.e.,

$$\begin{aligned}h_{1}\left(\mathbf{x}^{\nu}+\Delta\mathbf{x}\right)&=h_{1}\left(\mathbf{x}^{\nu}\right)+H\left(\Delta\mathbf{x}\right)\\ g\left(\mathbf{x}^{\nu}+\Delta\mathbf{x}\right)&=g\left(\mathbf{x}^{\nu}\right)+G\left(\Delta\mathbf{x}\right)\end{aligned} \tag{6.3.8}$$

And the update is given by:

$$\begin{aligned}\mathbf{x}^{\nu+1} &= \mathbf{x}^{\nu} + \Delta\mathbf{x} \\ \boldsymbol{\lambda}^{\nu+1} &= \boldsymbol{\lambda}^{\nu} + \Delta\boldsymbol{\lambda}\end{aligned} \tag{6.3.9}$$

Now the Lagrangian function becomes (6.3.10), and the solution is obtained via the necessary condition of this Lagrangian function as shown in (6.3.11):

$$\begin{aligned}L(\mathbf{x},\boldsymbol{\lambda}) = &\left(h_1\left(\mathbf{x}^{\nu}\right) + H\Delta\mathbf{x} - \mathbf{z}\right)^T W\left(h_1\left(\mathbf{x}^{\nu}\right) + H\Delta\mathbf{x} - \mathbf{z}\right) \\ &+2\left(\boldsymbol{\lambda}^{\nu} + \Delta\boldsymbol{\lambda}\right)^T\left(g\left(\mathbf{x}^{\nu}\right) + G\Delta\mathbf{x}\right)\end{aligned} \tag{6.3.10}$$

$$\begin{aligned}0 &= \frac{\partial L(\mathbf{x},\boldsymbol{\lambda})}{\partial\mathbf{x}} = 2H^T WH\Delta\mathbf{x} + 2H^T W\left(h_1\left(\mathbf{x}^{\nu}\right) - \mathbf{z}\right) + 2G^T\left(\boldsymbol{\lambda}^{\nu} + \Delta\boldsymbol{\lambda}\right) \\ 0 &= \frac{\partial L(\mathbf{x},\boldsymbol{\lambda})}{\partial\boldsymbol{\lambda}} = 2G\Delta\mathbf{x} + 2g\left(\mathbf{x}^{\nu}\right)\end{aligned} \tag{6.3.11}$$

Therefore, the solution is obtained by the iterative equation:

$$\begin{bmatrix}\Delta\mathbf{x} \\ \Delta\boldsymbol{\lambda}\end{bmatrix} = -\begin{bmatrix}H^T WH & G^T \\ G & 0\end{bmatrix}^{-1}\begin{bmatrix}H^T W\left(h_1\left(\mathbf{x}^{\nu}\right) - \mathbf{z}\right) + G^T\boldsymbol{\lambda}^{\nu} \\ g\left(\mathbf{x}^{\nu}\right)\end{bmatrix} \tag{6.3.12}$$

or

$$\begin{bmatrix}\mathbf{x}^{\nu+1} \\ \boldsymbol{\lambda}^{\nu+1}\end{bmatrix} = \begin{bmatrix}\mathbf{x}^{\nu} \\ \boldsymbol{\lambda}^{\nu}\end{bmatrix} - \begin{bmatrix}H^T WH & G^T \\ G & 0\end{bmatrix}^{-1}\begin{bmatrix}H^T W\left(h_1\left(\mathbf{x}^{\nu}\right) - \mathbf{z}\right) + G^T\boldsymbol{\lambda}^{\nu} \\ g\left(\mathbf{x}^{\nu}\right)\end{bmatrix} \tag{6.3.13}$$

Notice that the algorithm performs state estimation using two consecutive measurements (time t and t_m). In addition, the past history terms $\mathbf{x}(t\text{-}h)$ and $\mathbf{i}(t\text{-}h)$ are

updated by $\mathbf{x}(t)$ and $\mathbf{i}(t)$ at each time step, i.e., these past history terms constantly correct state estimation results at each time step.

As described in Section 6.2, after the solution is obtained, the parameterized chi-square test is performed immediately. The chi-square test is a mathematical method to check if the errors between measurements and estimated measurements are in an acceptable region, i.e., the consistency between the measurements and the network model. The procedure is as follows. First, the chi-square value is obtained by computing the objective value as shown in (6.3.14) with parameter *k*. Notice that only the measurement errors of non-virtual measurements are taken into account in chi-square computation, since the virtual measurements are now considered as constraints without any measurement errors.

$$\xi = \sum_i \left(\frac{h_{1,i}(\mathbf{x}) - z_i}{k\delta_i} \right)^2 \tag{6.3.14}$$

Next, the confidence level is obtained:

$$\mathrm{P} = 1 - \Pr(\xi, n) \tag{6.3.15}$$

where ξ is the chi-square, *n* is the degree of freedom (the difference between the number of measurements and states), parameter *k* denotes that we set the standard deviation of each measurement equal to the accuracy of the measurement error times *k*, Pr() is the probability function, P is the confidence level evaluating the consistency between the measurements and the system model. Setting *k* equals to one means that we set the standard deviation of each measurement the same as the actual measurement error from IEDs. A high confidence level (e.g., 100%) indicates the measurements matching the system model. Thus, the

estimated states and measurements are trustworthy, and the monitored system model is validated. A low confidence level (e.g., 0%) implies the occurrence of some bad data, hidden failures, or incorrect device models in the system.

6.4 Bad Data Detection and Identification

The existence of bad data can be detected by the chi-square test, i.e., if the network-level measurement model is free of bad data, the computed confidence level will be high. On the contrary, we will obtain a low confidence level if some bad data exist. However, the chi-square test is not able to identify the bad data, and the identification process is achieved by the chi-square test with some other techniques.

The bad data identification is divided into two steps. The first step is to check whether the measurements are in reasonable regions. This process is highly dependent on the monitored system. If some measurements are highly inconsistent with the rest of the measurements and their values are abnormal in the system (e.g., a negative voltage measurement or a measurement that is several times higher than its expected value), these measurements are listed as suspected measurements (suspected of being bad).

The second step is to check the residuals between measurements and estimated measurements from the state estimation. In weighted least square method, those measurements with relatively large residuals are suspected bad data. However, it is also possible that a measurement with a large residual may not be a bad measurement and a bad measurement may have a small residual. Therefore, a rather secure but computational demanding way to identify a bad measurement is hypothesis testing [72], which is feasible by the fact that the redundancy is available in DS-DQDSE with the introduction of derived,

virtual, and pseudo measurements. The hypothesis test is defined as “measurement *i* (or a set of measurements) is a bad datum”, where measurement *i* is a suspected bad data obtained from the aforementioned two steps. For each hypothesis test, the suspected measurement model equation with its measurement value is removed from the network-level measurement model, and the QDSE is rerun using the remaining measurements. A drastic improvement in the confidence level indicates that the data under consideration is bad.

6.5 Summary

This chapter introduces the algorithm of QDSE given the formulated network-level measurement model. Two state estimation algorithms are described here, i.e., (1) unconstrained weighted least square method, and (2) constrained weighted least square method. The QDSE provides the best estimates of the monitored system and check the consistency between measurements and the system model. If an inconsistency occurs (i.e., a low confidence level is obtained from the state estimation), a bad data detection and identification process is performed. The estimated states and validated model from the state estimator could be used for further applications, such as voltage regulation, distribution system optimal control, etc. [73]–[76]

CHAPTER 7. COMPARISON BETWEEN QUASI-DYNAMIC STATE ESTIMATION AND STATIC STATE ESTIMATION

7.1 Overview

This chapter presents a comparative performance study between QDSE and SSE. The comparison is for the purpose of assessing the differences between QDSE and SSE; the comparison revealed and identified certain advantages of QDSE against SSE. These advantages have been enabled with the better models used in QDSE and the high-sampling-rate of PMUs or other IEDs.

After the great northeast blackout in 1965 [23], state estimation started to be introduced and applied to power systems. The legacy state estimator collects redundant measurement data from power systems, performs state estimation, and gives the best estimates of the monitored transmission system [8], [9]. Many efforts have been done to develop more accurate state estimators. For example, three-phase models enable the researchers to alleviate the bias created from those legacy state estimators that employ positive sequence models [24]. In addition, with the introduction of GPS synchronization technology, PMU and other IEDs are developed. These measurement devices provide GPS-synchronized phasor measurements with higher accuracy [10]. With the help pf these technologies, legacy state estimators are being widely implemented in power systems. However, legacy state estimators employ SSE, which considers all the devices in a power system to be static, i.e., frequency domain models. Therefore, such type of state estimator is not able to reveal more detailed information (i.e., dynamics) in power systems.

The high-sampling rate of PMUs enables the development of QDSE. QDSE employs quasi-dynamic domain models that incorporate slow dynamics (e.g., electromechanical transients of rotating electrical machines, controls of power electronic devices, etc.) while neglecting fast electromagnetic transients. A large amount of research has been carried out in this area. For example, an induction motor model with electromechanical transients is considered in QDSE [19], while [21] incorporates dynamics of controls in converters into QDSE. Compared with SSE, the benefits of using QDSE include, but are not limited to: (1) Improving oscillations monitoring, (2) enhancing hierarchical decentralized control, (3) improving dependability and reliability of protection systems, and (4) enhancing reliability of the system models utilized for dynamic security assessment, etc. [77]

Recently, IEEE task force on power system dynamic state and parameter estimation recommends performing some comprehensive studies of the performance on different state estimators. As QDSE is drawing an increasing attention, this chapter carries out a comparative study of the different performance between QDSE and SSE on a generator model. In this study, generators are modeled with governor, turbine, and exciter models, which capture the slow dynamics. The QDSE adopts the full model of the generator incorporating the slow dynamics from the electromechanical transients in the rotor, control of the turbine, etc. SSE utilizes frequency domain models without dynamics, so it employs a simplified generator model. State estimation is applied to these two different modeling approaches, and an illustrative example is used to present the performance difference between these two state estimation methods. The results indicate that QDSE is capable of providing more accurate information of the monitored system compared with SSE. Table

7.1.1 summarizes the models and measurements used in this comparison study. The rest of this chapter is organized as follows. Section 7.2 describes the detailed quasi-dynamic domain and frequency domain modeling approaches for a generator set. Section 7.3 uses an example to demonstrate the comparison study, and Section 7.4 summarizes the results.

Table 7.1.1: Generator Set Model and Measurements Used in QDSE and SSE

State Estimation Method	Generator Model	Measurements
QDSE	Quasi-dynamic domain model	Three-phase voltage and currents at the terminal of the generator
		Rotating speed ω_m of the generator
SSE	Frequency domain model	Three-phase voltage and currents at the terminal of the generator

7.2 Modeling of a Generator

As mentioned in Table 7.1.1, QDSE employs quasi-dynamic domain models and SSE employs frequency domain models. This section introduces these two different device modeling approaches for a generator set. To be more specific, QDSE adopts the full model of a generator set including a generator, and peripherals including a governor, a turbine, and an exciter. For SSE, since it ignores all the dynamics by assuming the outputs from the peripherals are constant, the models of these peripherals are omitted. Thus, only the frequency domain model of the generator is considered.

7.2.1 Quasi-Dynamic Domain Model of a Generator

The quasi-dynamic domain model of a generator set is described in Appendix A in detail. It considers the dynamics in the rotor, turbine, governor, and exciter. The compact device model of the quasi-dynamic domain model of a generator set is listed from (A.1.1) to (A.1.16). After quadratization and separating those quadratized equations into real and imaginary parts, the standard SCQDM of a generator set could be obtained (described in Appendix A.2). The SCQDM of a generator set consists of 30 states and 30 equations at time *t*. Then, the SCAQCF of the generator set model (described in Appendix A.3) could be automatically obtained by the quadratic integration method.

7.2.2 Frequency Domain Model of a Generator

SSE employs the frequency domain model of a generator set, which is built with assumptions: (1) The mechanical power output from the governor and turbine is constant; (2) the terminal voltage is always the desired voltage without any control delay. Therefore, the dynamics in governor, turbine, and exciter are neglected. The generator, governor, turbine, and exciter model equations are simplified as (7.2.1) to (7.2.3).

$$\begin{bmatrix} \tilde{I}_a \\ \tilde{I}_b \\ \tilde{I}_c \end{bmatrix} = \begin{bmatrix} Y_{aa} & Y_{ab} & Y_{ac} \\ Y_{ba} & Y_{bb} & Y_{bc} \\ Y_{ca} & Y_{cb} & Y_{cc} \end{bmatrix} \begin{bmatrix} \tilde{V}_a - \tilde{V}_n - \tilde{E}_a \\ \tilde{V}_b - \tilde{V}_n - \tilde{E}_b \\ \tilde{V}_c - \tilde{V}_n - \tilde{E}_c \end{bmatrix} = y_{abc} \begin{bmatrix} \tilde{V}_a - \tilde{V}_n - \tilde{E}_a \\ \tilde{V}_b - \tilde{V}_n - \tilde{E}_b \\ \tilde{V}_c - \tilde{V}_n - \tilde{E}_c \end{bmatrix}$$
$$\tilde{I}_n = \begin{bmatrix} -1 & -1 & -1 \end{bmatrix} \begin{bmatrix} Y_{aa} & Y_{ab} & Y_{ac} \\ Y_{ba} & Y_{bb} & Y_{bc} \\ Y_{ca} & Y_{cb} & Y_{cc} \end{bmatrix} \begin{bmatrix} \tilde{V}_a - \tilde{V}_n - \tilde{E}_a \\ \tilde{V}_b - \tilde{V}_n - \tilde{E}_b \\ \tilde{V}_c - \tilde{V}_n - \tilde{E}_c \end{bmatrix} = \begin{bmatrix} -1 & -1 & -1 \end{bmatrix} y_{abc} \begin{bmatrix} \tilde{V}_a - \tilde{V}_n - \tilde{E}_a \\ \tilde{V}_b - \tilde{V}_n - \tilde{E}_b \\ \tilde{V}_c - \tilde{V}_n - \tilde{E}_c \end{bmatrix} \quad (7.2.1)$$

$$0 = \mathrm{Re}\left(\tilde{E}_a \tilde{I}_a^* + \tilde{E}_b \tilde{I}_b^* + \tilde{E}_c \tilde{I}_c^* \right) + P_m \quad (7.2.2)$$

$$0 = \left| \tilde{V}_a - \tilde{V}_b \right| - V_{pu} V_{rated} \quad (7.2.3)$$

where $\tilde{E}_a = Ee^{j\delta}$, $\tilde{E}_b = \tilde{E}_a e^{j-120^\circ}$, $\tilde{E}_c = \tilde{E}_a e^{j120^\circ}$; $\tilde{V}_a$, $\tilde{V}_b$, $\tilde{V}_c$, $\tilde{V}_n$ are the terminal phase voltages of the generator, $Ee^{j\delta}$ is the internal voltage of the generator, $\tilde{I}_a$, $\tilde{I}_b$, $\tilde{I}_c$, $\tilde{I}_n$ are the terminal phase currents flowing into the generator, y_{abc} is the admittance matrix, P_m is the constant power output from the turbine, and $V_{pu}V_{rated}$ is the constant voltage controlled by the exciter. For this model, the through variables are: $\tilde{I}_a$, $\tilde{I}_b$, $\tilde{I}_c$, and $\tilde{I}_n$. The states are: $\tilde{V}_a$, $\tilde{V}_b$, $\tilde{V}_c$, $\tilde{V}_n$, $Ee^{j\delta}$.

After splitting equations into real and imaginary parts, the frequency domain model of the generator is expressed as equations from (7.2.4) to (7.2.13), and it can be directly expressed in a general form as shown in (7.2.14), which has 10 states and 10 equations.

$$I_{ar} = Y_{aar}V_{ar} - Y_{aai}V_{ai} + Y_{abr}V_{br} - Y_{abi}V_{bi} + Y_{acr}V_{cr} - Y_{aci}V_{ci} - \left(Y_{aar} + Y_{abr} + Y_{acr}\right)V_{nr} + \left(Y_{aai} + Y_{abi} + Y_{aci}\right)V_{ni} - \left(Y_{aar} - \frac{1}{2}Y_{abr} + \frac{\sqrt{3}}{2}Y_{abi} - \frac{1}{2}Y_{acr} - \frac{\sqrt{3}}{2}Y_{aci}\right)\cdot E_r - \left(-Y_{aai} + \frac{\sqrt{3}}{2}Y_{abr} + \frac{1}{2}Y_{abi} - \frac{\sqrt{3}}{2}Y_{acr} + \frac{1}{2}Y_{aci}\right)\cdot E_i \quad (7.2.4)$$

$$I_{ai} = Y_{aai}V_{ar} + Y_{aar}V_{ai} + Y_{abi}V_{br} + Y_{abr}V_{bi} + Y_{aci}V_{cr} + Y_{acr}V_{ci} - \left(Y_{aai} + Y_{abi} + Y_{aci}\right)V_{nr} - \left(Y_{aar} + Y_{abr} + Y_{acr}\right)V_{ni} - \left(Y_{aai} - \frac{\sqrt{3}}{2}Y_{abr} - \frac{1}{2}Y_{abi} + \frac{\sqrt{3}}{2}Y_{acr} - \frac{1}{2}Y_{aci}\right)\cdot E_r - \left(Y_{aar} - \frac{1}{2}Y_{abr} + \frac{\sqrt{3}}{2}Y_{abi} - \frac{1}{2}Y_{acr} - \frac{\sqrt{3}}{2}Y_{aci}\right)\cdot E_i \quad (7.2.5)$$

$$I_{br} = Y_{bar}V_{ar} - Y_{bai}V_{ai} + Y_{bbr}V_{br} - Y_{bbi}V_{bi} + Y_{bcr}V_{cr} - Y_{bci}V_{ci} - \left(Y_{bar} + Y_{bbr} + Y_{bcr}\right)V_{nr} + \left(Y_{bai} + Y_{bbi} + Y_{bci}\right)V_{ni} - \left(Y_{bar} - \frac{1}{2}Y_{bbr} + \frac{\sqrt{3}}{2}Y_{bbi} - \frac{1}{2}Y_{bcr} - \frac{\sqrt{3}}{2}Y_{bci}\right)\cdot E_r - \left(-Y_{bai} + \frac{\sqrt{3}}{2}Y_{bbr} + \frac{1}{2}Y_{bbi} - \frac{\sqrt{3}}{2}Y_{bcr} + \frac{1}{2}Y_{bci}\right)\cdot E_i \quad (7.2.6)$$

$$I_{bi} = Y_{bai}V_{ar} + Y_{bar}V_{ai} + Y_{bbi}V_{br} + Y_{bbr}V_{bi} + Y_{bci}V_{cr} + Y_{bcr}V_{ci} - \left(Y_{bai} + Y_{bbi} + Y_{bci}\right)V_{nr} - \left(Y_{bar} + Y_{bbr} + Y_{bcr}\right)V_{ni}$$
$$-\left(Y_{bai} - \frac{\sqrt{3}}{2}Y_{bbr} - \frac{1}{2}Y_{bbi} + \frac{\sqrt{3}}{2}Y_{bcr} - \frac{1}{2}Y_{bci}\right)\cdot E_r - \left(Y_{bar} - \frac{1}{2}Y_{bbr} + \frac{\sqrt{3}}{2}Y_{bbi} - \frac{1}{2}Y_{bcr} - \frac{\sqrt{3}}{2}Y_{bci}\right)\cdot E_i$$

(7.2.7)

$$I_{cr} = Y_{car}V_{ar} - Y_{cai}V_{ai} + Y_{cbr}V_{br} - Y_{cbi}V_{bi} + Y_{ccr}V_{cr} - Y_{cci}V_{ci} - \left(Y_{car} + Y_{cbr} + Y_{ccr}\right)V_{nr} + \left(Y_{cai} + Y_{cbi} + Y_{cci}\right)V_{ni}$$
$$-\left(Y_{car} - \frac{1}{2}Y_{cbr} + \frac{\sqrt{3}}{2}Y_{cbi} - \frac{1}{2}Y_{ccr} - \frac{\sqrt{3}}{2}Y_{cci}\right)\cdot E_r - \left(-Y_{cai} + \frac{\sqrt{3}}{2}Y_{cbr} + \frac{1}{2}Y_{cbi} - \frac{\sqrt{3}}{2}Y_{ccr} + \frac{1}{2}Y_{cci}\right)\cdot E_i$$

(7.2.8)

$$I_{ci} = Y_{cai}V_{ar} + Y_{car}V_{ai} + Y_{cbi}V_{br} + Y_{cbr}V_{bi} + Y_{cci}V_{cr} + Y_{ccr}V_{ci} - \left(Y_{cai} + Y_{cbi} + Y_{cci}\right)V_{nr} - \left(Y_{car} + Y_{cbr} + Y_{ccr}\right)V_{ni}$$
$$-\left(Y_{cai} - \frac{\sqrt{3}}{2}Y_{cbr} - \frac{1}{2}Y_{cbi} + \frac{\sqrt{3}}{2}Y_{ccr} - \frac{1}{2}Y_{cci}\right)\cdot E_r - \left(Y_{car} - \frac{1}{2}Y_{cbr} + \frac{\sqrt{3}}{2}Y_{cbi} - \frac{1}{2}Y_{ccr} - \frac{\sqrt{3}}{2}Y_{cci}\right)\cdot E_i$$

(7.2.9)

$$I_{nr} = -\left(\begin{array}{l} Y_{aar}V_{ar} - Y_{aai}V_{ai} + Y_{abr}V_{br} - Y_{abi}V_{bi} + Y_{acr}V_{cr} - Y_{aci}V_{ci} - \left(Y_{aar} + Y_{abr} + Y_{acr}\right)V_{nr} + \left(Y_{aai} + Y_{abi} + Y_{aci}\right)V_{ni} \\ -\left(Y_{aar} - \frac{1}{2}Y_{abr} + \frac{\sqrt{3}}{2}Y_{abi} - \frac{1}{2}Y_{acr} - \frac{\sqrt{3}}{2}Y_{aci}\right)\cdot E_r - \left(-Y_{aai} + \frac{\sqrt{3}}{2}Y_{abr} + \frac{1}{2}Y_{abi} - \frac{\sqrt{3}}{2}Y_{acr} + \frac{1}{2}Y_{aci}\right)\cdot E_i \end{array}\right)$$
$$-\left(\begin{array}{l} Y_{bar}V_{ar} - Y_{bai}V_{ai} + Y_{bbr}V_{br} - Y_{bbi}V_{bi} + Y_{bcr}V_{cr} - Y_{bci}V_{ci} - \left(Y_{bar} + Y_{bbr} + Y_{bcr}\right)V_{nr} + \left(Y_{bai} + Y_{bbi} + Y_{bci}\right)V_{ni} \\ -\left(Y_{bar} - \frac{1}{2}Y_{bbr} + \frac{\sqrt{3}}{2}Y_{bbi} - \frac{1}{2}Y_{bcr} - \frac{\sqrt{3}}{2}Y_{bci}\right)\cdot E_r - \left(-Y_{bai} + \frac{\sqrt{3}}{2}Y_{bbr} + \frac{1}{2}Y_{bbi} - \frac{\sqrt{3}}{2}Y_{bcr} + \frac{1}{2}Y_{bci}\right)\cdot E_i \end{array}\right)$$
$$-\left(\begin{array}{l} Y_{car}V_{ar} - Y_{cai}V_{ai} + Y_{cbr}V_{br} - Y_{cbi}V_{bi} + Y_{ccr}V_{cr} - Y_{cci}V_{ci} - \left(Y_{car} + Y_{cbr} + Y_{ccr}\right)V_{nr} + \left(Y_{cai} + Y_{cbi} + Y_{cci}\right)V_{ni} \\ -\left(Y_{car} - \frac{1}{2}Y_{cbr} + \frac{\sqrt{3}}{2}Y_{cbi} - \frac{1}{2}Y_{ccr} - \frac{\sqrt{3}}{2}Y_{cci}\right)\cdot E_r - \left(-Y_{cai} + \frac{\sqrt{3}}{2}Y_{cbr} + \frac{1}{2}Y_{cbi} - \frac{\sqrt{3}}{2}Y_{ccr} + \frac{1}{2}Y_{cci}\right)\cdot E_i \end{array}\right)$$

(7.2.10)

$$
\begin{aligned}
I_{ni} = -&\left(\begin{array}{l} Y_{aai}V_{ar} + Y_{aar}V_{ai} + Y_{abi}V_{br} + Y_{abr}V_{bi} + Y_{aci}V_{cr} + Y_{acr}V_{ci} - \left(Y_{aai} + Y_{abi} + Y_{aci}\right)V_{nr} - \left(Y_{aar} + Y_{abr} + Y_{acr}\right)V_{ni} \\ -\left(Y_{aai} - \frac{\sqrt{3}}{2}Y_{abr} - \frac{1}{2}Y_{abi} + \frac{\sqrt{3}}{2}Y_{acr} - \frac{1}{2}Y_{aci}\right)\cdot E_r - \left(Y_{aar} - \frac{1}{2}Y_{abr} + \frac{\sqrt{3}}{2}Y_{abi} - \frac{1}{2}Y_{acr} - \frac{\sqrt{3}}{2}Y_{aci}\right)\cdot E_i \end{array}\right) \\
&-\left(\begin{array}{l} Y_{bai}V_{ar} + Y_{bar}V_{ai} + Y_{bbi}V_{br} + Y_{bbr}V_{bi} + Y_{bci}V_{cr} + Y_{bcr}V_{ci} - \left(Y_{bai} + Y_{bbi} + Y_{bci}\right)V_{nr} - \left(Y_{bar} + Y_{bbr} + Y_{bcr}\right)V_{ni} \\ -\left(Y_{bai} - \frac{\sqrt{3}}{2}Y_{bbr} - \frac{1}{2}Y_{bbi} + \frac{\sqrt{3}}{2}Y_{bcr} - \frac{1}{2}Y_{bci}\right)\cdot E_r - \left(Y_{bar} - \frac{1}{2}Y_{bbr} + \frac{\sqrt{3}}{2}Y_{bbi} - \frac{1}{2}Y_{bcr} - \frac{\sqrt{3}}{2}Y_{bci}\right)\cdot E_i \end{array}\right) \\
&-\left(\begin{array}{l} Y_{cai}V_{ar} + Y_{car}V_{ai} + Y_{cbi}V_{br} + Y_{cbr}V_{bi} + Y_{cci}V_{cr} + Y_{ccr}V_{ci} - \left(Y_{cai} + Y_{cbi} + Y_{cci}\right)V_{nr} - \left(Y_{car} + Y_{cbr} + Y_{ccr}\right)V_{ni} \\ -\left(Y_{cai} - \frac{\sqrt{3}}{2}Y_{cbr} - \frac{1}{2}Y_{cbi} + \frac{\sqrt{3}}{2}Y_{ccr} - \frac{1}{2}Y_{cci}\right)\cdot E_r - \left(Y_{car} - \frac{1}{2}Y_{cbr} + \frac{\sqrt{3}}{2}Y_{cbi} - \frac{1}{2}Y_{ccr} - \frac{\sqrt{3}}{2}Y_{cci}\right)\cdot E_i \end{array}\right)
\end{aligned}
\tag{7.2.11}
$$

$$
\begin{aligned}
0 = {} & E_r \cdot I_{ar} + E_i \cdot I_{ai} - \frac{1}{2}E_r \cdot I_{br} + \frac{\sqrt{3}}{2}E_i \cdot I_{br} - \frac{\sqrt{3}}{2}E_r \cdot I_{bi} - \frac{1}{2}E_i \cdot I_{bi} \\
& - \frac{1}{2}E_r \cdot I_{cr} - \frac{\sqrt{3}}{2}E_i \cdot I_{cr} + \frac{\sqrt{3}}{2}E_r \cdot I_{ci} - \frac{1}{2}E_i \cdot I_{ci} + P_m
\end{aligned}
\tag{7.2.12}
$$

$$
0 = V_{ar}^2 + V_{ai}^2 + V_{br}^2 + V_{bi}^2 - 2V_{ar}V_{br} - 2V_{ai}V_{bi} - V_{pu}^2 V_{rated}^2 \tag{7.2.13}
$$

$$
\begin{bmatrix} \mathbf{i}(t) \\ 0 \end{bmatrix} = Y_x \mathbf{x} + \begin{Bmatrix} \vdots \\ \mathbf{x}^T F_x^i \mathbf{x} \\ \vdots \end{Bmatrix} + C \tag{7.2.14}
$$

where $\mathbf{i}(t) = \begin{bmatrix} I_{ar} & I_{ai} & I_{br} & I_{bi} & I_{cr} & I_{ci} & I_{nr} & I_{ni} \end{bmatrix}^T$,

$\mathbf{x}(t) = \begin{bmatrix} V_{ar} & V_{ai} & V_{br} & V_{bi} & V_{cr} & V_{ci} & V_{nr} & V_{ni} & E_r & E_i \end{bmatrix}^T$,

7.3 Demonstrative Example

This section uses an illustrative example to compare the performance difference between QDSE and SSE. The example system is shown in Figure 7.3.1, and the generator of interest is G1 (encircled by the red dashed line) with 15 kV rated voltage and 150 MVA

rated power. The basic parameters of this generator set are shown in Table 7.3.1. A PMU is available to collect three-phase voltage and current measurements at the terminal of G1. In addition, a mechanical rotating speed measurement is also available to measure the rotating speed of the rotor. A 20-second event is simulated with some load changes at bus B11. The sampling rate is 60 samples per second. The simulation software is WinIGS. This event is stored in a COMTRADE file. The two state estimation approaches use this COMTRADE file and perform state estimation in MATLAB in a laptop (i7-5600U, 12GB RAM). Figure 7.3.2 shows the voltage and current measurements collected from G1. Notice some dynamics exist throughout the whole event because of the load changes. Figure 7.3.3 shows the simulated mechanical power output from the turbine as well as the rotating speed of the rotor. The mechanical power output and the rotating speed of the rotor change constantly in this event.

Table 7.3.1: Basic Parameters of G1 (15 kV, 150 MVA)

Positive Impedance	Negative Impedance	Zero Impedance	Inertia Constant	Number of Poles
0.01+j0.18 pu	0.01+j0.20 pu	0.01+j0.09 pu	2.8s	2

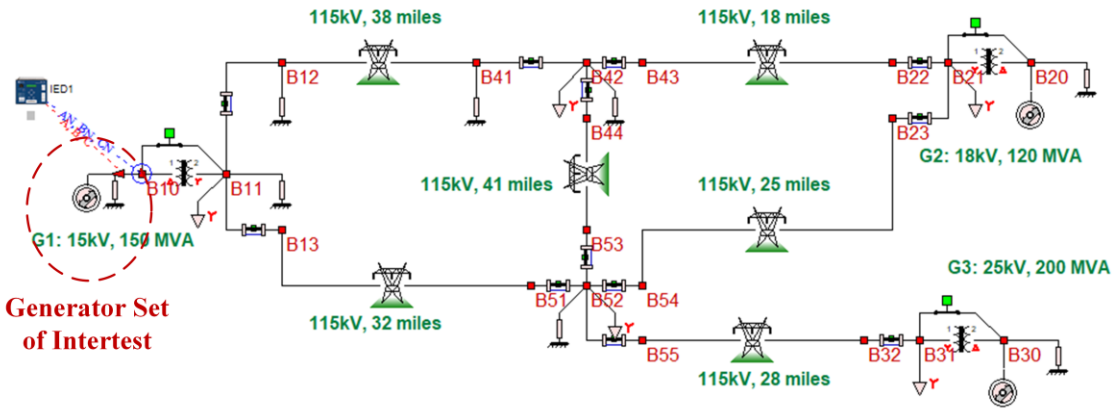

Figure 7.3.1: Single-Line Diagram of the Example System

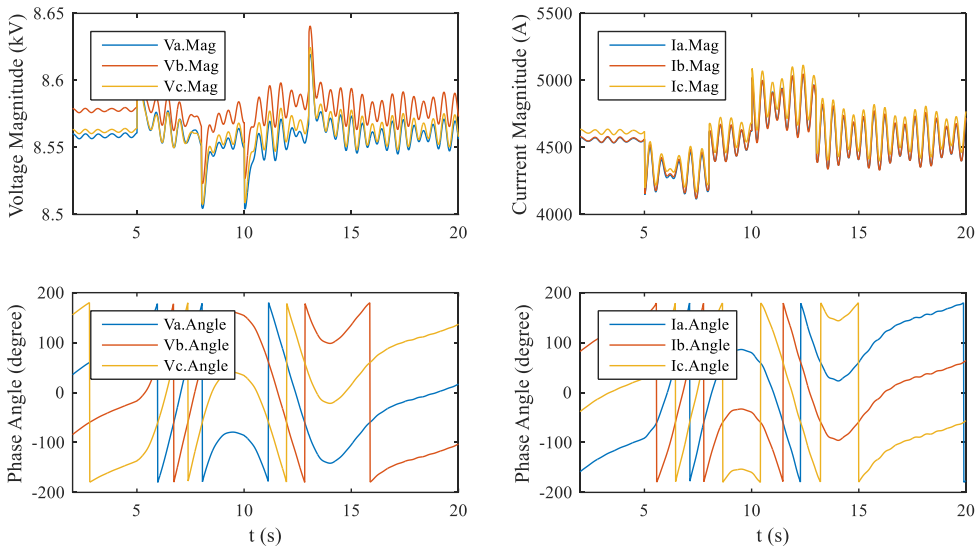

Figure 7.3.2: Voltage and Current Phasor Measurements from G1

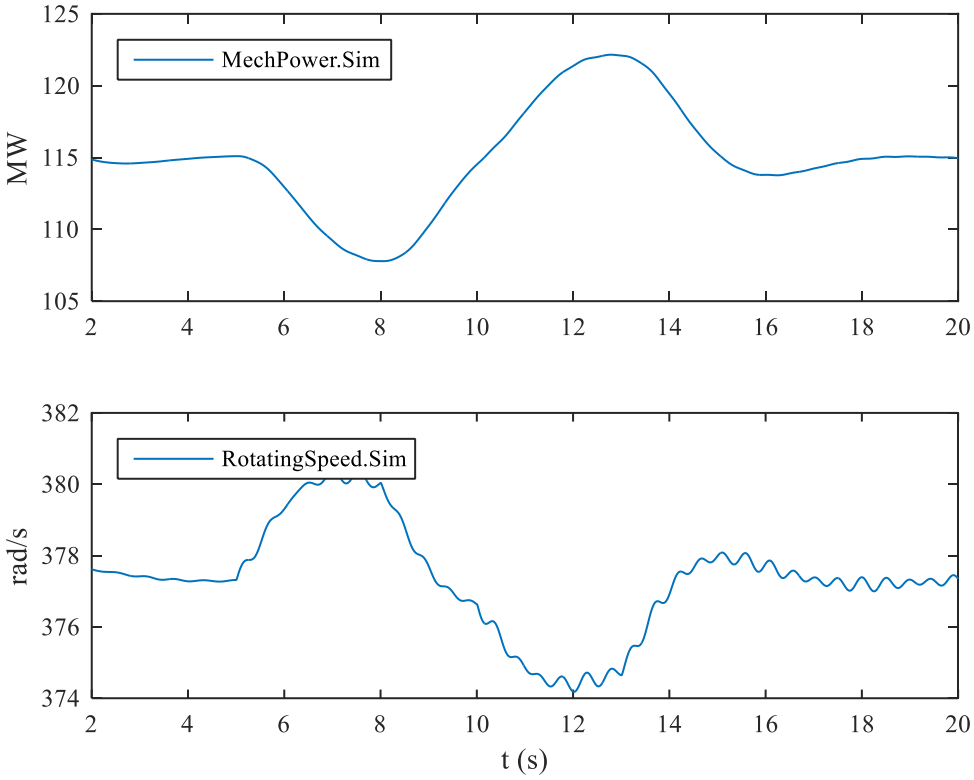

Figure 7.3.3: Mechanical Power from the Turbine and Rotor Rotating Speed from Simulation

7.3.1 Performance of QDSE

QDSE uses three-phase voltage and current measurements, and the rotating speed measurement of the rotor to estimate the states of G1. By splitting a phasor measurement into real and imaginary parts, the total number of actual measurements is 13. The measurement model of the generator is constructed as described in Chapter 5. Specifically, the voltage measurement and the rotating speed measurement model are constructed by a linear combination of the states of the measured generator with the errors from the meter. The current measurement models are constructed by extracting the corresponding

equations of the measured generator model plus the errors from the meter. In addition to these 13 actual measurements, we have 22 virtual measurements and two pseudo measurements. The 22 virtual measurements are those that describe the physical properties of the generator, i.e., internal equations of the generator. These measurements have zero values, and they are assigned with a very small measurement error since they are very accurate (obey the physical rules). Two pseudo measurements are those that assume the voltage at the neutral phase of G1 is close to zero during the normal operation. The entire measurement model for QDSE before quadratic integration is listed from (7.3.1) to (7.3.37).

$$z_{Vanr} = V_{ar} - V_{nr} + \eta_1 \tag{7.3.1}$$

$$z_{Vani} = V_{ai} - V_{ni} + \eta_2 \tag{7.3.2}$$

$$z_{Vbnr} = V_{br} - V_{nr} + \eta_3 \tag{7.3.3}$$

$$z_{Vbni} = V_{bi} - V_{ni} + \eta_4 \tag{7.3.4}$$

$$z_{Vcnr} = V_{cr} - V_{nr} + \eta_5 \tag{7.3.5}$$

$$z_{Vcni} = V_{ci} - V_{ni} + \eta_6 \tag{7.3.6}$$

$$\begin{aligned} z_{Iar} = {} & Y_{aar}V_{ar} - Y_{aai}V_{ai} + Y_{abr}V_{br} - Y_{abi}V_{bi} + Y_{acr}V_{cr} - Y_{aci}V_{ci} - \left(Y_{aar} + Y_{abr} + Y_{acr}\right)V_{nr} \\ & + \left(Y_{aai} + Y_{abi} + Y_{aci}\right)V_{ni} + \left(Y_{aar} - \frac{1}{2}Y_{abr} + \frac{\sqrt{3}}{2}Y_{abi} - \frac{1}{2}Y_{acr} - \frac{\sqrt{3}}{2}Y_{aci} \right) \cdot z_1 \\ & + \left(-Y_{aai} + \frac{\sqrt{3}}{2}Y_{abr} + \frac{1}{2}Y_{abi} - \frac{\sqrt{3}}{2}Y_{acr} + \frac{1}{2}Y_{aci} \right) \cdot z_2 + \eta_7 \end{aligned} \tag{7.3.7}$$

$$z_{Iai} = Y_{aai}V_{ar} + Y_{aar}V_{ai} + Y_{abi}V_{br} + Y_{abr}V_{bi} + Y_{aci}V_{cr} + Y_{acr}V_{ci} - \left(Y_{aai} + Y_{abi} + Y_{aci}\right)V_{nr}$$
$$-\left(Y_{aar} + Y_{abr} + Y_{acr}\right)V_{ni} + \left(Y_{aai} - \frac{\sqrt{3}}{2}Y_{abr} - \frac{1}{2}Y_{abi} + \frac{\sqrt{3}}{2}Y_{acr} - \frac{1}{2}Y_{aci}\right)\cdot z_1 \qquad (7.3.8)$$
$$+\left(Y_{aar} - \frac{1}{2}Y_{abr} + \frac{\sqrt{3}}{2}Y_{abi} - \frac{1}{2}Y_{acr} - \frac{\sqrt{3}}{2}Y_{aci}\right)\cdot z_2 + \eta_8$$

$$z_{Ibr} = Y_{bar}V_{ar} - Y_{bai}V_{ai} + Y_{bbr}V_{br} - Y_{bbi}V_{bi} + Y_{bcr}V_{cr} - Y_{bci}V_{ci} - \left(Y_{bar} + Y_{bbr} + Y_{bcr}\right)V_{nr}$$
$$+\left(Y_{bai} + Y_{bbi} + Y_{bci}\right)V_{ni} + \left(Y_{bar} - \frac{1}{2}Y_{bbr} + \frac{\sqrt{3}}{2}Y_{bbi} - \frac{1}{2}Y_{bcr} - \frac{\sqrt{3}}{2}Y_{bci}\right)\cdot z_1 \qquad (7.3.9)$$
$$+\left(-Y_{bai} + \frac{\sqrt{3}}{2}Y_{bbr} + \frac{1}{2}Y_{bbi} - \frac{\sqrt{3}}{2}Y_{bcr} + \frac{1}{2}Y_{bci}\right)\cdot z_2 + \eta_9$$

$$z_{Ibi} = Y_{bai}V_{ar} + Y_{bar}V_{ai} + Y_{bbi}V_{br} + Y_{bbr}V_{bi} + Y_{bci}V_{cr} + Y_{bcr}V_{ci} - \left(Y_{bai} + Y_{bbi} + Y_{bci}\right)V_{nr}$$
$$-\left(Y_{bar} + Y_{bbr} + Y_{bcr}\right)V_{ni} + \left(Y_{bai} - \frac{\sqrt{3}}{2}Y_{bbr} - \frac{1}{2}Y_{bbi} + \frac{\sqrt{3}}{2}Y_{bcr} - \frac{1}{2}Y_{bci}\right)\cdot z_1 \qquad (7.3.10)$$
$$+\left(Y_{bar} - \frac{1}{2}Y_{bbr} + \frac{\sqrt{3}}{2}Y_{bbi} - \frac{1}{2}Y_{bcr} - \frac{\sqrt{3}}{2}Y_{bci}\right)\cdot z_2 + \eta_{10}$$

$$z_{Icr} = Y_{car}V_{ar} - Y_{cai}V_{ai} + Y_{cbr}V_{br} - Y_{cbi}V_{bi} + Y_{ccr}V_{cr} - Y_{cci}V_{ci} - \left(Y_{car} + Y_{cbr} + Y_{ccr}\right)V_{nr}$$
$$+\left(Y_{cai} + Y_{cbi} + Y_{cci}\right)V_{ni} + \left(Y_{car} - \frac{1}{2}Y_{cbr} + \frac{\sqrt{3}}{2}Y_{cbi} - \frac{1}{2}Y_{ccr} - \frac{\sqrt{3}}{2}Y_{cci}\right)\cdot z_1 \qquad (7.3.11)$$
$$+\left(-Y_{cai} + \frac{\sqrt{3}}{2}Y_{cbr} + \frac{1}{2}Y_{cbi} - \frac{\sqrt{3}}{2}Y_{ccr} + \frac{1}{2}Y_{cci}\right)\cdot z_2 + \eta_{11}$$

$$z_{Ici} = Y_{cai}V_{ar} + Y_{car}V_{ai} + Y_{cbi}V_{br} + Y_{cbr}V_{bi} + Y_{cci}V_{cr} + Y_{ccr}V_{ci} - \left(Y_{cai} + Y_{cbi} + Y_{cci}\right)V_{nr}$$
$$-\left(Y_{car} + Y_{cbr} + Y_{ccr}\right)V_{ni} + \left(Y_{cai} - \frac{\sqrt{3}}{2}Y_{cbr} - \frac{1}{2}Y_{cbi} + \frac{\sqrt{3}}{2}Y_{ccr} - \frac{1}{2}Y_{cci}\right)\cdot z_1 \qquad (7.3.12)$$
$$+\left(Y_{car} - \frac{1}{2}Y_{cbr} + \frac{\sqrt{3}}{2}Y_{cbi} - \frac{1}{2}Y_{ccr} - \frac{\sqrt{3}}{2}Y_{cci}\right)\cdot z_2 + \eta_{12}$$

$$z_\omega = \omega_m + \eta_{13} \qquad (7.3.13)$$

$$0 = \frac{dc}{dt} + y_1 + \eta_{14} \qquad (7.3.14)$$

$$0 = \frac{ds}{dt} + y_2 + \eta_{15} \tag{7.3.15}$$

$$0 = \frac{d\omega}{dt} + x_1 + \eta_{16} \tag{7.3.16}$$

$$0 = T_G \frac{d\Delta P_T}{dt} + \Delta P_T + \frac{1}{2\pi R}\omega_m(t) - \Delta P_C - \frac{1}{2\pi R}\omega_{set}(t) + \eta_{17} \tag{7.3.17}$$

$$0 = \frac{d\Delta P_C}{dt} + \frac{k}{2\pi}\omega_m(t) - \frac{k}{2\pi}\omega_{set}(t) + \eta_{18} \tag{7.3.18}$$

$$0 = -T_t \frac{dP_{m,T}}{dt} - P_{m,T} - \Delta P_T + \eta_{19} \tag{7.3.19}$$

$$0 = T_A \frac{dV_R}{dt} + V_R + K_A V_t + K_A V_F - K_A V_{ref} + \eta_{20} \tag{7.3.20}$$

$$0 = T_E \frac{dV_{DC}}{dt} + K_E \cdot V_{DC} - V_R + \eta_{21} \tag{7.3.21}$$

$$0 = K_F \frac{dV_{DC}}{dt} - T_F \frac{dV_F}{dt} - V_F + \eta_{22} \tag{7.3.22}$$

$$0 = -V_{fd} + L_f \frac{di_{fd,G}}{dt} + R_f \cdot i_{fd,G} + \eta_{23} \tag{7.3.23}$$

$$\begin{aligned} 0 = {} & \frac{2 \cdot H \cdot S}{\omega_{m0}^2} \cdot \omega_m \cdot \frac{2}{p} \cdot x_1 - z_1 \cdot I_{ar} - z_2 \cdot I_{ai} + \frac{1}{2} z_1 \cdot I_{br} - \frac{\sqrt{3}}{2} z_2 \cdot I_{br} + \frac{\sqrt{3}}{2} z_1 \cdot I_{bi} + \frac{1}{2} z_2 \cdot I_{bi} \\ & + \frac{1}{2} z_1 \cdot I_{cr} + \frac{\sqrt{3}}{2} z_2 \cdot I_{cr} - \frac{\sqrt{3}}{2} z_1 \cdot I_{ci} + \frac{1}{2} z_2 \cdot I_{ci} + P_{m,G} + \eta_{24} \end{aligned} \tag{7.3.24}$$

$$0 = \frac{p}{2}\omega_m - \omega + \eta_{25} \tag{7.3.25}$$

$$0 = \omega_0 \cdot s + y_1 - \omega \cdot s + \eta_{26} \tag{7.3.26}$$

$$0 = -\omega_0 \cdot c + y_2 + \omega \cdot c + \eta_{27} \tag{7.3.27}$$

$$0 = V_t^2 - V_{ar}^2 - V_{ai}^2 + \eta_{28} \tag{7.3.28}$$

$$0 = z_1 + E \cdot c + \eta_{29} \tag{7.3.29}$$

$$0 = z_2 + E \cdot s + \eta_{30} \tag{7.3.30}$$

$$0 = E - \omega \cdot z_3 + \eta_{31} \tag{7.3.31}$$

$$0 = i_{fd,G} - \frac{\sqrt{2}}{M_f} \cdot z_3 + \eta_{32} \tag{7.3.32}$$

$$0 = \frac{1}{R_{DC}} V_{fd} - \frac{1}{R_{DC}} V_{DC} - i_{fd,E} + \eta_{33} \tag{7.3.33}$$

$$0 = P_{m,T} + P_{m,G} + \eta_{34} \tag{7.3.34}$$

$$0 = i_{fd,G} + i_{fd,E} + \eta_{35} \tag{7.3.35}$$

$$0 = V_{nr} + \eta_{36} \tag{7.3.36}$$

$$0 = V_{ni} + \eta_{37} \tag{7.3.37}$$

By combining all these measurements together, we have 37 measurements for G1 in total. In addition, a standard deviation is assigned to each measurement to represent its measurement error. The standard deviations of those actual measurements from meters are the meter errors, and we assign a typical value (i.e., 0.01 pu) to those actual measurements. Since virtual measurements are obtained from those equations obeying physical rules, their errors are much smaller than actual measurements. Therefore, their standard deviations are set to be a relatively small value, and in this case, we assign 0.001 pu to all the virtual measurements. As pseudo measurements are approximately known without actually measured, their standard deviations are set to be a relatively large value, and we assign 0.1 pu to all the pseudo measurements in this case.

In summary, we have 37 measurements for G1. As G1 has 30 states (described in Appendix A.2), the redundancy is 37/30 = 123%. The execution time for this case is 2.91

s. The average execution time for one state estimation is 2.43 ms, which is much less than the time interval between two samples, i.e., 16.67 ms. Figure 7.3.4 shows the actual and estimated voltage and current magnitude measurements from QDSE. The results show that the estimated measurements track the actual measurements very accurately. Figure 7.3.5 depicts the simulated and estimated mechanical power output from the turbine, and the confidence level of QDSE when parameter *k* equals to one. From the figure, we can observe that the estimated mechanical power tracks the simulated values precisely. In addition, during the whole event, the confidence level, the indicator of the performance of this state estimation, is always 100%. Therefore, the estimated states from this case are trustworthy.

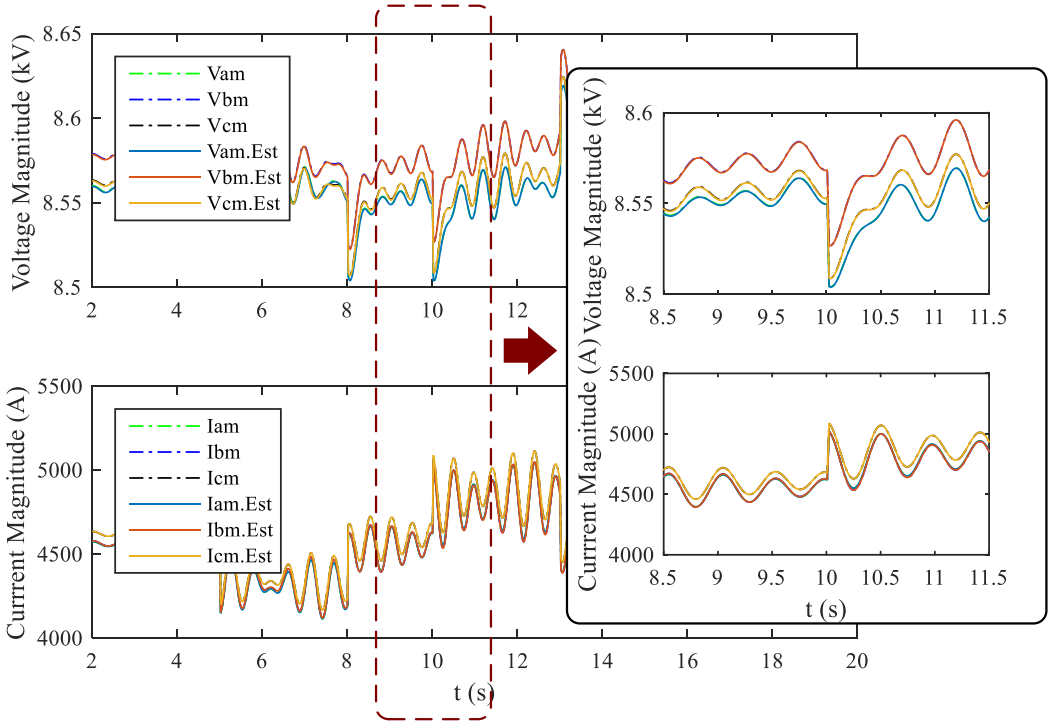

Figure 7.3.4: Actual and Estimated Voltage and Current Measurements from QDSE

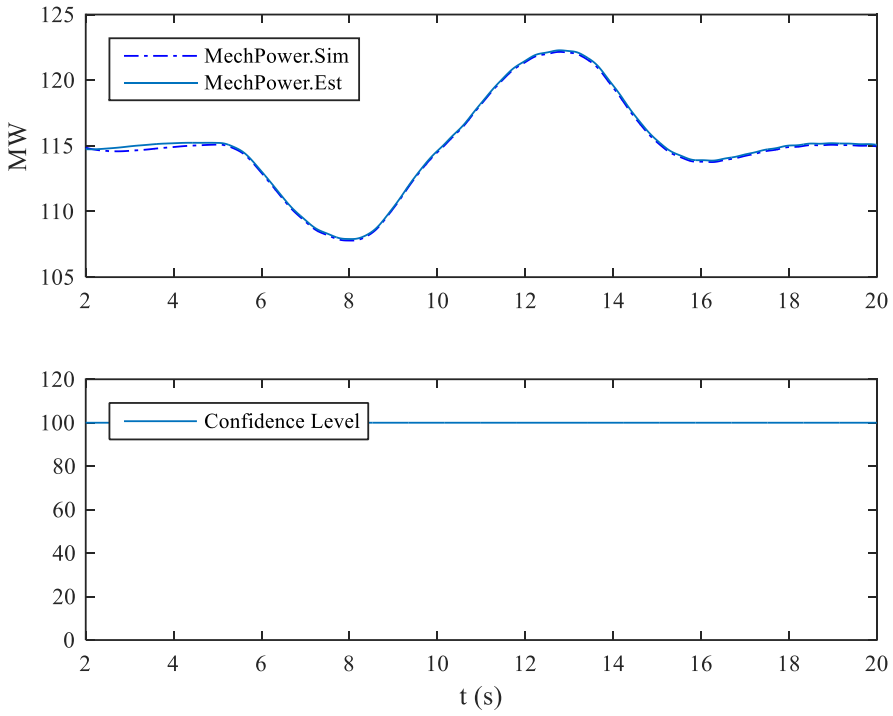

Figure 7.3.5: Simulated, Estimated Mechanical Power Output and Confidence Level

7.3.2 Performance of SSE

SSE uses three-phase voltage and current measurements to estimate the states of G1. By splitting a phasor measurement into real and imaginary parts, the total number of actual measurements is 12. Specifically, the voltage measurement models are constructed by a linear combination of the states of the measured frequency domain generator with the errors from the meter. The current measurement models are constructed by extracting the corresponding equations of the measured frequency domain generator plus the errors from the meter. Besides, we have two virtual measurements and two pseudo measurements. The two virtual measurements are those that describe the physical properties of the frequency generator, i.e., internal equations of the generator. These measurements have zero values,

and they are assigned with a very small measurement error since they are very accurate (obey the physical rules). Two pseudo measurements are those that assume the voltage at the neutral phase of G1 is close to zero during the normal operation. The entire measurement model for SSE is listed from (7.3.38) to (7.3.53).

$$z_{Vanr} = V_{ar} - V_{nr} + \eta_1 \tag{7.3.38}$$

$$z_{Vani} = V_{ai} - V_{ni} + \eta_2 \tag{7.3.39}$$

$$z_{Vbnr} = V_{br} - V_{nr} + \eta_3 \tag{7.3.40}$$

$$z_{Vbni} = V_{bi} - V_{ni} + \eta_4 \tag{7.3.41}$$

$$z_{Vcnr} = V_{cr} - V_{nr} + \eta_5 \tag{7.3.42}$$

$$z_{Vcni} = V_{ci} - V_{ni} + \eta_6 \tag{7.3.43}$$

$$\begin{aligned} z_{Iar} = {} & Y_{aar}V_{ar} - Y_{aai}V_{ai} + Y_{abr}V_{br} - Y_{abi}V_{bi} + Y_{acr}V_{cr} - Y_{aci}V_{ci} - \left(Y_{aar} + Y_{abr} + Y_{acr}\right)V_{nr} \\ & + \left(Y_{aai} + Y_{abi} + Y_{aci}\right)V_{ni} - \left(Y_{aar} - \frac{1}{2}Y_{abr} + \frac{\sqrt{3}}{2}Y_{abi} - \frac{1}{2}Y_{acr} - \frac{\sqrt{3}}{2}Y_{aci}\right)\cdot E_r \\ & - \left(-Y_{aai} + \frac{\sqrt{3}}{2}Y_{abr} + \frac{1}{2}Y_{abi} - \frac{\sqrt{3}}{2}Y_{acr} + \frac{1}{2}Y_{aci}\right)\cdot E_i + \eta_7 \end{aligned} \tag{7.3.44}$$

$$\begin{aligned} z_{Iai} = {} & Y_{aai}V_{ar} + Y_{aar}V_{ai} + Y_{abi}V_{br} + Y_{abr}V_{bi} + Y_{aci}V_{cr} + Y_{acr}V_{ci} - \left(Y_{aai} + Y_{abi} + Y_{aci}\right)V_{nr} \\ & - \left(Y_{aar} + Y_{abr} + Y_{acr}\right)V_{ni} - \left(Y_{aai} - \frac{\sqrt{3}}{2}Y_{abr} - \frac{1}{2}Y_{abi} + \frac{\sqrt{3}}{2}Y_{acr} - \frac{1}{2}Y_{aci}\right)\cdot E_r \\ & - \left(Y_{aar} - \frac{1}{2}Y_{abr} + \frac{\sqrt{3}}{2}Y_{abi} - \frac{1}{2}Y_{acr} - \frac{\sqrt{3}}{2}Y_{aci}\right)\cdot E_i + \eta_8 \end{aligned} \tag{7.3.45}$$

$$\begin{aligned} z_{Ibr} = {} & Y_{bar}V_{ar} - Y_{bai}V_{ai} + Y_{bbr}V_{br} - Y_{bbi}V_{bi} + Y_{bcr}V_{cr} - Y_{bci}V_{ci} - \left(Y_{bar} + Y_{bbr} + Y_{bcr}\right)V_{nr} \\ & + \left(Y_{bai} + Y_{bbi} + Y_{bci}\right)V_{ni} - \left(Y_{bar} - \frac{1}{2}Y_{bbr} + \frac{\sqrt{3}}{2}Y_{bbi} - \frac{1}{2}Y_{bcr} - \frac{\sqrt{3}}{2}Y_{bci}\right)\cdot E_r \\ & - \left(-Y_{bai} + \frac{\sqrt{3}}{2}Y_{bbr} + \frac{1}{2}Y_{bbi} - \frac{\sqrt{3}}{2}Y_{bcr} + \frac{1}{2}Y_{bci}\right)\cdot E_i + \eta_9 \end{aligned} \tag{7.3.46}$$

$$z_{Ibi} = Y_{bai}V_{ar} + Y_{bar}V_{ai} + Y_{bbi}V_{br} + Y_{bbr}V_{bi} + Y_{bci}V_{cr} + Y_{bcr}V_{ci} - \left(Y_{bai} + Y_{bbi} + Y_{bci}\right)V_{nr}$$
$$-\left(Y_{bar} + Y_{bbr} + Y_{bcr}\right)V_{ni} - \left(Y_{bai} - \frac{\sqrt{3}}{2}Y_{bbr} - \frac{1}{2}Y_{bbi} + \frac{\sqrt{3}}{2}Y_{bcr} - \frac{1}{2}Y_{bci}\right)\cdot E_r \qquad (7.3.47)$$
$$-\left(Y_{bar} - \frac{1}{2}Y_{bbr} + \frac{\sqrt{3}}{2}Y_{bbi} - \frac{1}{2}Y_{bcr} - \frac{\sqrt{3}}{2}Y_{bci}\right)\cdot E_i + \eta_{10}$$

$$z_{Icr} = Y_{car}V_{ar} - Y_{cai}V_{ai} + Y_{cbr}V_{br} - Y_{cbi}V_{bi} + Y_{ccr}V_{cr} - Y_{cci}V_{ci} - \left(Y_{car} + Y_{cbr} + Y_{ccr}\right)V_{nr}$$
$$+\left(Y_{cai} + Y_{cbi} + Y_{cci}\right)V_{ni} - \left(Y_{car} - \frac{1}{2}Y_{cbr} + \frac{\sqrt{3}}{2}Y_{cbi} - \frac{1}{2}Y_{ccr} - \frac{\sqrt{3}}{2}Y_{cci}\right)\cdot E_r \qquad (7.3.48)$$
$$-\left(-Y_{cai} + \frac{\sqrt{3}}{2}Y_{cbr} + \frac{1}{2}Y_{cbi} - \frac{\sqrt{3}}{2}Y_{ccr} + \frac{1}{2}Y_{cci}\right)\cdot E_i + \eta_{11}$$

$$z_{Ici} = Y_{cai}V_{ar} + Y_{car}V_{ai} + Y_{cbi}V_{br} + Y_{cbr}V_{bi} + Y_{cci}V_{cr} + Y_{ccr}V_{ci} - \left(Y_{cai} + Y_{cbi} + Y_{cci}\right)V_{nr}$$
$$-\left(Y_{car} + Y_{cbr} + Y_{ccr}\right)V_{ni} - \left(Y_{cai} - \frac{\sqrt{3}}{2}Y_{cbr} - \frac{1}{2}Y_{cbi} + \frac{\sqrt{3}}{2}Y_{ccr} - \frac{1}{2}Y_{cci}\right)\cdot E_r \qquad (7.3.49)$$
$$-\left(Y_{car} - \frac{1}{2}Y_{cbr} + \frac{\sqrt{3}}{2}Y_{cbi} - \frac{1}{2}Y_{ccr} - \frac{\sqrt{3}}{2}Y_{cci}\right)\cdot E_i + \eta_{12}$$

$$0 = E_r \cdot I_{ar} + E_i \cdot I_{ai} - \frac{1}{2}E_r \cdot I_{br} + \frac{\sqrt{3}}{2}E_i \cdot I_{br} - \frac{\sqrt{3}}{2}E_r \cdot I_{bi} - \frac{1}{2}E_i \cdot I_{bi}$$
$$-\frac{1}{2}E_r \cdot I_{cr} - \frac{\sqrt{3}}{2}E_i \cdot I_{cr} + \frac{\sqrt{3}}{2}E_r \cdot I_{ci} - \frac{1}{2}E_i \cdot I_{ci} + P_m + \eta_{13} \qquad (7.3.50)$$

$$0 = V_{ar}^2 + V_{ai}^2 + V_{br}^2 + V_{bi}^2 - 2V_{ar}V_{br} - 2V_{ai}V_{bi} - V_{pu}^2 V_{rated}^2 + \eta_{14} \qquad (7.3.51)$$

$$0 = V_{nr} + \eta_{15} \qquad (7.3.52)$$

$$0 = V_{ni} + \eta_{16} \qquad (7.3.53)$$

In summary, we have 16 measurements for G1. Similar as QDSE, a standard deviation is assigned to each measurement to represent its measurement error. The standard deviation of actual, virtual, and pseudo measurements are assigned to be the same as those in QDSE, that is, 0.01 pu, 0.001 pu, and 0.1 pu, respectively. As G1 has 10 states, the

redundancy is 16/10 = 160%. The execution time for this case is 1.21 s. Figure 7.3.6 shows actual and estimated voltage and current magnitude measurements from SSE, and Figure 7.3.7 shows the confidence level of the whole event when parameter *k* equals to one. The confidence level is 100% at the beginning when the system is in steady state. However, since some dynamics occur in the system after *t*=5s and the frequency domain model of the generator is not able to reflect the dynamics inside the generator, the confidence level drops to a low value and oscillates. Meanwhile, relatively large deviations are observed between estimated measurements and measurements after *t*=5s in Figure 7.3.6 compared with the results from Figure 7.3.4. For example, the maximum difference between the magnitude of phase A current measurement and estimated measurement is 0.059 pu from SSE, while the value is 0.008 pu from QDSE. The oscillating confidence level during the transients indicates the measurements are not quite consistent with the generator model. Therefore, the estimated states from this case are not reliable.

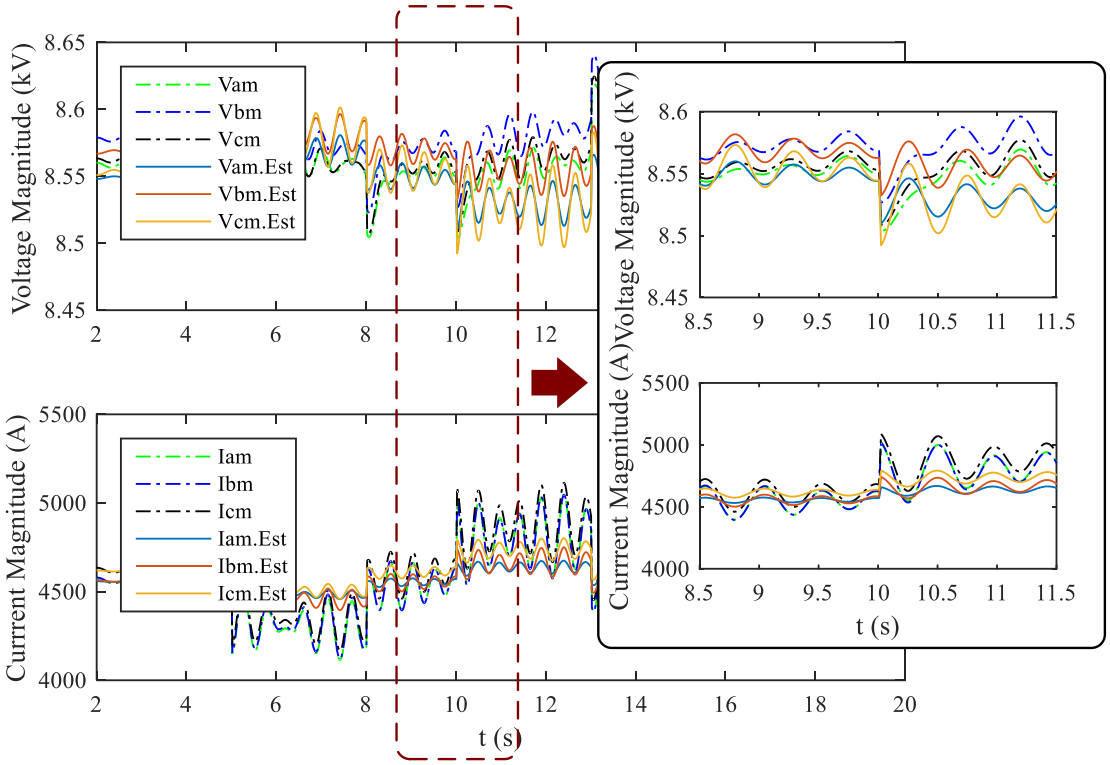

Figure 7.3.6: Actual and Estimated Voltage and Current Measurements from SSE

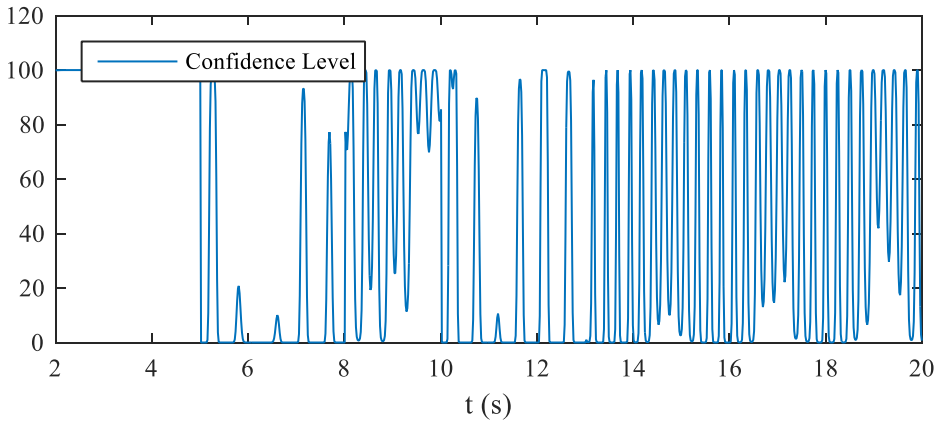

Figure 7.3.7: Confidence Level of SSE

7.4 Summary

With the increasing number of installed PMUs and other IEDs, QDSE has become a possibility for power systems. This chapter compared the performance between QDSE and SSE on an example power system with several generators. In this study, generators are modeled with governor, turbine, and exciter models, which capture the slow dynamics. Results for one of the generators have been presented. QDSE considers the full model of the generator incorporating all the slow dynamics in power systems, while SSE utilizes frequency domain models without dynamics, so it employs a simplified generator. As a consequence, with the aid of high-sampling-rate PMUs, QDSE is able to provide more accurate information (e.g., dynamics in the rotating rotor, etc.) of the monitored power system compared with SSE. The confidence level of the QDSE is very high while the confidence level of the SSE is good during steady state operation but rapidly deteriorates when transients occur. On the other hand, QDSE involves more states than SSE and the computational burden is heavier in QDSE. This issue could be resolved by a distributed architecture of the state estimator [21], which is proposed in this dissertation and will be illustrated by an actual feeder in the next chapter.

CHAPTER 8. DEMONSTRATION EXAMPLES FOR THE PROPOSED STATE ESTIMATOR

8.1 Overview

This chapter demonstrates the performance of the proposed distribution system distributed quasi-dynamic state estimator (DS-DQDSE) on a real feeder model provided by a utility. The state estimation results for the reduced feeder model are first demonstrated to test the effectiveness of the proposed state estimator. Then, the state estimation results for the full feeder model are provided. The rest of this chapter is organized as follows. Section 8.2 presents the performance of the state estimator for the reduced feeder model. Section 8.3 presents the performance of the state estimator for the full feeder model. Section 8.4 summarizes this chapter.

8.2 Example 1: The Reduced Feeder Model

This section presents the performance of the DS-DQDSE for the reduced feeder model. First, the detailed information of this reduced feeder model is described. Then the state estimator setup and simulation event creation follow. Finally, the results of the DS-DQDSE on this reduced feeder model are presented.

8.2.1 Example System Description

This subsection presents the detailed information of the reduced feeder model with 15 three-phase buses. The GPS coordinates of these buses are available. This allows the visualization of the feeder topology as shown in Figure 8.2.1. The feeder model consists of

various types of devices, including loads (three-phase, single-phase), capacitor banks, three-phase two-winding transformers, three-phase distribution line segments, synchronous generators, and PV sources, etc. Table 8.2.1 shows the detailed information of these devices in this feeder. The feeder model has been debugged in WinIGS software.

The reduced feeder model consists of 2 three-phase loads (12.47kV/0.48 kV) and 12 single-phase loads (7.2 kV). The real and reactive power consumption of these loads are 2568.60 kW and 1418.71 kVar, respectively. The reduced feeder also consists of one capacitor bank (12.47 kV, 1800 kVar, wye connection), 12 three-phase distribution line segments (12.47 kV), 2 three-phase two-winding transformers and three PV sources. The detailed information of transformers and PV sources is illustrated in Table 8.2.2 and Table 8.2.3. The feeder is connected to a synchronous generator (115 kV) as the power supply from the transmission system.

Table 8.2.1: Devices in the Reduced Feeder Model

Device Type		Number
Load	Three-Phase	2
	Single-Phase	12
Capacitor Bank	Three-Phase	1
Transformer	Three-Phase Two-Winding	2
Distribution Line Segment	Three-Phase	12
Synchronous Generator	Three-Phase	1
PV Source	Three-Phase	3

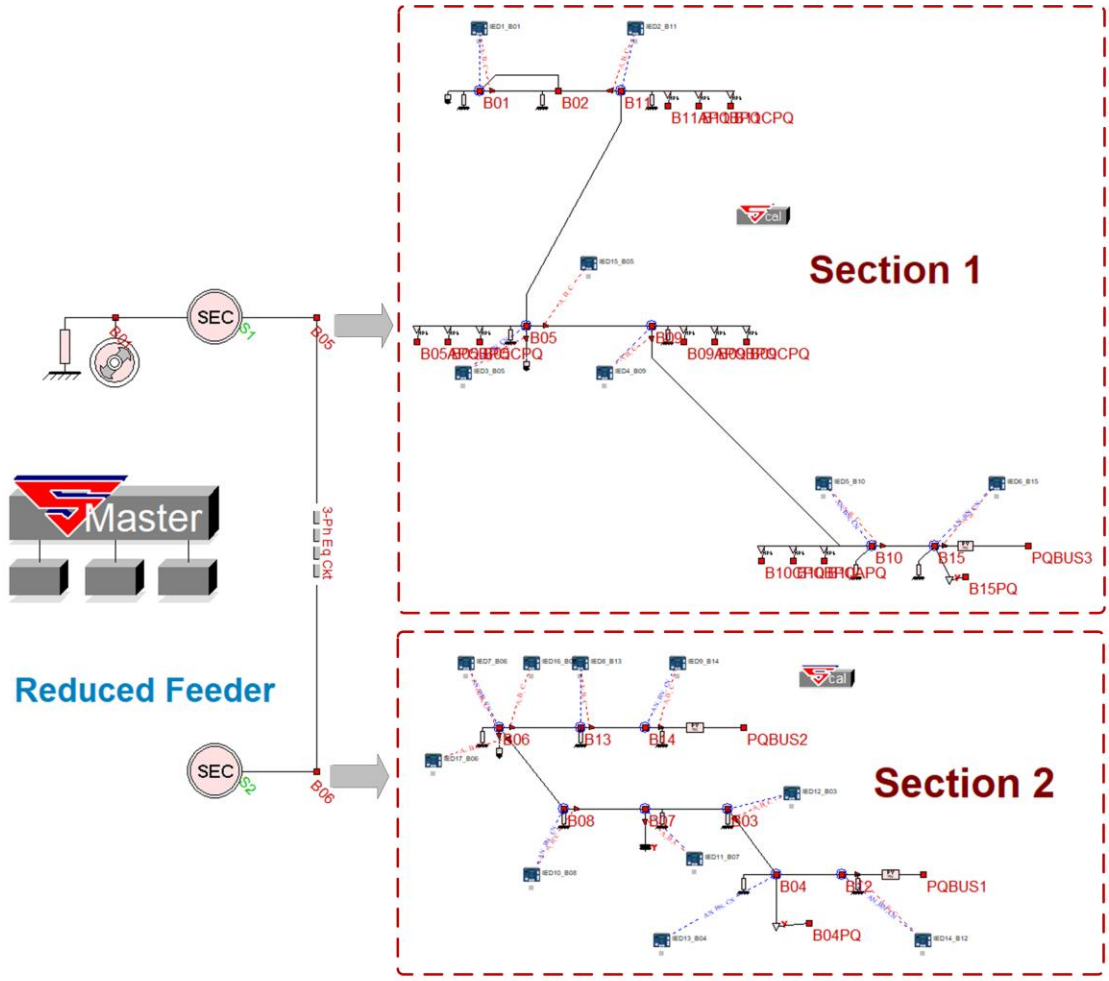

Figure 8.2.1: Single-Line Diagram with IEDs and State Estimators of the Reduced Feeder

Table 8.2.2: Parameters of Three-Phase Two-Winding Transformers in the Reduced Feeder Model

Three-Phase Two-Winding Transformer					
#	Device Name	Bus Name	Rated Power (MVA)	Rated Voltage (kV)	Connection Type
1	Tran1	B01, B02	30	115/12.47	DELTA/WYE
2	Tran20	B10, B15	0.5	12.47/0.48	WYE/WYE

Table 8.2.3: Parameters of Three-Phase PV Sources in the Reduced Feeder Model

Three-Phase PV Source					
#	Device Name	Bus Name	Rated Voltage (kV)	Rated Power (MVA)	Power Factor
1	PVSy1	B12	12.47	1.0	1.0
2	PVSy2	B14	12.47	10.0	1.0
3	PVSy3	B15	0.48	0.258	1.0

8.2.2 State Estimator Setup and Event Creation

This subsection presents the details of how the state estimator is set up for the given reduced feeder model and how the simulation event is created. As shown in Figure 8.2.1, DS-DQDSE separates the feeder model into two sections. Each section has several IEDs that collect voltage and current measurements from the devices in this section. To be more specific, section 1 has 7 IEDs, and section 2 has 10 IEDs. The total number of phasor measurement is 90. Each measurement channel is defined by IED's instrumentation channel in detail. The installed IEDs and their measurement channels in section 1 and 2 are listed in Table 8.2.4 and Table 8.2.5, respectively. A local state estimator is installed in each section. The local state estimator automatically collects the measurement channel information (measurement definition) and measurement data in this section, then performs QDSE for this section. Meanwhile, a master state estimator collects the data from the local state estimators and synthesizes the states and the validated model for the whole feeder.

Table 8.2.4: Measurement Channels of IEDs in Section 1

IED Name	Voltage Channels	Current Channels	# of channels of this IED
IED1_B01	AN, BN, CN at B01	A, B, C at B01, from B01 to B02 (Tran1)	6
IED2_B11	AN, BN, CN at B11	A, B, C at B11, from B11 to B02 (Line149)	6
IED3_B05	AN, BN, CN at B05	A, B, C at B05, from B05 to B06 (Line59)	6
IED4_B09	AN, BN, CN at B09	A, B, C at B09, from B09 to B10 (Line105)	6
IED5_B10	AN, BN, CN at B10	A, B, C at B10, from B10 to B15 (Tran20)	6
IED6_B15	AN, BN, CN at B15	A, B, C at B15, into the PV Source (PVSy3)	6
IED15_B05		A, B, C at B05, from B05 to B09 (Line135)	3

Table 8.2.5: Measurement Channels of IEDs in Section 2

IED Name	Voltage Channels	Current Channels	# of channels of this IED
IED7_B06	AN, BN, CN at B06	A, B, C at B06, from B06 to B05 (Line59)	6
IED8_B13	AN, BN, CN at B13	A, B, C at B13, from B13 to B14 (Line196)	6
IED9_B14	AN, BN, CN at B14	A, B, C at B14, into the PV Source (PVSy2)	6

IED10_B08	AN, BN, CN at B08	A, B, C at B08, from B08 to B07 (Line97)	6
IED11_B07	AN, BN, CN at B07	A, B, C at B07, into the capacitor bank (Capa1)	6
IED12_B03	AN, BN, CN at B03	A, B, C at B03, from B03 to B04 (Line4)	6
IED13_B04	AN, BN, CN at B04		3
IED14_B12	AN, BN, CN at B12	A, B, C at B12, into the PV Source (PVSy1)	6
IED16_B06		A, B, C at B06, from B06 to B13 (Line167)	3
IED17_B06		A, B, C at B06, from B06 to B08 (Line188)	3

A sixty-second event is created and stored in COMTRADE files for testing the state estimator. The time step is selected to be 1 sample per cycle in this example, i.e., 60 samples per second. During the event, we simulate some power output changes of three PV sources. Since the generated data are very large, we present the data obtained from some specific relays as shown in Figure 8.2.2. Figure 8.2.2 presents two sets of three-phase voltage and current measurements from IED2_B11 and IED14_B12, respectively. Notice that since the PVs are not constant power sources, some dynamics exist during the whole event.

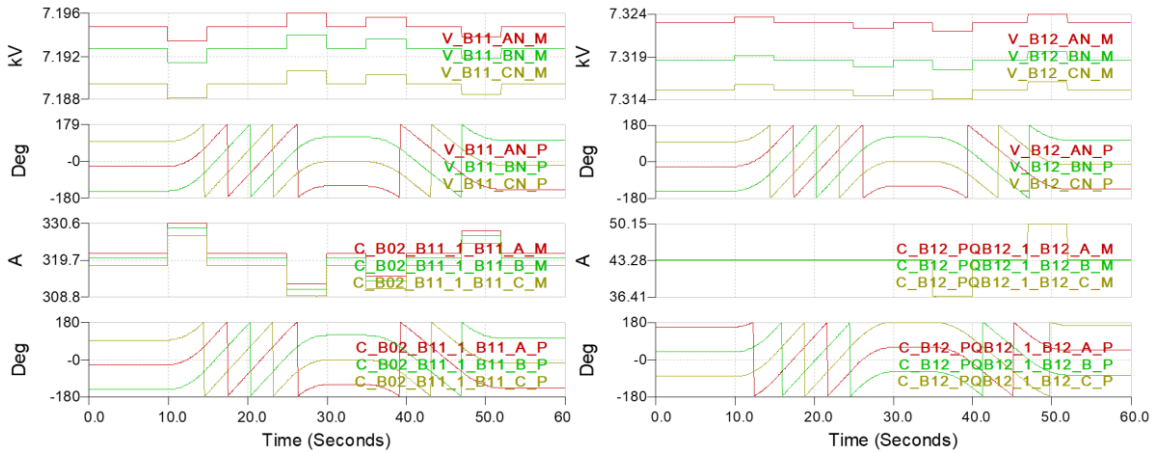

Figure 8.2.2: Measurements from IED2_B11 (Section 1), and IED14_B12 (Section 2)

8.2.3 State Estimation Results

This subsection presents the state estimation results obtained from the two local state estimators during the event.

8.2.3.1 State Estimation Result of Section 1

In section 1, we have 18 voltage phasor measurements and 21 current phasor measurements collected from IEDs. Since the state estimator divides each phasor measurement into real and imaginary parts, we have 78 actual measurements in total. Furthermore, according to Chapter 5, the state estimator automatically creates type I derived, type II derived, pseudo, and virtual measurements: (1) 120 type I derived measurements, (2) 30 type II derived measurements, (3) 42 virtual measurements, and (4) 14 pseudo measurements. In summary, we have 284 measurements at time *t*. Since section 1 consists of 114 states at time *t*, the redundancy is 284/114 = 249.12%.

The local state estimator at section 1 uses section-wise measurements to estimate the states of the whole section. Since the generated data are very large in size, we depict the state estimation results by some specific data. Figure 8.2.3 presents the voltage and current actual and estimated phasor measurements from IED2_B11. Figure 8.2.4 presents the voltage and current actual and estimated phasor measurements from IED6_B15. These figures indicate that the estimated measurements track the measurements accurately. Figure 8.2.5 snapshots actual/estimated measurements and their differences of all the voltage measurements in section 1. Notice that all the errors are in small values. In addition, the confidence level (when parameter *k* equals to 1) of the whole section remains at 100% during the event, which indicates a strong consistency between the measurements and the system model, i.e., the estimated states of this section are trustworthy, and the system model of this section is validated.

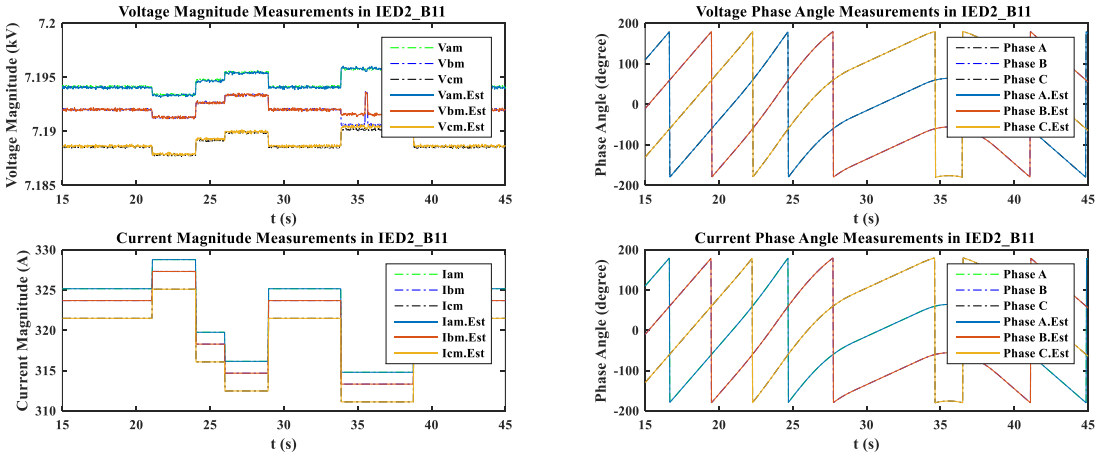

Figure 8.2.3: Actual and Estimated Measurements from IED2_B11

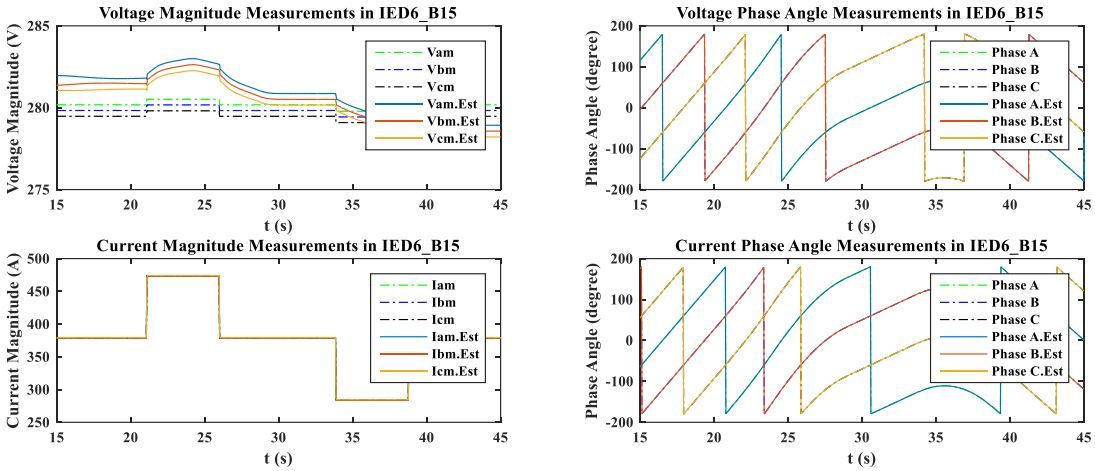

Figure 8.2.4: Actual and Estimated Measurements from IED6_B15

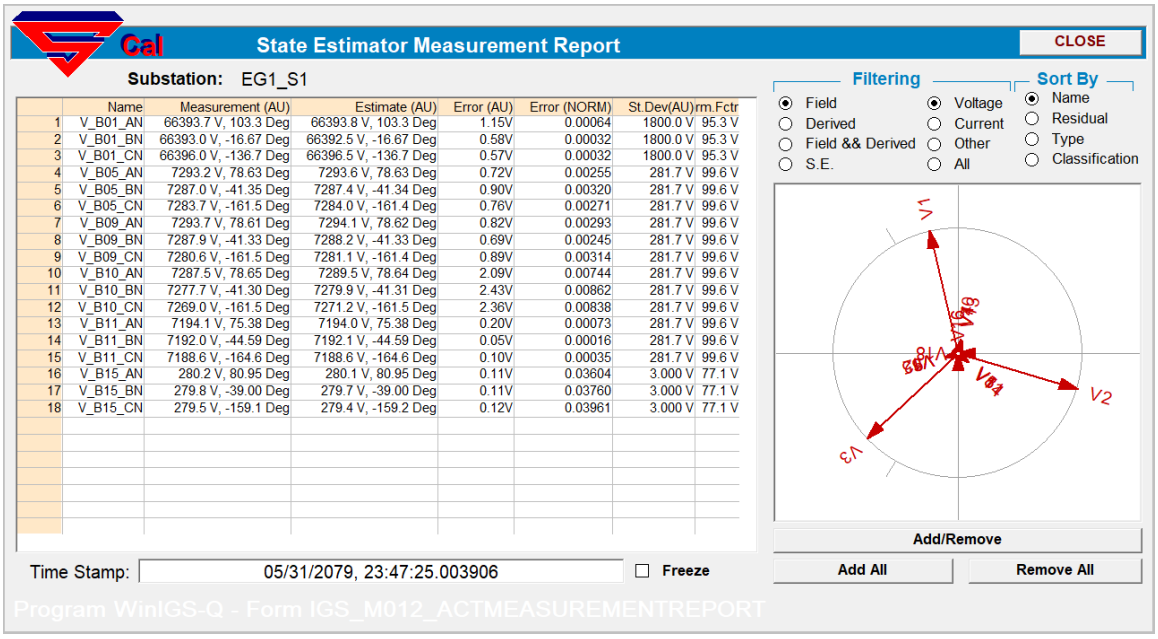

	Name	Measurement (AU)	Estimate (AU)	Error (AU)	Error (NORM)	St.Dev(AU)	rm.Fctr
1	V_B01_AN	66393.7 V, 103.3 Deg	66393.8 V, 103.3 Deg	1.15V	0.00064	1800.0 V	95.3 V
2	V_B01_BN	66393.0 V, -16.67 Deg	66392.5 V, -16.67 Deg	0.58V	0.00032	1800.0 V	95.3 V
3	V_B01_CN	66396.0 V, -136.7 Deg	66396.5 V, -136.7 Deg	0.57V	0.00032	1800.0 V	95.3 V
4	V_B05_AN	7293.2 V, 78.63 Deg	7293.6 V, 78.63 Deg	0.72V	0.00255	281.7 V	99.6 V
5	V_B05_BN	7287.0 V, -41.35 Deg	7287.4 V, -41.34 Deg	0.90V	0.00320	281.7 V	99.6 V
6	V_B05_CN	7283.7 V, -161.5 Deg	7284.0 V, -161.4 Deg	0.76V	0.00271	281.7 V	99.6 V
7	V_B09_AN	7293.7 V, 78.61 Deg	7294.1 V, 78.62 Deg	0.82V	0.00293	281.7 V	99.6 V
8	V_B09_BN	7287.9 V, -41.33 Deg	7288.2 V, -41.33 Deg	0.69V	0.00245	281.7 V	99.6 V
9	V_B09_CN	7280.6 V, -161.5 Deg	7281.1 V, -161.4 Deg	0.89V	0.00314	281.7 V	99.6 V
10	V_B10_AN	7287.5 V, 78.65 Deg	7289.5 V, 78.64 Deg	2.09V	0.00744	281.7 V	99.6 V
11	V_B10_BN	7277.7 V, -41.30 Deg	7279.9 V, -41.31 Deg	2.43V	0.00862	281.7 V	99.6 V
12	V_B10_CN	7269.0 V, -161.5 Deg	7271.2 V, -161.5 Deg	2.36V	0.00838	281.7 V	99.6 V
13	V_B11_AN	7194.1 V, 75.38 Deg	7194.0 V, 75.38 Deg	0.20V	0.00073	281.7 V	99.6 V
14	V_B11_BN	7192.0 V, -44.59 Deg	7192.1 V, -44.59 Deg	0.05V	0.00016	281.7 V	99.6 V
15	V_B11_CN	7188.6 V, -164.6 Deg	7188.6 V, -164.6 Deg	0.10V	0.00035	281.7 V	99.6 V
16	V_B15_AN	280.2 V, 80.95 Deg	280.1 V, 80.95 Deg	0.11V	0.03604	3.000 V	77.1 V
17	V_B15_BN	279.8 V, -39.00 Deg	279.7 V, -39.00 Deg	0.11V	0.03760	3.000 V	77.1 V
18	V_B15_CN	279.5 V, -159.1 Deg	279.4 V, -159.2 Deg	0.12V	0.03961	3.000 V	77.1 V

Figure 8.2.5: State Estimator Voltage Measurement Report, Section 1

8.2.3.2 State Estimation Result of Section 2

In section 2, IEDs collect 24 voltage phasor measurements and 27 current phasor measurements. Since the state estimator divides each phasor measurement into real and

imaginary parts, we have 102 actual measurements in total. Furthermore, according to Chapter 5, the state estimator automatically creates type I derived, type II derived, pseudo, and virtual measurements: (1) 66 type I derived measurements, (2) 14 type II derived measurements, (3) 20 virtual measurements, and (4) 16 pseudo measurements. In summary, we have 218 measurements at time *t*. Since section 2 consists of 88 states at time *t*, the redundancy is 218/88 = 247.73%.

The local state estimator at section 2 uses section-wise measurements and estimates the states of the whole section. Since the generated data are very large in size, we depict the state estimation results by some specific data. Figure 8.2.6 shows the voltage and current actual and estimated phasor measurements from IED9_B14. Figure 8.2.7 presents the voltage and current actual and estimated phasor measurements from IED14_B12. These figures indicate that the estimated measurements track the measurements accurately. Figure 8.2.8 snapshots actual/estimated measurements and their differences of all the current measurements in section 2. Notice that all the errors are in small values. In addition, the confidence level (when parameter *k* equals to one) of the whole section remains at 100% during the event, which indicates a strong consistency between the measurements and the system model, i.e., the estimated states of this section are trustworthy, and the system model of this section is validated.

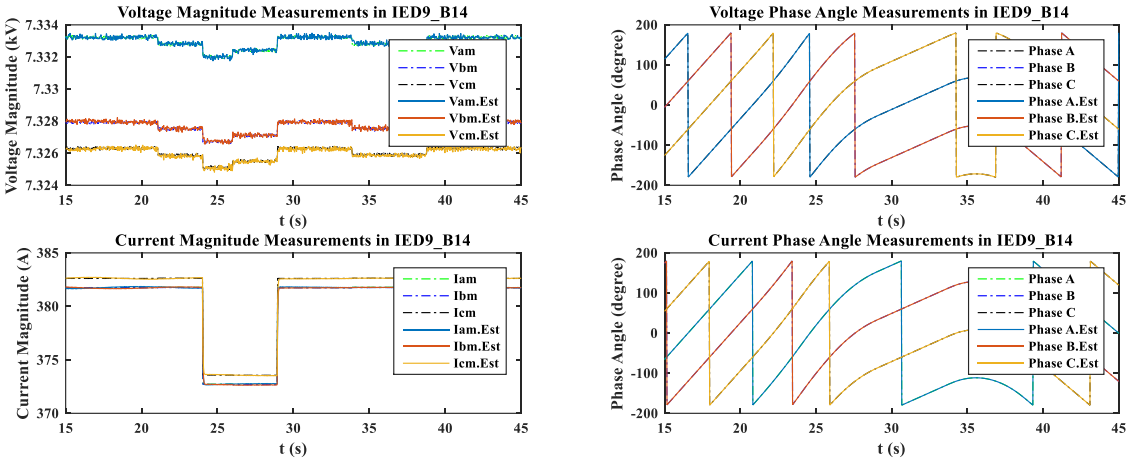

Figure 8.2.6: Actual and Estimated Voltage Measurements from IED9_B14

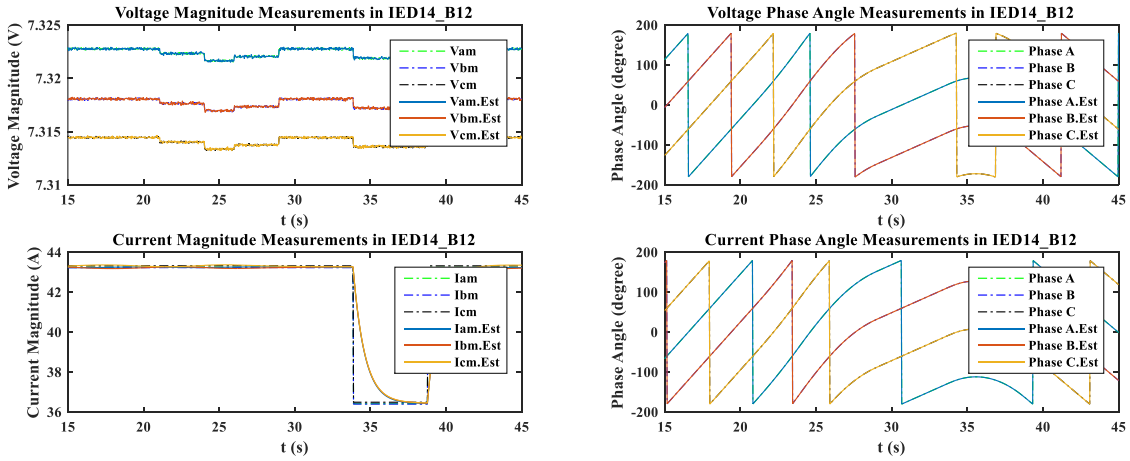

Figure 8.2.7: Actual and Estimated Voltage Measurements from IED14_B12

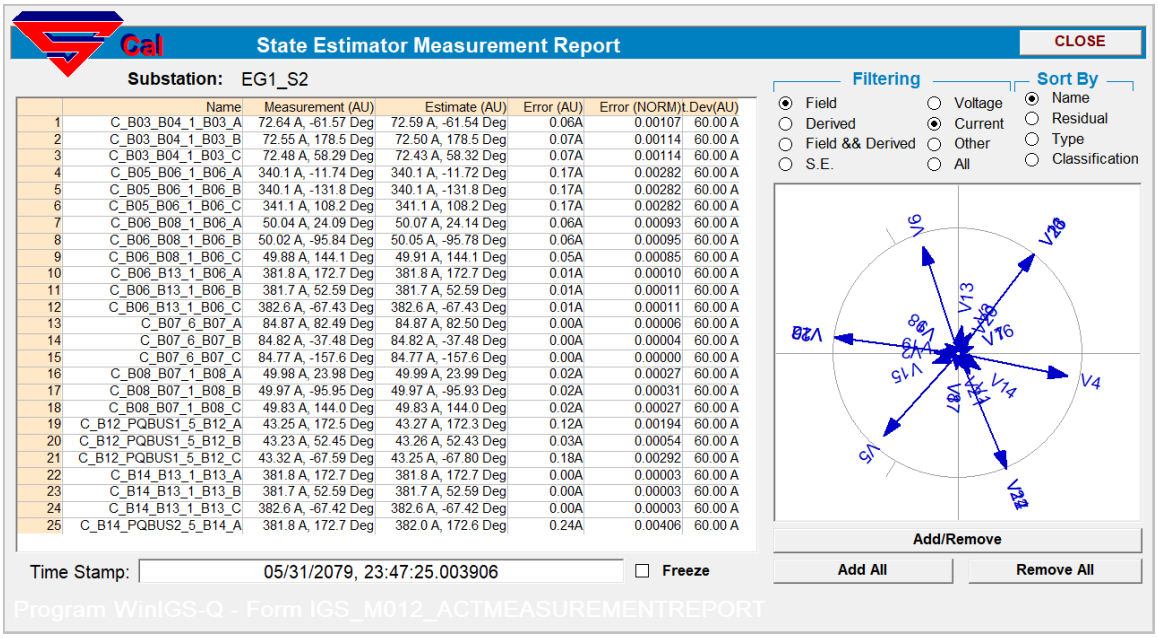

	Name	Measurement (AU)	Estimate (AU)	Error (AU)	Error (NORM)	t.Dev(AU)
1	C_B03_B04_1_B03_A	72.64 A, -61.57 Deg	72.59 A, -61.54 Deg	0.06A	0.00107	60.00 A
2	C_B03_B04_1_B03_B	72.55 A, 178.5 Deg	72.50 A, 178.5 Deg	0.07A	0.00114	60.00 A
3	C_B03_B04_1_B03_C	72.48 A, 58.29 Deg	72.43 A, 58.32 Deg	0.07A	0.00114	60.00 A
4	C_B05_B06_1_B06_A	340.1 A, -11.74 Deg	340.1 A, -11.72 Deg	0.17A	0.00282	60.00 A
5	C_B05_B06_1_B06_B	340.1 A, -131.8 Deg	340.1 A, -131.8 Deg	0.17A	0.00282	60.00 A
6	C_B05_B06_1_B06_C	341.1 A, 108.2 Deg	341.1 A, 108.2 Deg	0.17A	0.00282	60.00 A
7	C_B06_B08_1_B06_A	50.04 A, 24.09 Deg	50.07 A, 24.14 Deg	0.06A	0.00093	60.00 A
8	C_B06_B08_1_B06_B	50.02 A, -95.84 Deg	50.05 A, -95.78 Deg	0.06A	0.00095	60.00 A
9	C_B06_B08_1_B06_C	49.88 A, 144.1 Deg	49.91 A, 144.1 Deg	0.05A	0.00085	60.00 A
10	C_B06_B13_1_B06_A	381.8 A, 172.7 Deg	381.8 A, 172.7 Deg	0.01A	0.00010	60.00 A
11	C_B06_B13_1_B06_B	381.7 A, 52.59 Deg	381.7 A, 52.59 Deg	0.01A	0.00011	60.00 A
12	C_B06_B13_1_B06_C	382.6 A, -67.43 Deg	382.6 A, -67.43 Deg	0.01A	0.00011	60.00 A
13	C_B07_6_B07_A	84.87 A, 82.49 Deg	84.87 A, 82.50 Deg	0.00A	0.00006	60.00 A
14	C_B07_6_B07_B	84.82 A, -37.48 Deg	84.82 A, -37.48 Deg	0.00A	0.00004	60.00 A
15	C_B07_6_B07_C	84.77 A, -157.6 Deg	84.77 A, -157.6 Deg	0.00A	0.00000	60.00 A
16	C_B08_B07_1_B08_A	49.98 A, 23.98 Deg	49.99 A, 23.99 Deg	0.02A	0.00027	60.00 A
17	C_B08_B07_1_B08_B	49.97 A, -95.95 Deg	49.97 A, -95.93 Deg	0.02A	0.00031	60.00 A
18	C_B08_B07_1_B08_C	49.83 A, 144.0 Deg	49.83 A, 144.0 Deg	0.02A	0.00027	60.00 A
19	C_B12_PQBUS1_5_B12_A	43.25 A, 172.5 Deg	43.27 A, 172.3 Deg	0.12A	0.00194	60.00 A
20	C_B12_PQBUS1_5_B12_B	43.23 A, 52.45 Deg	43.26 A, 52.43 Deg	0.03A	0.00054	60.00 A
21	C_B12_PQBUS1_5_B12_C	43.32 A, -67.59 Deg	43.25 A, -67.80 Deg	0.18A	0.00292	60.00 A
22	C_B14_B13_1_B13_A	381.8 A, 172.7 Deg	381.8 A, 172.7 Deg	0.00A	0.00003	60.00 A
23	C_B14_B13_1_B13_B	381.7 A, 52.59 Deg	381.7 A, 52.59 Deg	0.00A	0.00003	60.00 A
24	C_B14_B13_1_B13_C	382.6 A, -67.42 Deg	382.6 A, -67.42 Deg	0.00A	0.00003	60.00 A
25	C_B14_PQBUS2_5_B14_A	381.8 A, 172.7 Deg	382.0 A, 172.6 Deg	0.24A	0.00406	60.00 A

Figure 8.2.8: State Estimator Current Measurement Report, Section 2

8.3 Example 2: The Full Feeder Model

This section presents the performance of the state estimator for the full feeder model. Similar as Section 8.2, the detailed information including the topology of the feeder model is first described. Then, the state estimator setup and simulation event creation follow. Finally, the results of the state estimator from four separate sections are presented.

8.3.1 Example System Description

This subsection presents the detailed information of the full feeder model. This feeder model has 217 buses. Of these buses, 193 are three-phase buses, 14 are single-phase buses, and 10 are secondary buses. The GPS coordinates of the buses are available. This allows the visualization of the feeder topology, which is shown in Figure 8.3.1. The feeder model consists of various types of devices, including 31 loads (three-phase, single-phase),

two capacitor banks, six switches, 20 transformers (three-phase two-winding, single-phase with secondary center-tap), 190 distribution lines (three-phase, single-phase), 3 PV sources, and 3 distributed generators. The real and reactive power consumption of these loads are 3971.40 kW and 1707.06 kVar, respectively. The devices of this feeder are listed in Table 8.3.1. Since the system is quite large, only the detailed information of some devices is listed here. Table 8.3.2 and Table 8.3.3 list the parameters of three-phase two-winding transformers and distributed generators, respectively. The feeder model has been debugged in WinIGS software.

Table 8.3.1: Devices in the Full Feeder Model

Device Type		Number
Transformer	Three-Phase Two-Winding Transformer	10
	Single-Phase Transformer with Secondary Center-tap	10
Distribution Line	Three-Phase Distribution Line	176
	Single-Phase Distribution Line	14
Load	Three-Phase Load	11
	Single-Phase Load	20
Capacitor Bank	Three-Phase	2
Switch	Three-Phase	6
PV Source	Three-Phase	3
Distributed Generator	Three-Phase	3

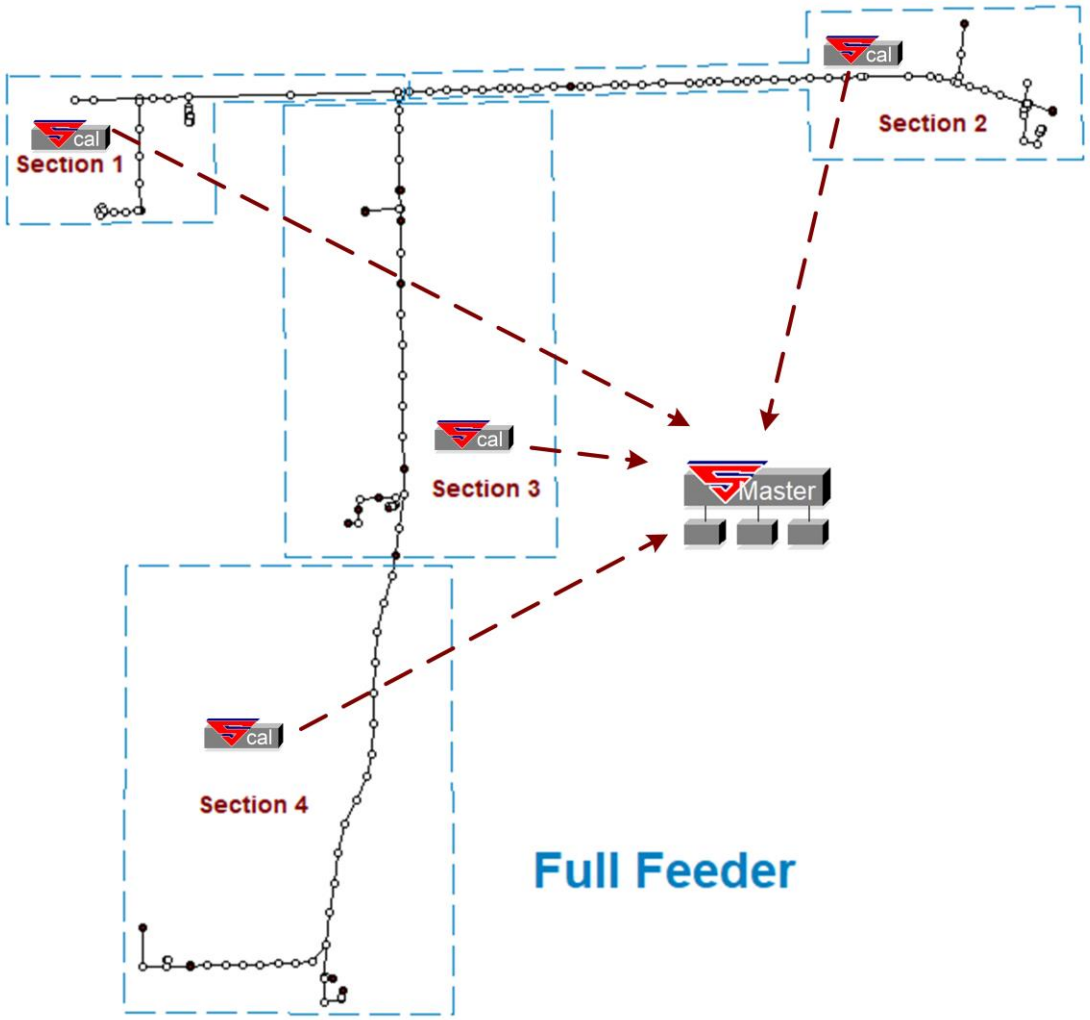

Figure 8.3.1: Topology of the Full Feeder Model

Table 8.3.2: Parameters of Three-Phase Two-Winding Transformers in the Full Feeder

#	Device Name	Bus Name	Rated Power (MVA)	Rated Voltage (kV)	Connection Type
1	32634	B093, B199	0.075	12.47/0.48	WYE/WYE
2	33012	B089, B200	0.3	12.47/0.48	WYE/WYE
3	29322	B082, B206	0.075	12.47/0.48	WYE/WYE
4	34475	B092, B208	0.15	12.47/0.48	WYE/WYE
5	30090	B031, B209	0.3	12.47/0.48	WYE/WYE
6	52370	B098, B211	0.75	12.47/0.48	WYE/WYE

7	29321	B157, B212	0.03	12.47/0.48	WYE/WYE
8	29323	B133, B213	0.3	12.47/0.48	WYE/WYE
9	53433	B198, B217	0.5	12.47/0.48	WYE/WYE
10	Sub	B001, B002	30	115/12.47	DELTA/WYE

Table 8.3.3: Parameters of Distributed Generators (12.47 kV, 1.5 MVA) in the Full Feeder

#	Device Name	Positive Impedance	Negative Impedance	Zero Impedance	Inertia Constant	Number of Poles
1	DG1	0.01+j0.10 pu	0.01+j0.10 pu	0.01+j0.10 pu	2.5s	2
2	DG2	0.01+j0.10 pu	0.01+j0.10 pu	0.01+j0.10 pu	2.5s	2
3	DG3	0.01+j0.10 pu	0.01+j0.10 pu	0.01+j0.10 pu	2.5s	2

8.3.2 State Estimator Setup and Event Creation

As shown in Figure 8.3.1, DS-DQDSE separates the feeder model into four sections. Each section has several IEDs that collect voltage and current measurements from the devices in this section. For those distributed generators, rotating speed measurements are assumed to be available, and the IEDs measure these generator's rotating speed as additional measurements. To be more specific, section 1 has 13 IEDs, section 2 has 9 IEDs, section 3 has 13 IEDs, and section 4 has 9 IEDs. Each measurement is defined by IED's instrumentation channel in detail. The installed IEDs and their measurements in section 1

to 4 are listed in Table 8.3.4, Table 8.3.5, Table 8.3.6, and Table 8.3.7, respectively. A local state estimator is installed in each section. The local state estimator automatically collects the measurement information (measurement definition) and measurement data in this section and performs QDSE for this section. Meanwhile, a master state estimator collects the data from the local state estimators and synthesizes the states and the validated model for the whole feeder. A sixty-second event is created and stored in COMTRADE files for testing the state estimator at each section. The time step is 1 sample per cycle in this example, i.e., 60 samples per second. During the event, we simulate some power output changes of PV sources and load changes.

Table 8.3.4: Measurements of IEDs in Section 1

IED Name	Voltage Channels	Current Channels	# of measurements of this IED
IED_B021	AN, BN, CN at B021	A, B, C at B021, from B021 to B071	6
IED_B149	AN, BN, CN at B149	A, B, C at B149, from B149 to B077	6
IED_B074	AN, BN, CN at B074	A, B, C at B074, from B074 to B173	6
IED_B189	AN, BN, CN at B189	A, B, C at B189, from B189 to B183	6
IED_B183	AN, BN, CN at B183	A, B, C at B183, from B183 to B192	6
IED_B181	AN, BN, CN at B181	A, B, C at B181, from B181 to B184, from B181 to B185	9
IED_B177	AN, BN, CN at B177	A, B, C at B177, from B177 to B179	6

IED_B196	AN, BN, CN at B196; Rotating speed measurement for DG1	A, B, C at B196, into DG1	7
IED_B026	AN, BN, CN at B026	A, B, C at B026, from B026 to B027	6
IED_B103	AN, BN, CN at B103	A, B, C at B103, into the capacitor bank and the load at B103	9
IED_B007	AN, BN, CN at B007	A, B, C at B007, into the capacitor bank and the load at B007	9
IED_B099	AN, BN, CN at B099	A, B, C at B099, into the load at B099	6
IED_B170	AN, BN, CN at B170	A, B, C at B170, into the PV source	6

Table 8.3.5: Measurements of IEDs in Section 2

IED Name	Voltage Channels	Current Channels	# of measurements of this IED
IED_B001	AN, BN, CN at B001; AN, BN, CN at B002	A, B, C from B001 to B002; A, B, C from B002 to B001 (transformer)	12
IED_B107	AN, BN, CN at B107	A, B, C from B107 to B108	6
IED_B121	AN, BN, CN at B121	A, B, C from B121 to B035	6
IED_B068	BN at B068; L1N, L2N at B207	B from B068 to B207; L1, L2 from B068 to B207	6

IED_B036	AN, BN, CN at B036	A, B, C from B036 to B037, from B036 to B084	9
IED_B038	AN, BN, CN at B038	A, B, C from B038 to B039	6
IED_B155	CN at B155; L1N, L2N at B204	C from B155 to B204; L1, L2 from B204 to B155	6
IED_B010	BN at B010; L1N, L2N at B201	B from B010 to B201; L1, L2 from B201 to B010	6
IED_B019	AN, BN, CN at B019 (Non-synchronized)	A, B, C from B019 to B020 (Non-Synchronized)	6

Table 8.3.6: Measurements of IEDs in Section 3

IED Name	Voltage Channels	Current Channels	# of measurements of this IED
IED_B119	AN, BN, CN at B119	A, B, C from B119 to B120	6
IED_B093	AN, BN, CN at B093; AN, BN, CN at B199	A, B, C from B093 to B199; A, B, C from B199 to B093 (transformer)	12
IED_B089	AN, BN, CN at B089; AN, BN, CN at B200	A, B, C from B089 to B200; A, B, C from B200 to B089 (transformer)	12
IED_B076	CN at B076; L1N, L2N at B202	C from B076 to B202; L1, L2 from B202 to B076	6
IED_B106	CN at B106; L1N, L2N at B205	C from B106 to B205; L1, L2 from B205 to B106	6
IED_B166	AN, BN, CN at B166; Rotating speed measurement for DG2	A, B, C at B166 (into DG2)	7
IED_B169	AN at B169;	A from B169 to B210;	6

	L1N, L2N at B210	L1, L2 from B210 to B169	
IED_B150	CN at B150; L1N, L2N at B203	C from B150 to B203; L1, L2 from B203 to B150	6
IED_B079	CN at B079; L1N, L2N at B215	C from B079 to B215; L1, L2 from B215 to B079	6
IED_B082	AN, BN, CN at B082; AN, BN, CN at B206	A, B, C from B082 to B206; A, B, C from B206 to B082 (transformer)	12
IED_B118	BN at B118; L1N, L2N at B214	B from B118 to B214; L1, L2 from B214 to B118	6
IED_B112	AN, BN, CN at B112	A, B, C at B112 (into the PV source)	6
IED_B133	AN, BN, CN at B133; AN, BN, CN at B213	A, B, C from B133 to B213; A, B, C from B213 to B133 (transformer)	12

Table 8.3.7: Measurements of IEDs in Section 4

IED Name	Voltage Channels	Current Channels	# of measurements of this IED
IED_B137	AN, BN, CN at B137	A, B, C from B137 to B138	6
IED_B130	CN at B130; L1N, L2N at B216	C from B130 to B216; L1, L2 from B216 to B130	6
IED_B157	AN, BN, CN at B157; AN, BN, CN at B212	A, B, C from B157 to B212; A, B, C from B212 to B157 (transformer)	12
IED_B198	AN, BN, CN at B198; AN, BN, CN at B217	A, B, C from B198 to B217; A, B, C from B217 to B198 (transformer)	12

IED_B217	AN, BN, CN at B217	A, B, C at B217 (into the PV source)	6
IED_B092	AN, BN, CN at B092; AN, BN, CN at B208	A, B, C from B092 to B208; A, B, C from B208 to B092 (transformer)	12
IED_B031	AN, BN, CN at B031; AN, BN, CN at B209	A, B, C from B031 to B209; A, B, C from B209 to B031 (transformer)	12
IED_B070	AN, BN, CN at B070; Rotating speed measurement for DG3	A, B, C at B070 (into DG3)	7
IED_B098	AN, BN, CN at B098; AN, BN, CN at B211	A, B, C from B098 to B211; A, B, C from B211 to B098 (transformer)	12

8.3.2.1 State Estimator Setup and Event Creation for Section 1

As shown in Figure 8.3.2, section 1 consists of 43 three-phase distribution lines, five single-phase distribution lines, two capacitor banks, two three-phase loads, one PV source, one distributed generator, and four switches. 13 IEDs are installed in this section. The measurements of these IEDs are described in Table 8.3.4. According to Table 8.3.4, section 1 has 87 phasor measurements and one rotating speed measurement. By splitting a phasor measurement into real and imaginary parts, we have 175 measurements in total. The COMTRADE files for the IEDs in section 1 are created with sampling rate to be 60 samples per second. Since the generated data are very large, we present the data obtained from some specific relays as shown in Figure 8.3.3 and Figure 8.3.4. Figure 8.3.3 presents voltage and current measurements from IED_B196, i.e., voltage and currents of a distributed generator

(DG1). Figure 8.3.4 presents voltage and current measurements from IED_B026 from a distribution line. Notice that since the PVs and loads are not constant throughout the whole event, some dynamics exist during the event.

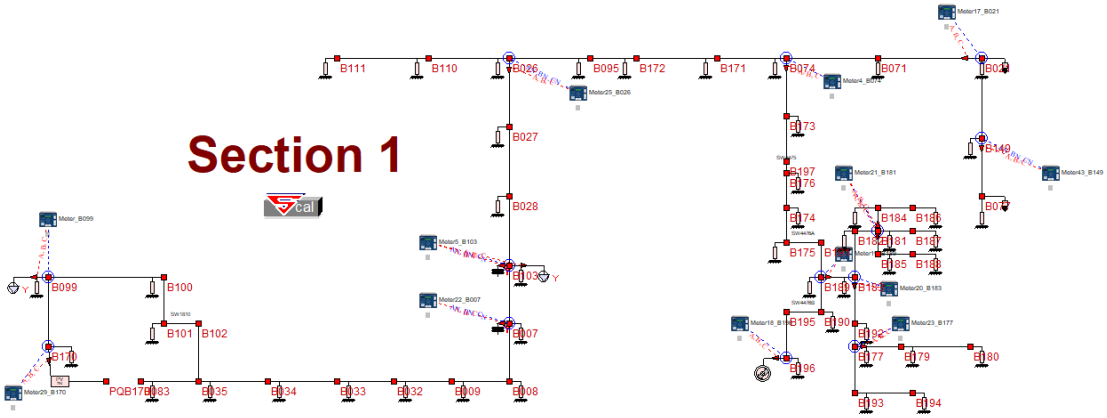

Figure 8.3.2: Section 1 with Installed IEDs and Local State Estimator

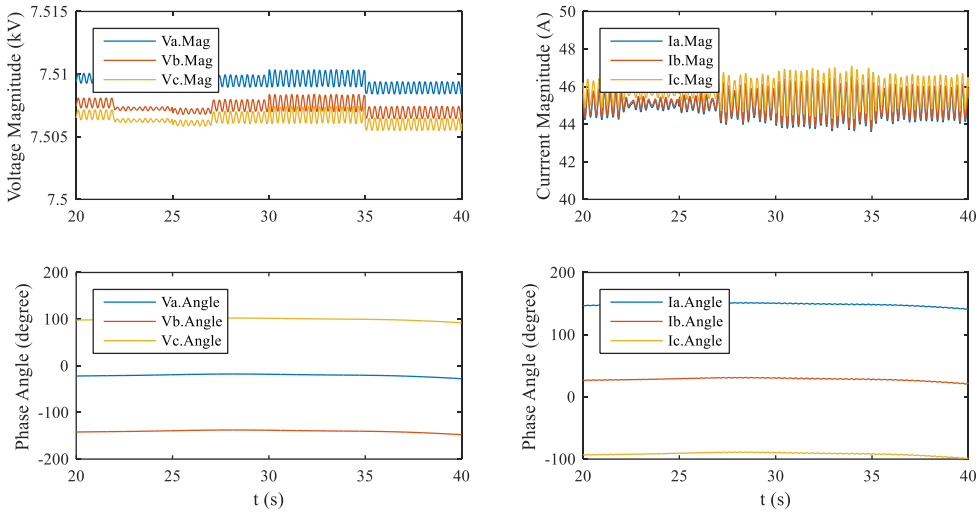

Figure 8.3.3: Voltage and Current Phasor Measurements from IED_B196

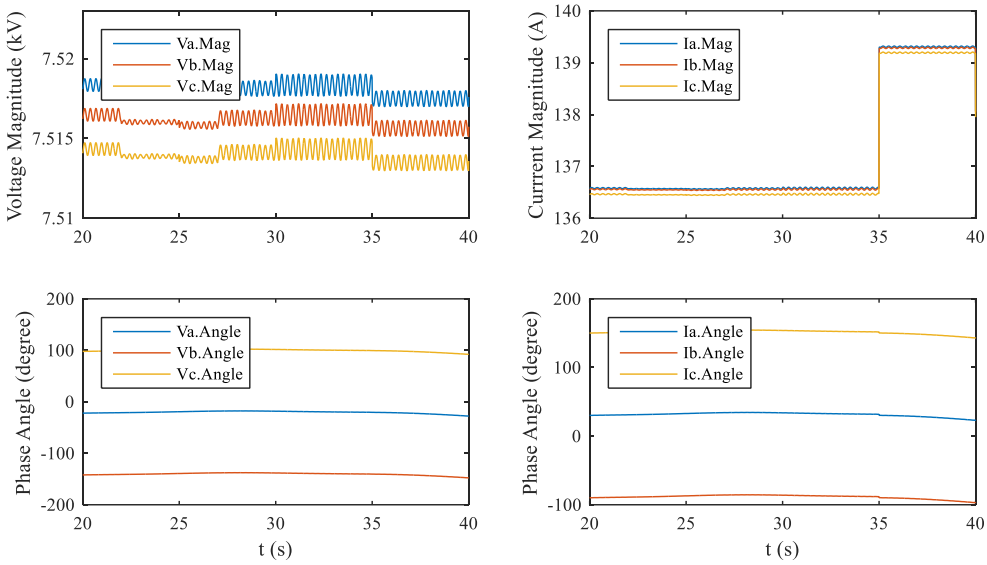

Figure 8.3.4: Voltage and Current Phasor Measurements from IED_B026

8.3.2.2 State Estimator Setup and Event Creation for Section 2

As shown in Figure 8.3.5, section 2 consists of 55 three-phase distribution lines, six single-phase distribution lines, six single-phase loads, one three-phase transformer, three

single-phase transformers with center-tap, and one switch. 9 IEDs are installed in this section. The measurements from these IEDs are described in Table 8.3.5. According to this table, section 2 has 63 phasor measurements. By splitting a phasor measurement into real and imaginary parts, we have 126 measurements in total. The COMTRADE files for the IEDs in section 2 are created with sampling rate to be 60 samples per second. Since the generated data are very large, we present the data obtained from one specific relay as shown in Figure 8.3.6. Figure 8.3.6 presents voltage and current measurements from the secondary side of the transformer between B001 and B002 from IED_B001. Notice that since the PVs and loads are not constant throughout the whole event, some dynamics exist during the event.

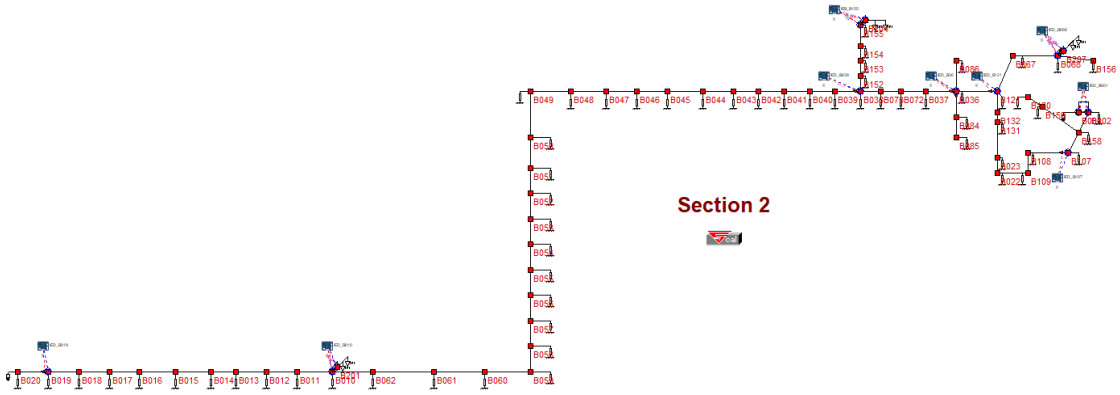

Figure 8.3.5: Section 2 with Installed IEDs and Local State Estimator

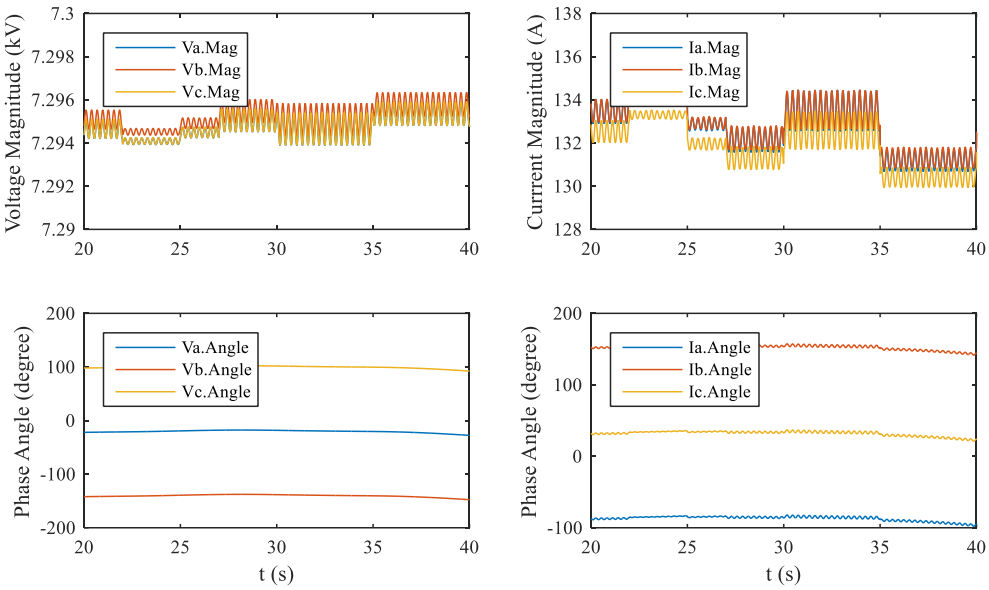

Figure 8.3.6: Voltage and Current Phasor Measurements from IED_B001

8.3.2.3 State Estimator Setup and Event Creation for Section 3

As shown in Figure 8.3.7, section 3 consists of 40 three-phase distribution lines, two single-phase distribution lines, four three-phase loads, 12 single-phase loads, one PV source, one distributed generator, and one switch. 13 IEDs are installed in this section. The measurements from these IEDs are described in Table 8.3.6. According to this table, section 3 has 102 phasor measurements and one rotating speed measurement. By splitting a phasor measurement into real and imaginary parts, we have 205 measurements in total. The COMTRADE files for the IEDs in section 3 are created with sampling rate to be 60 samples per second. Since the generated data are very large, we present the data obtained from some specific relays as shown in Figure 8.3.8 and Figure 8.3.9. Figure 8.3.8 presents voltage and current measurements from IED_B166, i.e., voltage and currents of a

distributed generator (DG2). Figure 8.3.9 presents voltage and current measurements from IED_B119 from a distribution line. Notice that since the PVs and loads are not constant throughout the whole event, some dynamics exist during the event.

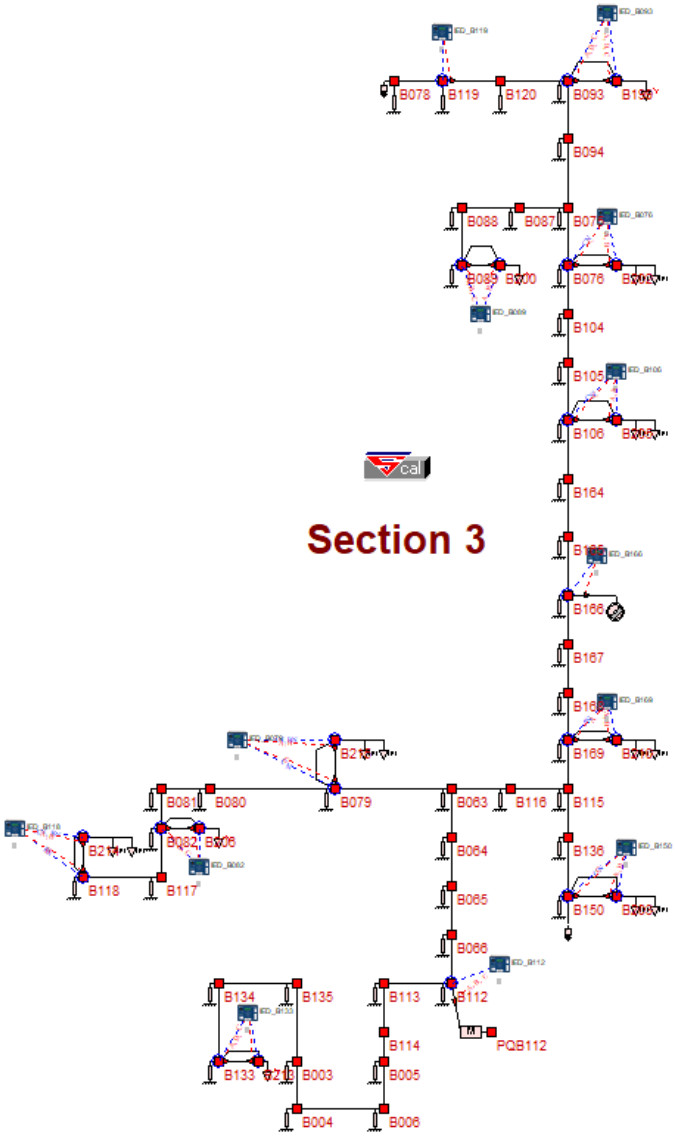

Figure 8.3.7: Section 3 with Installed IEDs and Local State Estimator

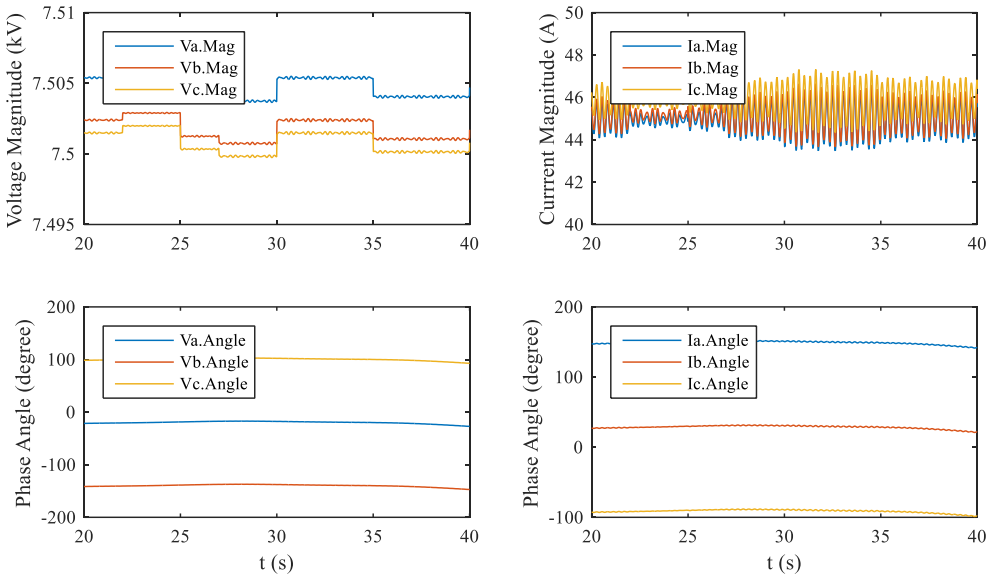

Figure 8.3.8: Voltage and Current Phasor Measurements from IED_B166

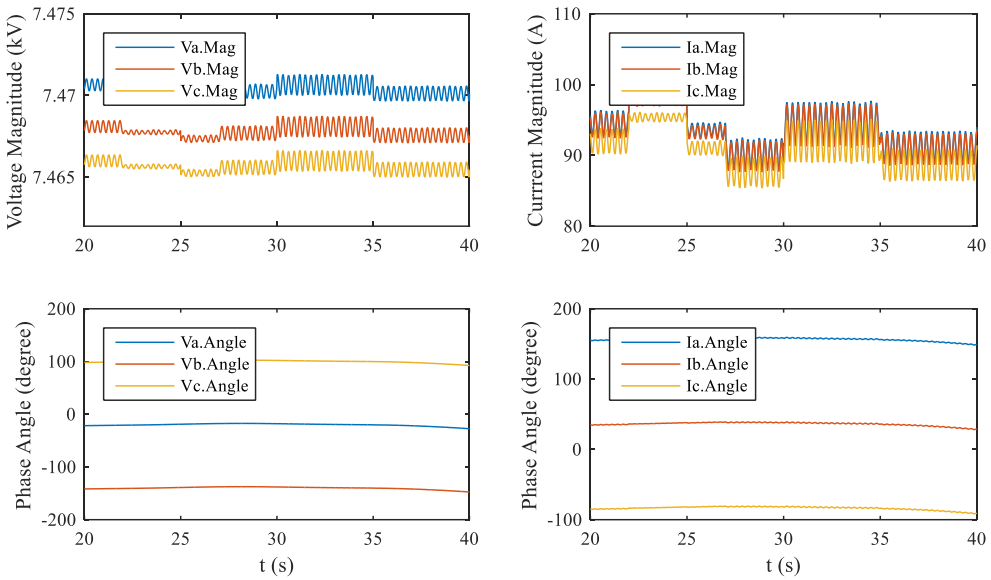

Figure 8.3.9: Voltage and Current Phasor Measurements from IED_B119

8.3.2.4 State Estimator Setup and Event Creation for Section 4

As shown in Figure 8.3.10, section 4 consists of 40 three-phase distribution lines, five three-phase loads, two single-phase loads, five three-phase two-winding transformers, one single-phase transformer with center-tap, one PV source, and one distributed generator. 9 IEDs are installed in this section. The measurements from these IEDs are described in Table 8.3.7. According to this table, section 4 has 84 phasor measurements and one rotating speed measurement. If we split a phasor measurement into real and imaginary parts, we have 169 measurements in total. The COMTRADE files for the IEDs in section 4 are created with sampling rate to be 60 samples per second. Since the generated data are very large, we present the data obtained from a specific relay as shown in Figure 8.3.11. Figure 8.3.11 presents voltage and current measurements from IED_B070, i.e., voltage and currents of a distributed generator (DG3). Notice that since the PVs and loads are not constant throughout the whole event, some dynamics exist during the event.

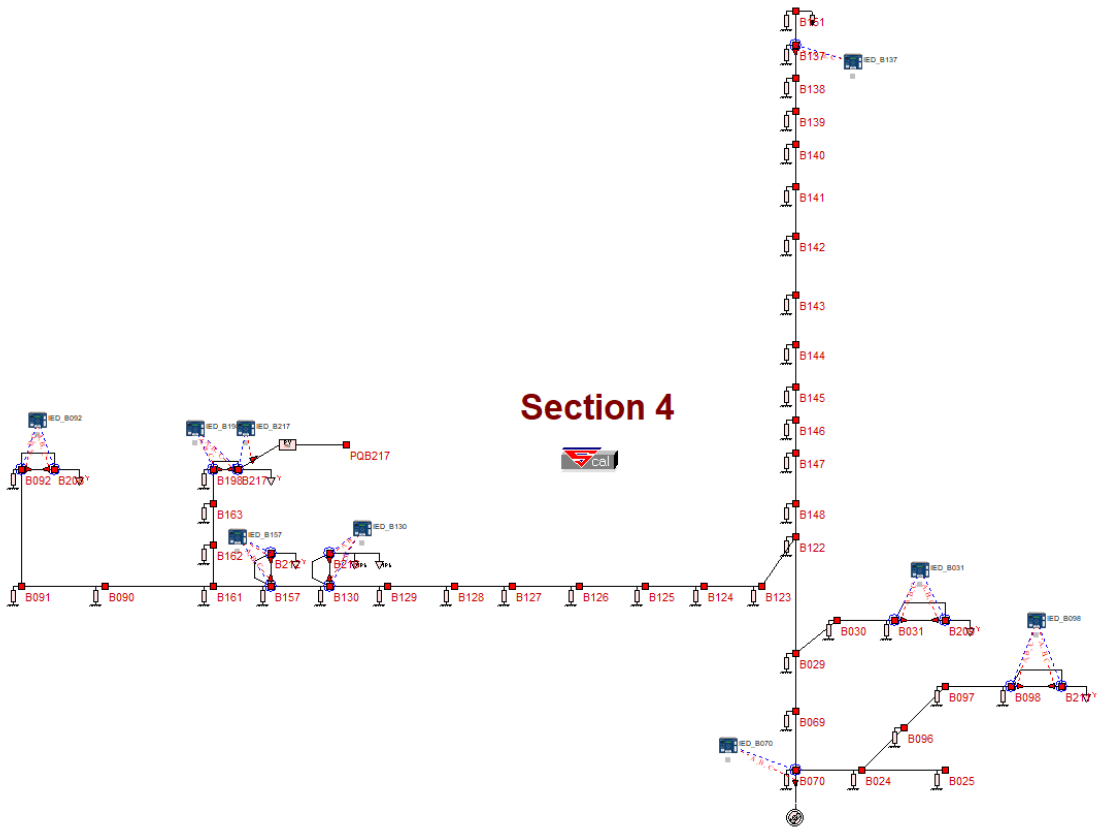

Figure 8.3.10: Section 4 with Installed IEDs and Local State Estimator

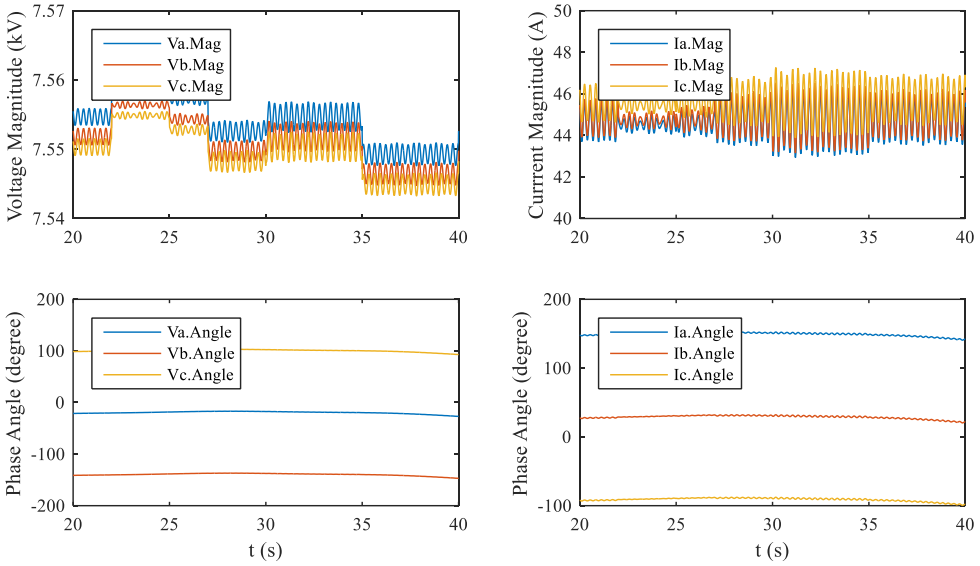

Figure 8.3.11: Voltage and Current Phasor Measurements from IED_B070

8.3.3 State Estimator Results

This subsection presents the state estimation results obtained from the four local state estimators during the event.

8.3.3.1 State Estimation Results of Section 1

In section 1, we have 39 voltage phasor measurements, 48 current phasor measurements, and one rotating speed measurement collected from IEDs. Since the state estimator divides each phasor measurement into real and imaginary parts, we have 175 actual measurements in total. Furthermore, according to Chapter 5, the local state estimator of section 1 automatically creates type I derived, type II derived, pseudo, and virtual measurements: (1) 482 type I derived measurements, (2) 12 type II derived measurements, (3) 94 pseudo measurements, and (4) 12 virtual measurements. In summary, we have 775 measurements at time *t*. Since section 1 consists of 384 states at time *t*, the redundancy is 775/384 = 201.82%.

The local state estimator at section 1 uses section-wise measurements to estimate the states of the whole section. Since the generated data are very large in size, we depict the state estimation results by some specific data. Figure 8.3.12 presents the current actual and estimated phasor measurements from IED_B196. Figure 8.3.13 presents the simulated and estimated rotor position of the monitored distributed generator (DG1). Figure 8.3.14 and Figure 8.3.15 present the actual and estimated voltage and current measurements from IED_B026. These figures indicate that the estimated values track the measurements accurately. Figure 8.3.16 snapshots estimated states of section 1. Figure 8.3.17 snapshots actual/estimated measurements and their differences of all the voltage measurements in

section 1. Notice that all the errors are in small values. In addition, the confidence level of the whole section (when parameter *k* equals to one) remains at 100% during the event, which indicates a strong consistency between the measurements and the system model, i.e., the estimated states of this section are trustworthy, and the system model of this section is validated.

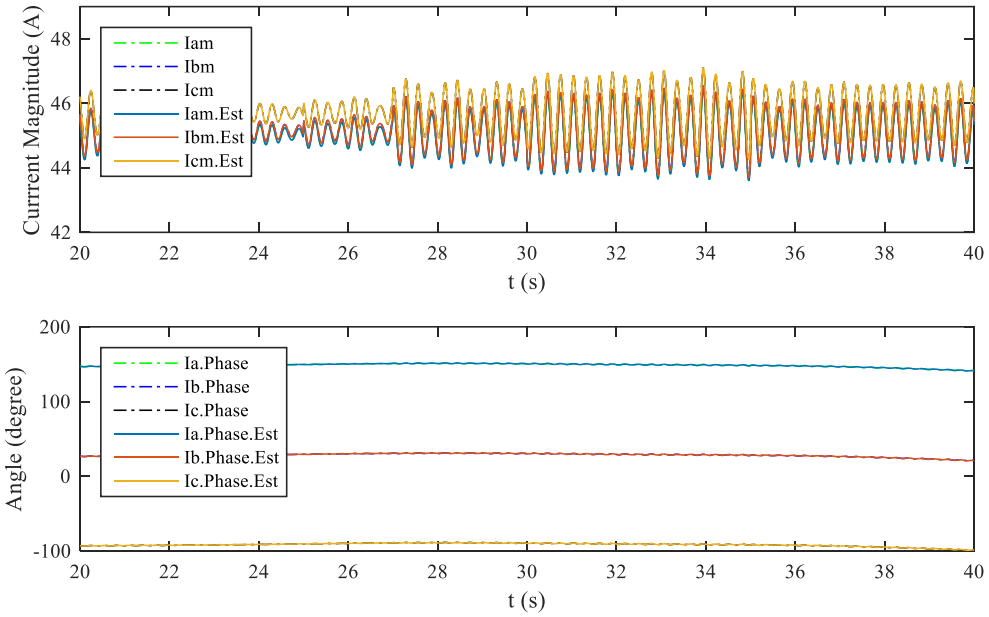

Figure 8.3.12: Actual and Estimated Current Measurements from IED_B196

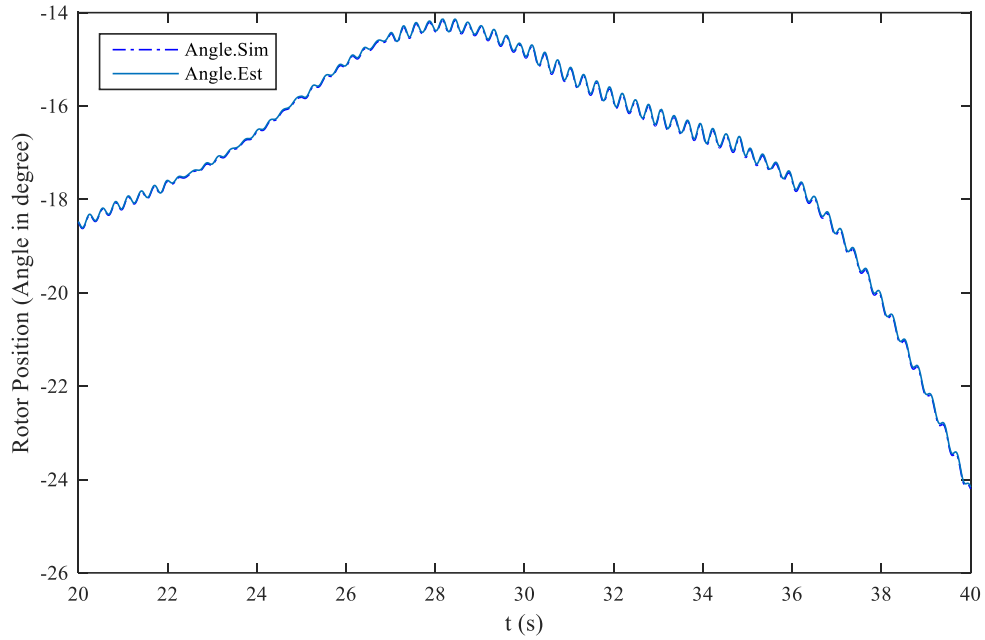

Figure 8.3.13: Simulated and Estimated Rotor Position of DG1

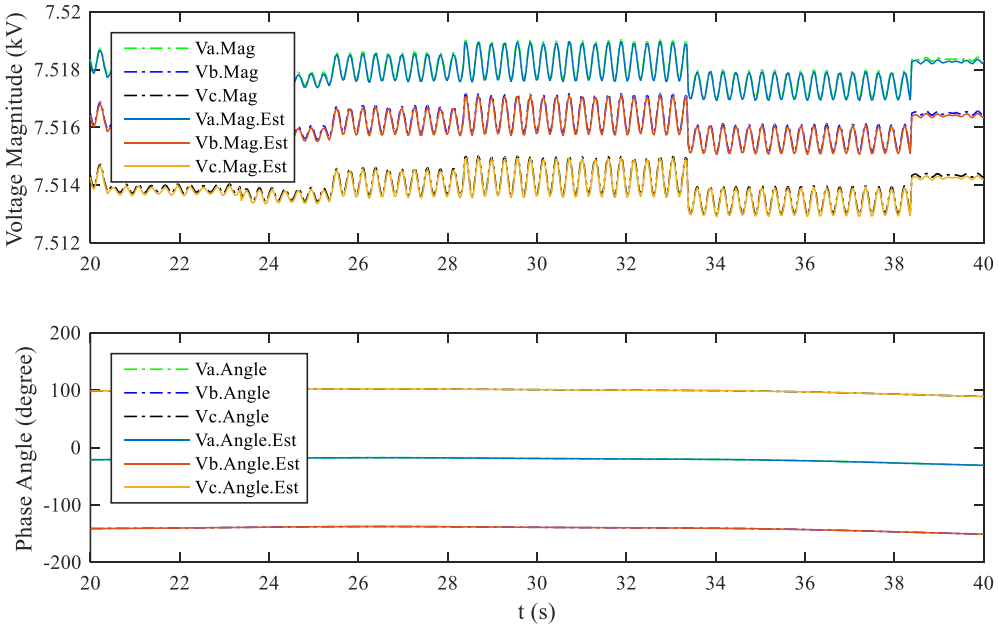

Figure 8.3.14: Actual and Estimated Voltage Measurements from IED_B026

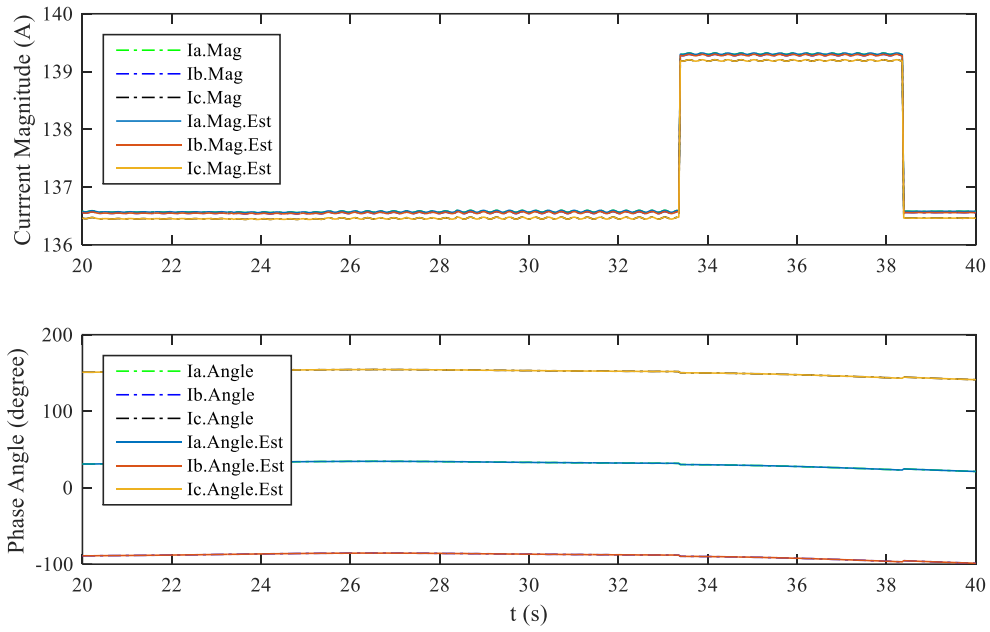

Figure 8.3.15: Actual and Estimated Current Measurements from IED_B026

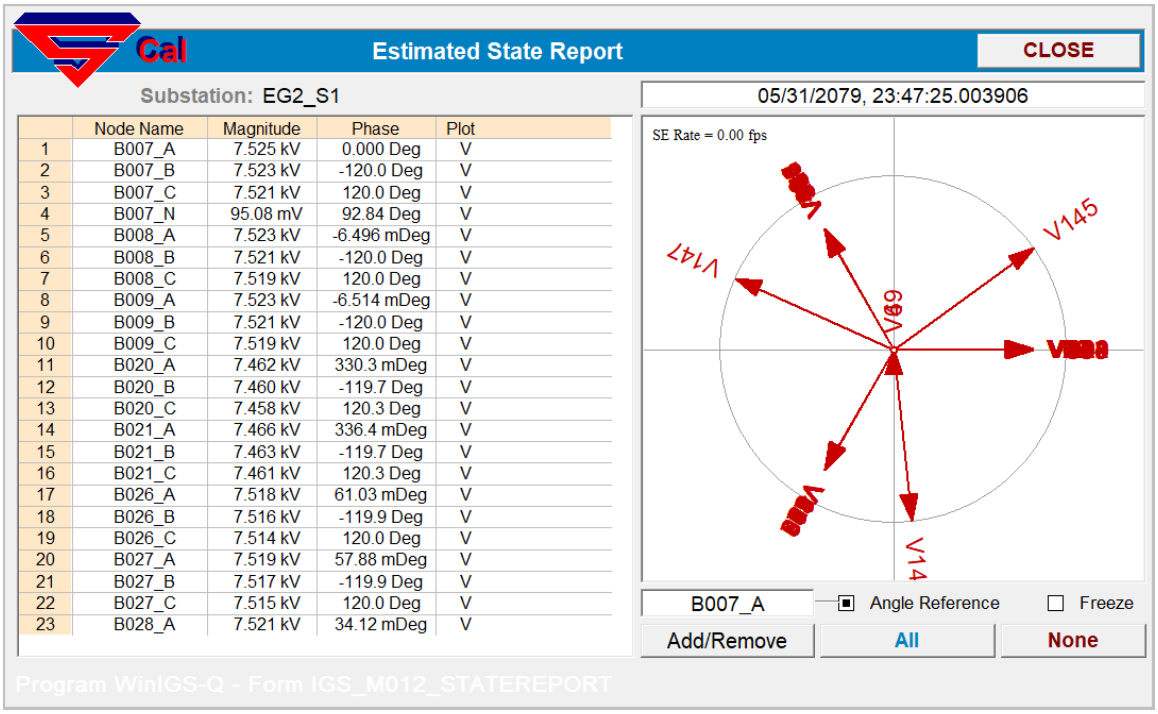

	Node Name	Magnitude	Phase	Plot
1	B007_A	7.525 kV	0.000 Deg	V
2	B007_B	7.523 kV	-120.0 Deg	V
3	B007_C	7.521 kV	120.0 Deg	V
4	B007_N	95.08 mV	92.84 Deg	V
5	B008_A	7.523 kV	-6.496 mDeg	V
6	B008_B	7.521 kV	-120.0 Deg	V
7	B008_C	7.519 kV	120.0 Deg	V
8	B009_A	7.523 kV	-6.514 mDeg	V
9	B009_B	7.521 kV	-120.0 Deg	V
10	B009_C	7.519 kV	120.0 Deg	V
11	B020_A	7.462 kV	330.3 mDeg	V
12	B020_B	7.460 kV	-119.7 Deg	V
13	B020_C	7.458 kV	120.3 Deg	V
14	B021_A	7.466 kV	336.4 mDeg	V
15	B021_B	7.463 kV	-119.7 Deg	V
16	B021_C	7.461 kV	120.3 Deg	V
17	B026_A	7.518 kV	61.03 mDeg	V
18	B026_B	7.516 kV	-119.9 Deg	V
19	B026_C	7.514 kV	120.0 Deg	V
20	B027_A	7.519 kV	57.88 mDeg	V
21	B027_B	7.517 kV	-119.9 Deg	V
22	B027_C	7.515 kV	120.0 Deg	V
23	B028_A	7.521 kV	34.12 mDeg	V

Figure 8.3.16: State Estimator Estimated State Report, Section 1

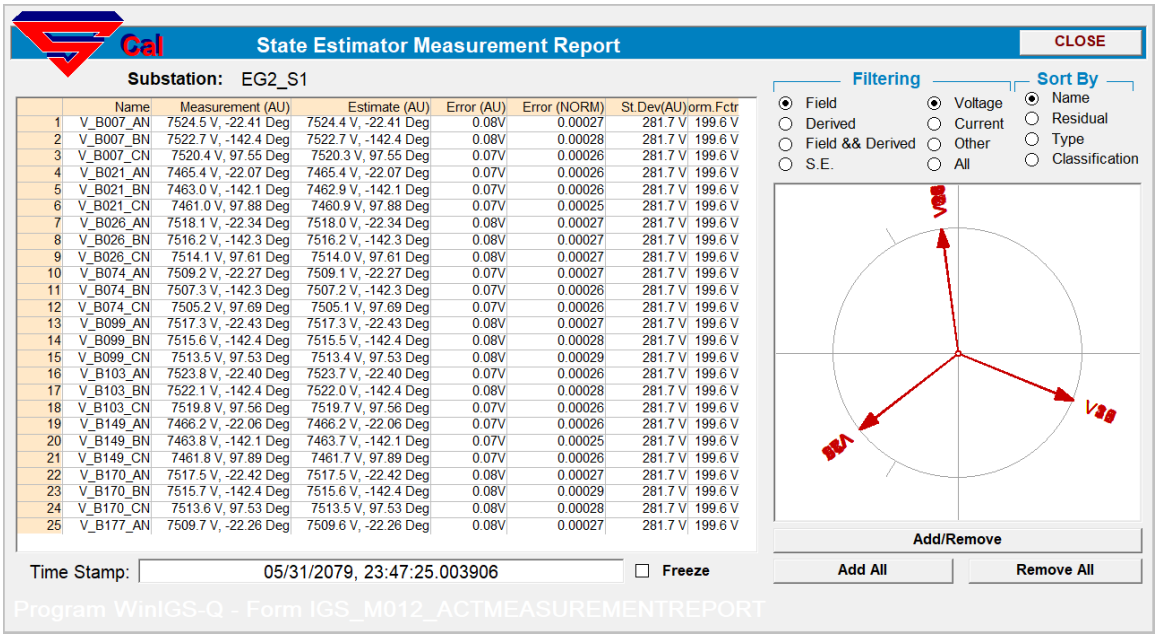

	Name	Measurement (AU)	Estimate (AU)	Error (AU)	Error (NORM)	St.Dev(AU)	orm.Fctr
1	V_B007_AN	7524.5 V, -22.41 Deg	7524.4 V, -22.41 Deg	0.08V	0.00027	281.7 V	199.6 V
2	V_B007_BN	7522.7 V, -142.4 Deg	7522.7 V, -142.4 Deg	0.08V	0.00028	281.7 V	199.6 V
3	V_B007_CN	7520.4 V, 97.55 Deg	7520.3 V, 97.55 Deg	0.07V	0.00026	281.7 V	199.6 V
4	V_B021_AN	7465.4 V, -22.07 Deg	7465.4 V, -22.07 Deg	0.07V	0.00026	281.7 V	199.6 V
5	V_B021_BN	7463.0 V, -142.1 Deg	7462.9 V, -142.1 Deg	0.07V	0.00026	281.7 V	199.6 V
6	V_B021_CN	7461.0 V, 97.88 Deg	7460.9 V, 97.88 Deg	0.07V	0.00025	281.7 V	199.6 V
7	V_B026_AN	7518.1 V, -22.34 Deg	7518.0 V, -22.34 Deg	0.08V	0.00027	281.7 V	199.6 V
8	V_B026_BN	7516.2 V, -142.3 Deg	7516.2 V, -142.3 Deg	0.08V	0.00027	281.7 V	199.6 V
9	V_B026_CN	7514.1 V, 97.61 Deg	7514.0 V, 97.61 Deg	0.08V	0.00027	281.7 V	199.6 V
10	V_B074_AN	7509.2 V, -22.27 Deg	7509.1 V, -22.27 Deg	0.07V	0.00027	281.7 V	199.6 V
11	V_B074_BN	7507.3 V, -142.3 Deg	7507.2 V, -142.3 Deg	0.07V	0.00026	281.7 V	199.6 V
12	V_B074_CN	7505.2 V, 97.69 Deg	7505.1 V, 97.69 Deg	0.07V	0.00026	281.7 V	199.6 V
13	V_B099_AN	7517.3 V, -22.43 Deg	7517.3 V, -22.43 Deg	0.08V	0.00027	281.7 V	199.6 V
14	V_B099_BN	7515.6 V, -142.4 Deg	7515.5 V, -142.4 Deg	0.08V	0.00028	281.7 V	199.6 V
15	V_B099_CN	7513.5 V, 97.53 Deg	7513.4 V, 97.53 Deg	0.08V	0.00029	281.7 V	199.6 V
16	V_B103_AN	7523.8 V, -22.40 Deg	7523.7 V, -22.40 Deg	0.07V	0.00026	281.7 V	199.6 V
17	V_B103_BN	7522.1 V, -142.4 Deg	7522.0 V, -142.4 Deg	0.08V	0.00028	281.7 V	199.6 V
18	V_B103_CN	7519.8 V, 97.56 Deg	7519.7 V, 97.56 Deg	0.07V	0.00026	281.7 V	199.6 V
19	V_B149_AN	7466.2 V, -22.06 Deg	7466.2 V, -22.06 Deg	0.07V	0.00026	281.7 V	199.6 V
20	V_B149_BN	7463.8 V, -142.1 Deg	7463.7 V, -142.1 Deg	0.07V	0.00025	281.7 V	199.6 V
21	V_B149_CN	7461.8 V, 97.89 Deg	7461.7 V, 97.89 Deg	0.07V	0.00026	281.7 V	199.6 V
22	V_B170_AN	7517.5 V, -22.42 Deg	7517.5 V, -22.42 Deg	0.08V	0.00027	281.7 V	199.6 V
23	V_B170_BN	7515.7 V, -142.4 Deg	7515.6 V, -142.4 Deg	0.08V	0.00029	281.7 V	199.6 V
24	V_B170_CN	7513.6 V, 97.53 Deg	7513.5 V, 97.53 Deg	0.08V	0.00028	281.7 V	199.6 V
25	V_B177_AN	7509.7 V, -22.26 Deg	7509.6 V, -22.26 Deg	0.08V	0.00027	281.7 V	199.6 V

Figure 8.3.17: State Estimator Voltage Measurement Report, Section 1

8.3.3.2 State Estimation Results of Section 2

In section 2, we have 30 voltage phasor measurements (27 GPS-synchronized, 3 non-synchronized), and 33 current phasor measurements (30 GPS-synchronized, 3 non-synchronized) from IEDs in this section. Since the state estimator divides each phasor measurement into real and imaginary parts, we have 126 actual measurements in total. Furthermore, according to Chapter 5, the state estimator automatically creates type I derived, type II derived, pseudo, and virtual measurements: (1) 684 type I derived measurements, (2) 8 type II derived measurements, (3) 122 pseudo measurements, and (4) 12 virtual measurements. In summary, we have 952 measurements at time *t*. Since section 2 consists of 508 states at time *t*, the redundancy is 952/508 = 187.40%.

The local state estimator at section 2 uses section-wise measurements to estimate the states of the whole section. Since the generated data are very large in size, we depict

the state estimation results by some specific data. Figure 8.3.18 presents the actual and estimated non-synchronized voltage measurements from IED_B019 (a non-synchronized IED). Figure 8.3.19 presents the estimated synchronous angle between this non-synchronized IED and the synchronized reference phase angle. Figure 8.3.20 snapshots actual/estimated measurements and their differences of all the voltage measurements in section 2. Notice that all the errors are in small values. In addition, the confidence level of the whole section (when parameter *k* equals to one) remains at 100% during the event. This indicates that the non-synchronous measurements in this section are properly processed and the computed synchronous angle between the non-synchronized IED and the synchronized reference phase angle is estimated accurately. In addition, such high confidence level indicates a strong consistency between the measurements and the system model, i.e., the estimated states of this section are trustworthy, and the system model of this section is validated.

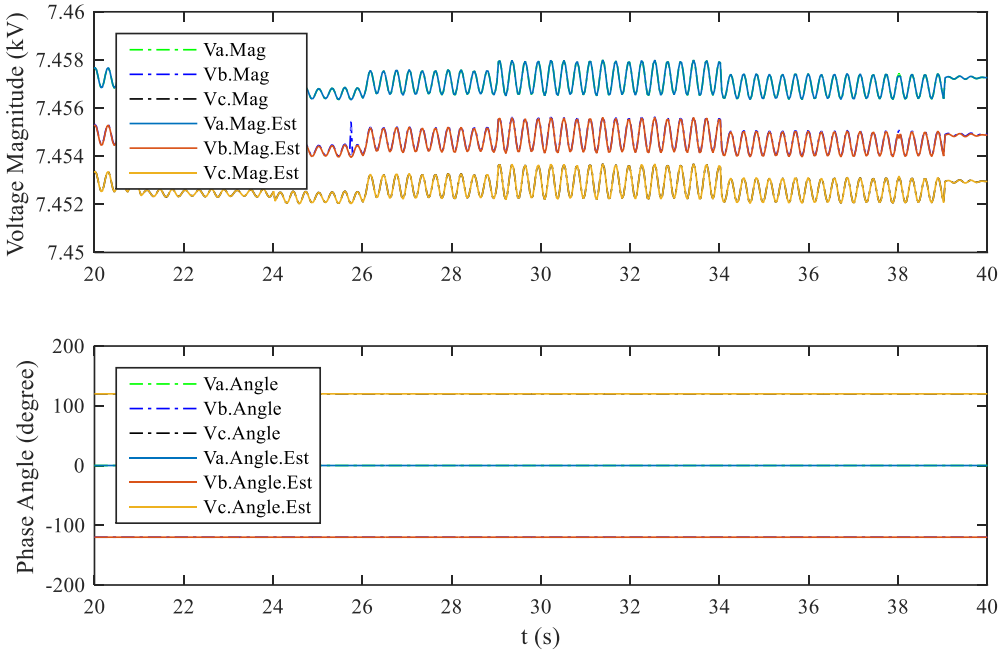

Figure 8.3.18: Actual and Estimated Voltage Measurements from IED_B019

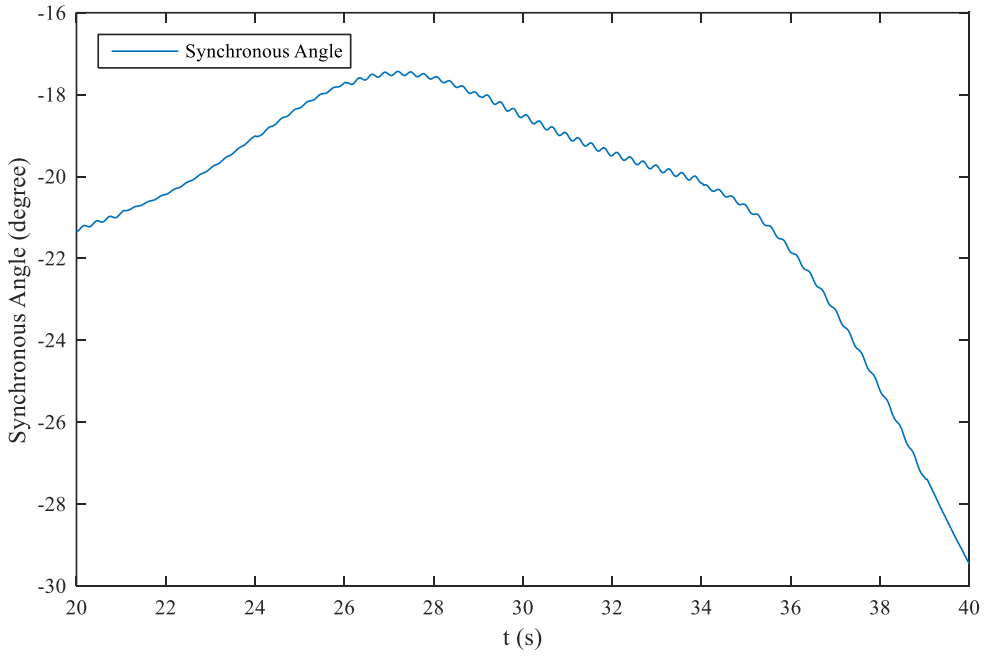

Figure 8.3.19: Estimated Synchronous Phase Angle of IED_B019

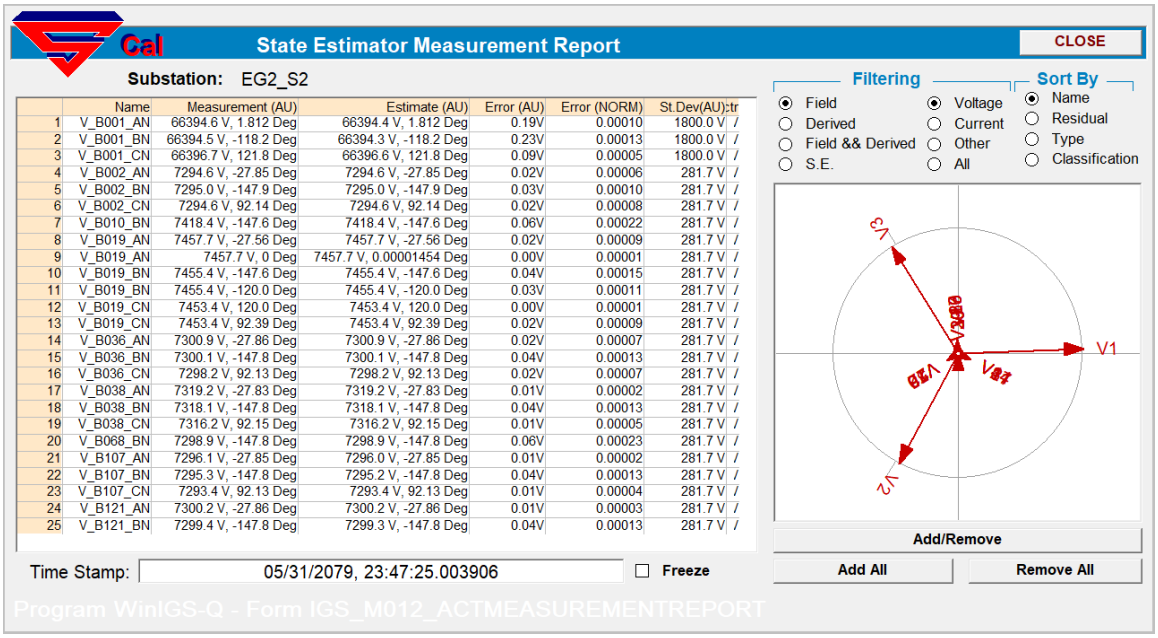

	Name	Measurement (AU)	Estimate (AU)	Error (AU)	Error (NORM)	St.Dev(AU):tr	
1	V_B001_AN	66394.6 V, 1.812 Deg	66394.4 V, 1.812 Deg	0.19V	0.00010	1800.0 V	/
2	V_B001_BN	66394.5 V, -118.2 Deg	66394.3 V, -118.2 Deg	0.23V	0.00013	1800.0 V	/
3	V_B001_CN	66396.7 V, 121.8 Deg	66396.6 V, 121.8 Deg	0.09V	0.00005	1800.0 V	/
4	V_B002_AN	7294.6 V, -27.85 Deg	7294.6 V, -27.85 Deg	0.02V	0.00006	281.7 V	/
5	V_B002_BN	7295.0 V, -147.9 Deg	7295.0 V, -147.9 Deg	0.03V	0.00010	281.7 V	/
6	V_B002_CN	7294.6 V, 92.14 Deg	7294.6 V, 92.14 Deg	0.02V	0.00008	281.7 V	/
7	V_B010_BN	7418.4 V, -147.6 Deg	7418.4 V, -147.6 Deg	0.06V	0.00022	281.7 V	/
8	V_B019_AN	7457.7 V, -27.56 Deg	7457.7 V, -27.56 Deg	0.02V	0.00009	281.7 V	/
9	V_B019_AN	7457.7 V, 0 Deg	7457.7 V, 0.00001454 Deg	0.00V	0.00001	281.7 V	/
10	V_B019_BN	7455.4 V, -147.6 Deg	7455.4 V, -147.6 Deg	0.04V	0.00015	281.7 V	/
11	V_B019_BN	7455.4 V, -120.0 Deg	7455.4 V, -120.0 Deg	0.03V	0.00011	281.7 V	/
12	V_B019_CN	7453.4 V, 120.0 Deg	7453.4 V, 120.0 Deg	0.00V	0.00001	281.7 V	/
13	V_B019_CN	7453.4 V, 92.39 Deg	7453.4 V, 92.39 Deg	0.02V	0.00009	281.7 V	/
14	V_B036_AN	7300.9 V, -27.86 Deg	7300.9 V, -27.86 Deg	0.02V	0.00007	281.7 V	/
15	V_B036_BN	7300.1 V, -147.8 Deg	7300.1 V, -147.8 Deg	0.04V	0.00013	281.7 V	/
16	V_B036_CN	7298.2 V, 92.13 Deg	7298.2 V, 92.13 Deg	0.02V	0.00007	281.7 V	/
17	V_B038_AN	7319.2 V, -27.83 Deg	7319.2 V, -27.83 Deg	0.01V	0.00002	281.7 V	/
18	V_B038_BN	7318.1 V, -147.8 Deg	7318.1 V, -147.8 Deg	0.04V	0.00013	281.7 V	/
19	V_B038_CN	7316.2 V, 92.15 Deg	7316.2 V, 92.15 Deg	0.01V	0.00005	281.7 V	/
20	V_B068_BN	7298.9 V, -147.8 Deg	7298.9 V, -147.8 Deg	0.06V	0.00023	281.7 V	/
21	V_B107_AN	7296.1 V, -27.85 Deg	7296.0 V, -27.85 Deg	0.01V	0.00002	281.7 V	/
22	V_B107_BN	7295.3 V, -147.8 Deg	7295.2 V, -147.8 Deg	0.04V	0.00013	281.7 V	/
23	V_B107_CN	7293.4 V, 92.13 Deg	7293.4 V, 92.13 Deg	0.01V	0.00004	281.7 V	/
24	V_B121_AN	7300.2 V, -27.86 Deg	7300.2 V, -27.86 Deg	0.01V	0.00003	281.7 V	/
25	V_B121_BN	7299.4 V, -147.8 Deg	7299.3 V, -147.8 Deg	0.04V	0.00013	281.7 V	/

Figure 8.3.20: State Estimator Voltage Measurement Report, Section 2

8.3.3.3 State Estimation Results of Section 3

In section 3, we have 51 voltage phasor measurements, 51 current phasor measurements, and one rotating speed measurement from IEDs in this section. Since the state estimator divides each phasor measurement into real and imaginary parts, we have 205 actual measurements in total. Furthermore, according to Chapter 5, the state estimator automatically creates type I derived, type II derived, pseudo, and virtual measurements: (1) 578 type I derived measurements, (2) 40 type II derived measurements, (3) 84 pseudo measurements, and (4) 48 virtual measurements. In summary, we have 955 measurements at time *t*. Since section 3 consists of 456 states at time *t*, the redundancy is 955/456 = 209.43%.

The local state estimator at section 3 uses section-wise measurements to estimate the states of the whole section. Since the generated data are very large in size, we depict

the state estimation results by some specific data. Figure 8.3.21 presents the current actual and estimated phasor measurements from IED_B166. Figure 8.3.22 presents the simulated and estimated rotor position of the monitored distributed generator (DG2). Figure 8.3.23 and Figure 8.3.24 present the actual and estimated voltage and current measurements from IED_B119. These figures indicate that the estimated values track the measurements accurately. Figure 8.3.25 snapshots actual/estimated voltage measurements and their differences in Section 3. Notice that all the errors are in small values. In addition, the confidence level of the whole section (when parameter *k* equals to one) remains at 100% during the event, which indicates a strong consistency between the measurements and the system model, i.e., the estimated states of this section are trustworthy, and the system model of this section is validated.

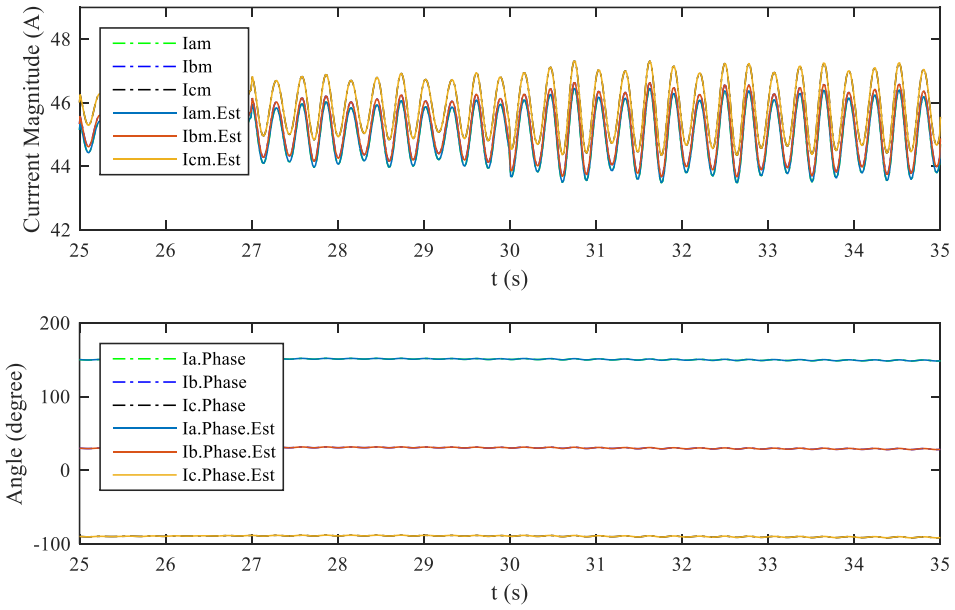

Figure 8.3.21: Actual and Estimated Current Measurements from IED_B166

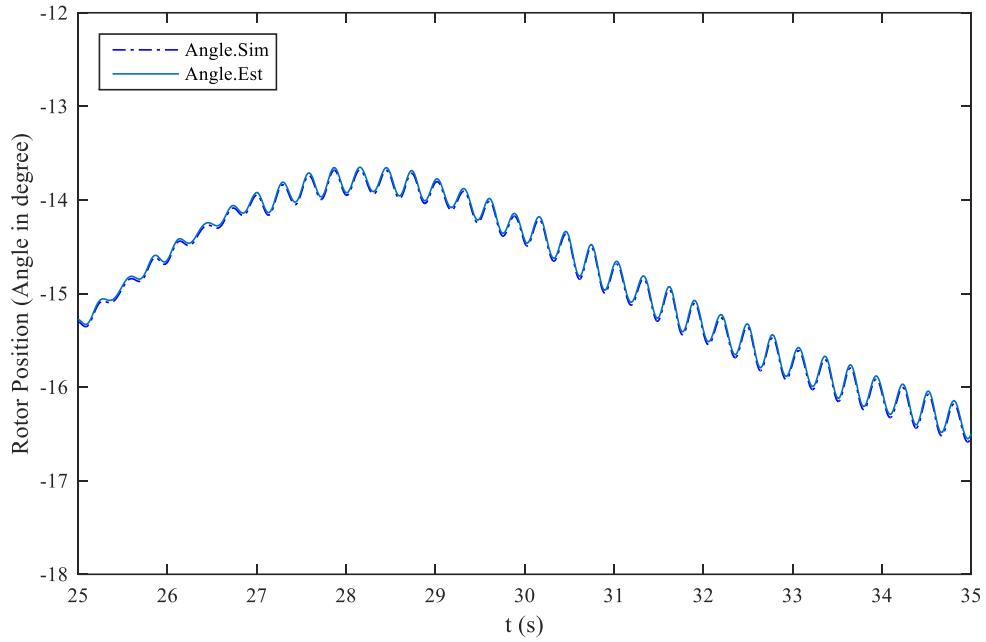

Figure 8.3.22: Simulated and Estimated Rotor Position of DG2

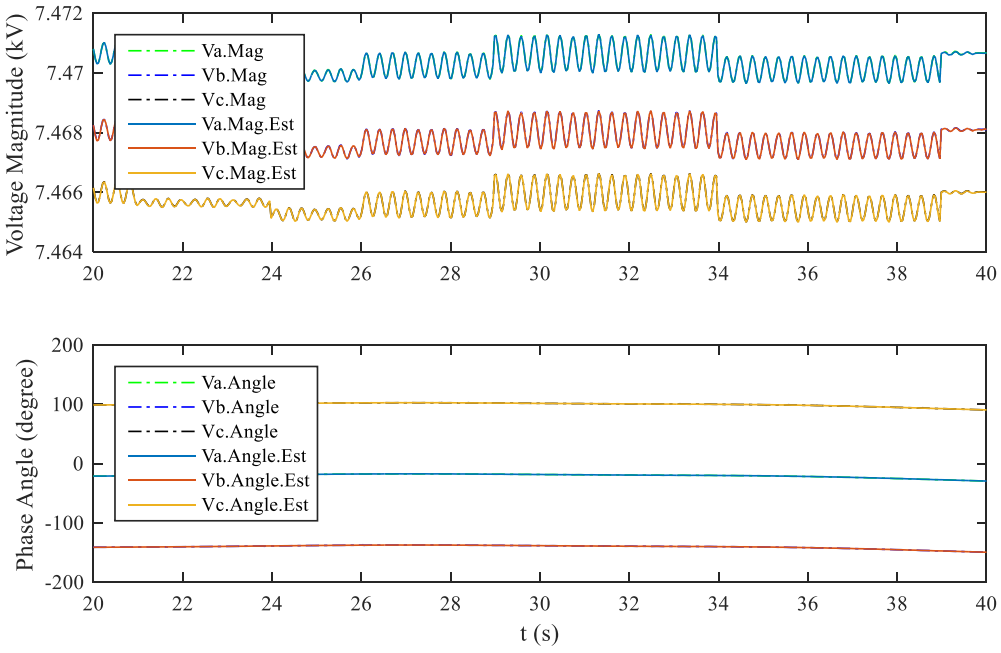

Figure 8.3.23: Actual and Estimated Voltage Measurements from IED_B119

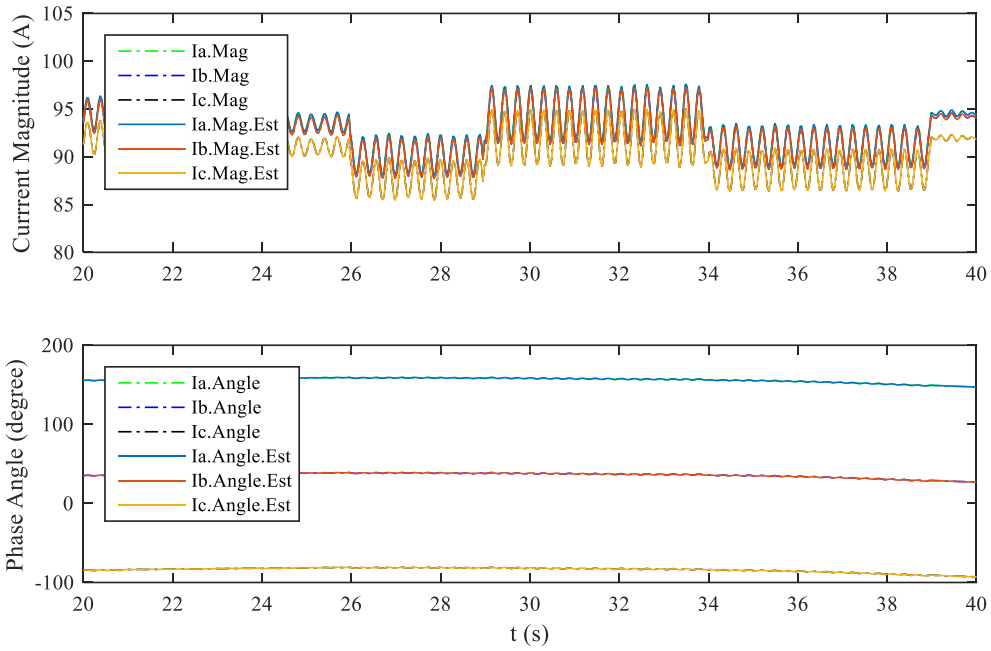

Figure 8.3.24: Actual and Estimated Current Measurements from IED_B119

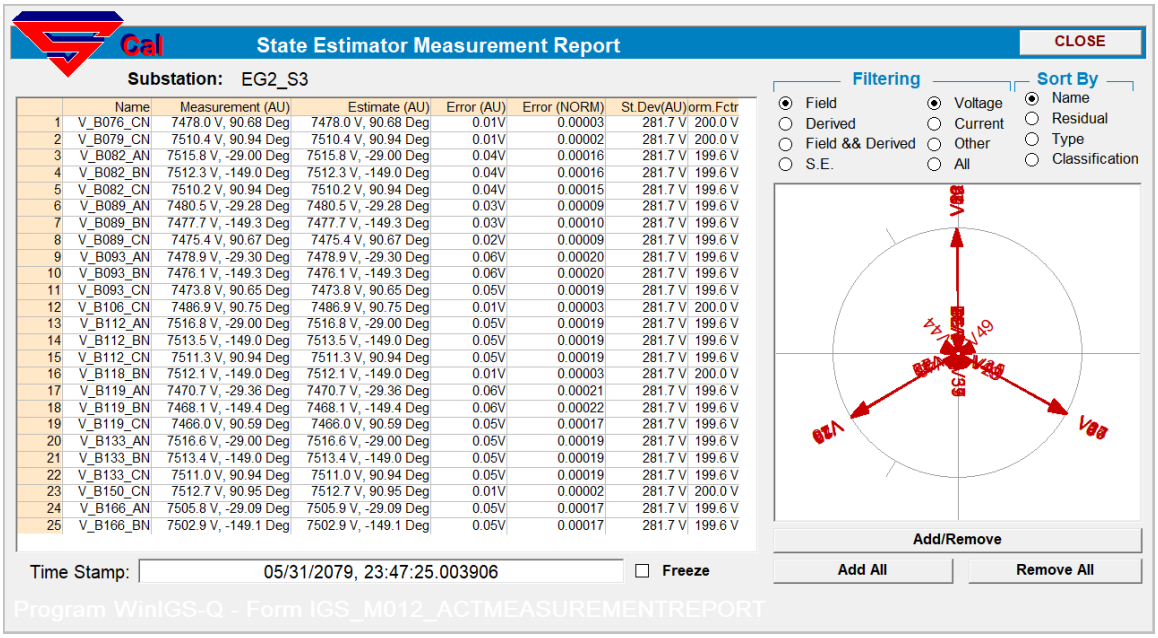

	Name	Measurement (AU)	Estimate (AU)	Error (AU)	Error (NORM)	St.Dev(AU)	orm.Fctr
1	V_B076_CN	7478.0 V, 90.68 Deg	7478.0 V, 90.68 Deg	0.01V	0.00003	281.7 V	200.0 V
2	V_B079_CN	7510.4 V, 90.94 Deg	7510.4 V, 90.94 Deg	0.01V	0.00002	281.7 V	200.0 V
3	V_B082_AN	7515.8 V, -29.00 Deg	7515.8 V, -29.00 Deg	0.04V	0.00016	281.7 V	199.6 V
4	V_B082_BN	7512.3 V, -149.0 Deg	7512.3 V, -149.0 Deg	0.04V	0.00016	281.7 V	199.6 V
5	V_B082_CN	7510.2 V, 90.94 Deg	7510.2 V, 90.94 Deg	0.04V	0.00015	281.7 V	199.6 V
6	V_B089_AN	7480.5 V, -29.28 Deg	7480.5 V, -29.28 Deg	0.03V	0.00009	281.7 V	199.6 V
7	V_B089_BN	7477.7 V, -149.3 Deg	7477.7 V, -149.3 Deg	0.03V	0.00010	281.7 V	199.6 V
8	V_B089_CN	7475.4 V, 90.67 Deg	7475.4 V, 90.67 Deg	0.02V	0.00009	281.7 V	199.6 V
9	V_B093_AN	7478.9 V, -29.30 Deg	7478.9 V, -29.30 Deg	0.06V	0.00020	281.7 V	199.6 V
10	V_B093_BN	7476.1 V, -149.3 Deg	7476.1 V, -149.3 Deg	0.06V	0.00020	281.7 V	199.6 V
11	V_B093_CN	7473.8 V, 90.65 Deg	7473.8 V, 90.65 Deg	0.05V	0.00019	281.7 V	199.6 V
12	V_B106_CN	7486.9 V, 90.75 Deg	7486.9 V, 90.75 Deg	0.01V	0.00003	281.7 V	200.0 V
13	V_B112_AN	7516.8 V, -29.00 Deg	7516.8 V, -29.00 Deg	0.05V	0.00019	281.7 V	199.6 V
14	V_B112_BN	7513.5 V, -149.0 Deg	7513.5 V, -149.0 Deg	0.05V	0.00019	281.7 V	199.6 V
15	V_B112_CN	7511.3 V, 90.94 Deg	7511.3 V, 90.94 Deg	0.05V	0.00019	281.7 V	199.6 V
16	V_B118_BN	7512.1 V, -149.0 Deg	7512.1 V, -149.0 Deg	0.01V	0.00003	281.7 V	200.0 V
17	V_B119_AN	7470.7 V, -29.36 Deg	7470.7 V, -29.36 Deg	0.06V	0.00021	281.7 V	199.6 V
18	V_B119_BN	7468.1 V, -149.4 Deg	7468.1 V, -149.4 Deg	0.06V	0.00022	281.7 V	199.6 V
19	V_B119_CN	7466.0 V, 90.59 Deg	7466.0 V, 90.59 Deg	0.05V	0.00017	281.7 V	199.6 V
20	V_B133_AN	7516.6 V, -29.00 Deg	7516.6 V, -29.00 Deg	0.05V	0.00019	281.7 V	199.6 V
21	V_B133_BN	7513.4 V, -149.0 Deg	7513.4 V, -149.0 Deg	0.05V	0.00019	281.7 V	199.6 V
22	V_B133_CN	7511.0 V, 90.94 Deg	7511.0 V, 90.94 Deg	0.05V	0.00019	281.7 V	199.6 V
23	V_B150_CN	7512.7 V, 90.95 Deg	7512.7 V, 90.95 Deg	0.01V	0.00002	281.7 V	200.0 V
24	V_B166_AN	7505.8 V, -29.09 Deg	7505.9 V, -29.09 Deg	0.05V	0.00017	281.7 V	199.6 V
25	V_B166_BN	7502.9 V, -149.1 Deg	7502.9 V, -149.1 Deg	0.05V	0.00017	281.7 V	199.6 V

Figure 8.3.25: State Estimator Voltage Measurement Report, Section 3

8.3.3.4 State Estimation Results of Section 4

In section 4, we have 42 voltage phasor measurements, and 42 current phasor measurements, and one rotating speed measurement from IEDs in this section. Since the state estimator divides each phasor measurement into real and imaginary parts, we have 169 actual measurements in total. Furthermore, according to Chapter 5, the state estimator automatically creates type I derived, type II derived, pseudo, and virtual measurements: (1) 514 type I derived measurements, (2) 36 type II derived measurements, (3) 80 pseudo measurements, and (4) 44 virtual measurements. In summary, we have 843 measurements at time *t*. Since section 4 consists of 416 states at time *t*, the redundancy is 843/416 = 202.64%.

The local state estimator at section 4 uses section-wise measurements to estimate the states of the whole section. Since the generated data are very large in size, we depict the state estimation results by some specific data. Figure 8.3.26 presents the voltage actual and estimated phasor measurements from IED_B070. Figure 8.3.27 depicts the simulated and estimated rotor position of the monitored distributed generator (DG3). Figure 8.3.28 and Figure 8.3.29 present the actual and estimated voltage and current measurements from IED_B137. These figures indicate that the estimated values track the measurements accurately. Figure 8.3.30 snapshots actual/estimated voltage measurements and their differences in Section 4. Notice that all the errors are in small values. In addition, the confidence level of the whole section (when parameter *k* equals to one) remains at 100% during the event, which indicates a strong consistency between the measurements and the system model, i.e., the estimated states of this section are trustworthy, and the system model of this section is validated.

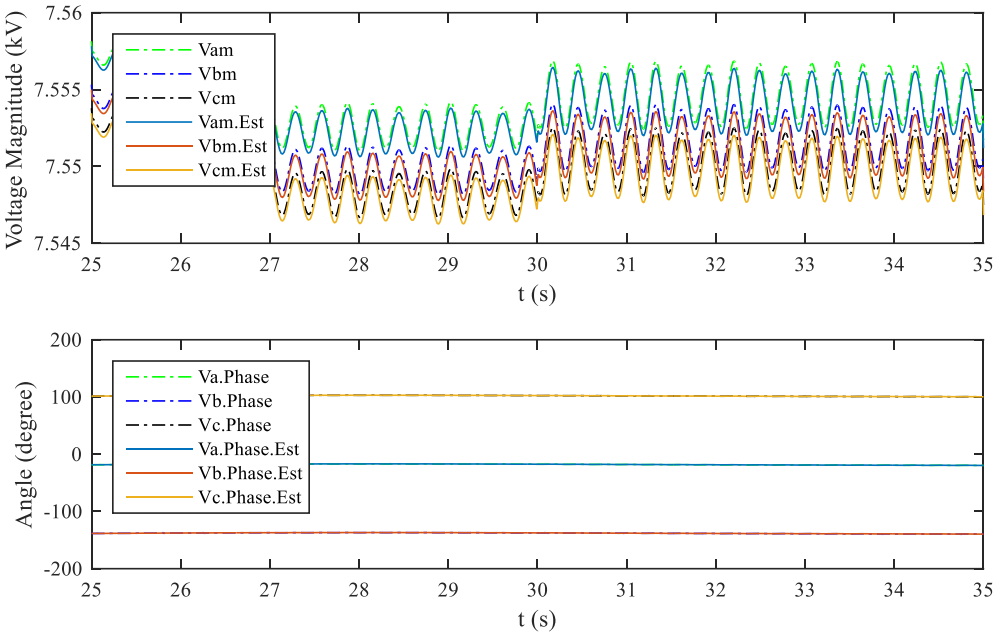

Figure 8.3.26: Actual and Estimated Current Measurements from IED_B070

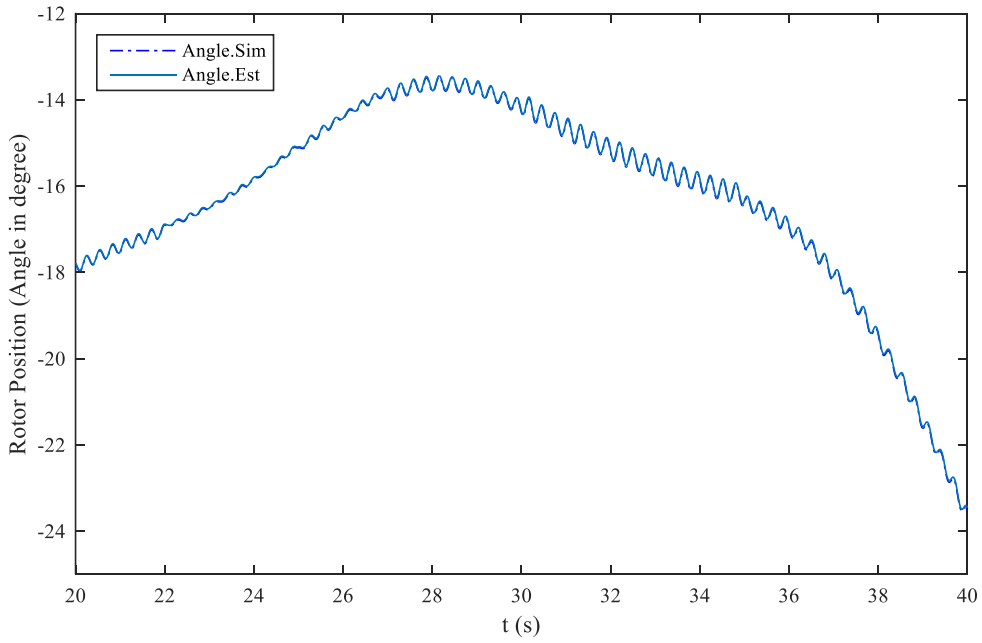

Figure 8.3.27: Simulated and Estimated Rotor Position of DG3

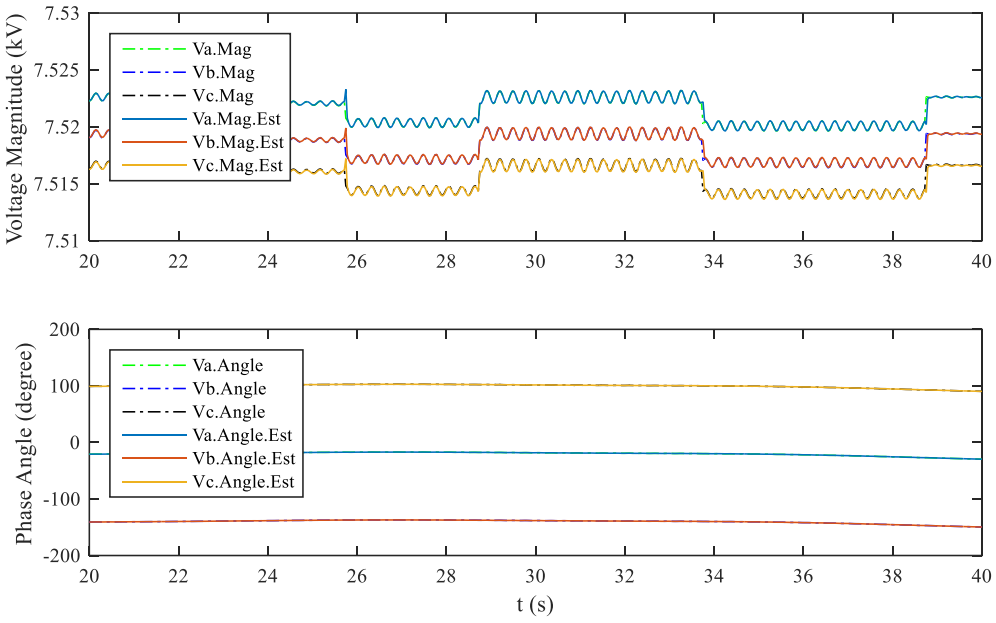

Figure 8.3.28: Actual and Estimated Voltage Measurements from IED_B137

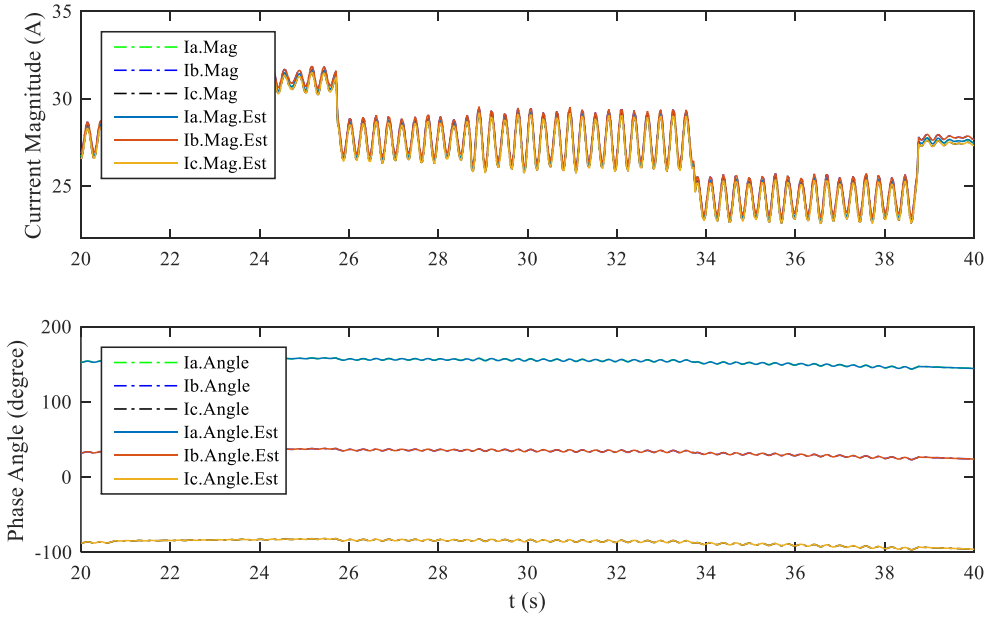

Figure 8.3.29: Actual and Estimated Current Measurements from IED_B137

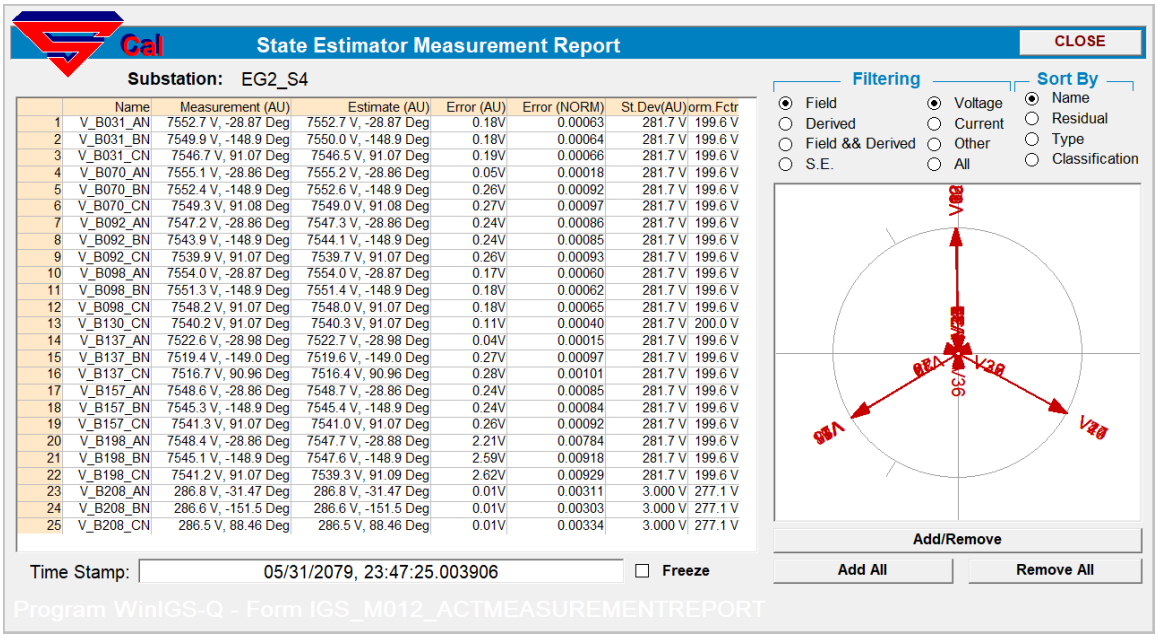

	Name	Measurement (AU)	Estimate (AU)	Error (AU)	Error (NORM)	St.Dev(AU)	orm.Fctr
1	V_B031_AN	7552.7 V, -28.87 Deg	7552.7 V, -28.87 Deg	0.18V	0.00063	281.7 V	199.6 V
2	V_B031_BN	7549.9 V, -148.9 Deg	7550.0 V, -148.9 Deg	0.18V	0.00064	281.7 V	199.6 V
3	V_B031_CN	7546.7 V, 91.07 Deg	7546.5 V, 91.07 Deg	0.19V	0.00066	281.7 V	199.6 V
4	V_B070_AN	7555.1 V, -28.86 Deg	7555.2 V, -28.86 Deg	0.05V	0.00018	281.7 V	199.6 V
5	V_B070_BN	7552.4 V, -148.9 Deg	7552.6 V, -148.9 Deg	0.26V	0.00092	281.7 V	199.6 V
6	V_B070_CN	7549.3 V, 91.08 Deg	7549.0 V, 91.08 Deg	0.27V	0.00097	281.7 V	199.6 V
7	V_B092_AN	7547.2 V, -28.86 Deg	7547.3 V, -28.86 Deg	0.24V	0.00086	281.7 V	199.6 V
8	V_B092_BN	7543.9 V, -148.9 Deg	7544.1 V, -148.9 Deg	0.24V	0.00085	281.7 V	199.6 V
9	V_B092_CN	7539.9 V, 91.07 Deg	7539.7 V, 91.07 Deg	0.26V	0.00093	281.7 V	199.6 V
10	V_B098_AN	7554.0 V, -28.87 Deg	7554.0 V, -28.87 Deg	0.17V	0.00060	281.7 V	199.6 V
11	V_B098_BN	7551.3 V, -148.9 Deg	7551.4 V, -148.9 Deg	0.18V	0.00062	281.7 V	199.6 V
12	V_B098_CN	7548.2 V, 91.07 Deg	7548.0 V, 91.07 Deg	0.18V	0.00065	281.7 V	199.6 V
13	V_B130_CN	7540.2 V, 91.07 Deg	7540.3 V, 91.07 Deg	0.11V	0.00040	281.7 V	200.0 V
14	V_B137_AN	7522.6 V, -28.98 Deg	7522.7 V, -28.98 Deg	0.04V	0.00015	281.7 V	199.6 V
15	V_B137_BN	7519.4 V, -149.0 Deg	7519.6 V, -149.0 Deg	0.27V	0.00097	281.7 V	199.6 V
16	V_B137_CN	7516.7 V, 90.96 Deg	7516.4 V, 90.96 Deg	0.28V	0.00101	281.7 V	199.6 V
17	V_B157_AN	7548.6 V, -28.86 Deg	7548.7 V, -28.86 Deg	0.24V	0.00085	281.7 V	199.6 V
18	V_B157_BN	7545.3 V, -148.9 Deg	7545.4 V, -148.9 Deg	0.24V	0.00084	281.7 V	199.6 V
19	V_B157_CN	7541.3 V, 91.07 Deg	7541.0 V, 91.07 Deg	0.26V	0.00092	281.7 V	199.6 V
20	V_B198_AN	7548.4 V, -28.86 Deg	7547.7 V, -28.88 Deg	2.21V	0.00784	281.7 V	199.6 V
21	V_B198_BN	7545.1 V, -148.9 Deg	7547.6 V, -148.9 Deg	2.59V	0.00918	281.7 V	199.6 V
22	V_B198_CN	7541.2 V, 91.07 Deg	7539.3 V, 91.09 Deg	2.62V	0.00929	281.7 V	199.6 V
23	V_B208_AN	286.8 V, -31.47 Deg	286.8 V, -31.47 Deg	0.01V	0.00311	3.000 V	277.1 V
24	V_B208_BN	286.6 V, -151.5 Deg	286.6 V, -151.5 Deg	0.01V	0.00303	3.000 V	277.1 V
25	V_B208_CN	286.5 V, 88.46 Deg	286.5 V, 88.46 Deg	0.01V	0.00334	3.000 V	277.1 V

Figure 8.3.30: State Estimator Voltage Measurement Report, Section 4

8.4 Discussion

This section discusses some issues together with the quasi-dynamic state estimation in this dissertation. Initialization is first discussed in this section. The DS-DQDSE initializes the estimated states and through variables using measurement values if available, or rated values if measurements are not available. This is based on the fact that the estimated variables are always around the measurements or rated values. However, the effect on the state estimation output if the estimated states and through variables are initialized in different values is not discussed, and this section takes it as an opportunity to discuss this issue. To simplify the problem, we investigate the performance of the state estimation on a distributed generator (nonlinear model) in the full feeder model described in Section 8.3, i.e., DG1 at bus B196. The initialized states and through variables are set to 5, 10, and 20 times as large as those set in Section 8.3. For each case, the average chi-

square and the average confidence level (when k=1, described in Section 6.2) for the whole event is computed and listed in Table 8.4.1. According to this table, we can find that the initialization does affect the performance of the state estimation. Specifically, if the initialized variables are set to be unreasonable, for example, 20 times as large as the original values, the average chi-square becomes much larger and as a result, the average confidence level is below 50%. However, if we set the initialized values to reasonable values (i.e., around rated values), the estimated results are satisfying. This discussion further substantiates that the estimated variables should be initialized to reasonable values, as what is designed in DS-DQDSE.

Table 8.4.1: Average Chi-square and Confidence Level of DG1 under Different Initialization Conditions

# of times as large as the original values	1.0	5.0	10.0	20.0
Average chi-square	1.9364	23.1907	106.1723	460.4753
Average confidence level (%)	99.8153	98.8464	93.9485	47.4345

Secondly, as described in Chapter 5, measurements obtained from IEDs are supplemented with derived, virtual, and pseudo measurements, and they together form the network-level measurement model, which is then processed by the quasi-dynamic state estimation. The observability of the state estimation depends on if the rank of the network-level measurement model is equal to the number of the states in this network-level measurement model. Because of these additional types of measurements, the observability of the state estimation is enhanced, and the accuracy of state estimation is improved. In addition, with increasing deployment of smart meters and other grid sensors in the

distribution system, the amount of available measurements is growing. As a consequence, we assume we have sufficient IEDs in the example systems.

Thirdly, the effect of noisy measurements on the performance of state estimation is also investigated in this section. Taking DG1 as an example, we compare the performance of state estimation on DG1 in four cases, i.e., measurements without noise, noise with 0.01 pu standard deviation, noise with 0.02 pu standard deviation, and noise with 0.05 pu standard deviation. The results are listed in Table 8.4.2. Recall that we assume measurements obtained from IEDs are with 0.01 pu measurement errors. According to Table 8.4.2, when the noise with 0.01 pu standard deviation are injected to the measurements, the average confidence level when k=1 is still very high, which indicates that the measurements are consistent with the device model when we set the standard deviation of each measurement to be the same as each real measurement error. However, when 0.02 pu noise are injected to the measurements while k is still equal to one in the chi-square test, the average confidence level goes down to a low level (15.7693%). This is because the state estimator still considers the measurement errors to be 0.01 pu, but they are now 0.02 pu instead. By setting k=2, i.e., we set standard deviation of each measurement to 0.02 pu, the average confidence level goes up again (over 90%), which substantiates the fact that we actually inject 0.02 pu noise to those measurements. A similar case is obtained when we inject 0.05 pu noise to the measurements. Similarly, the average confidence level is very low (i.e., 0%) since the state estimator still considers the measurement errors are 0.01 pu and the measurements with 0.05 pu noise are not consistent with the device model. However, when we set correct standard deviations to the measurements, i.e., k=5, the confidence level rises to a high value (85.3320%), which

substantiates the fact that we actually inject 0.05 pu noise to those measurements. In summary, the performance of state estimation deteriorates when larger noise is injected. However, with the aid of parameterized chi-square test and the knowledge of standard deviation of measurement errors, we are still able to obtain trustworthy results from the state estimator.

Table 8.4.2: Average Confidence Level under Different Noise Level

	No noise	0.01 pu noise	0.02 pu noise		0.05 pu noise	
Parameter *k*	*k*=1	*k*=1	*k*=1	*k*=2	*k*=1	*k*=5
Average confidence level (%)	99.8153	93.0795	15.7693	93.3931	0.0	85.3320

8.5 Summary

This chapter demonstrated the proposed DS-DQDSE using the real feeder model provided by a utility company. The DS-DQDSE is first applied on the reduced feeder model. Then the application of DS-DQDSE on the full feeder model with over 200 buses is presented. The state estimation results show that the proposed DS-DQDSE is able to constantly monitor the operating states of the system including those dynamic states such as the rotor position of distributed generators in a fast rate (60 samples per second). In addition, DS-DQDSE is able to operate on both GPS-synchronized data and non-synchronized data.

CHAPTER 9. CONCLUSION AND FUTURE WORK DIRECTION

9.1 Conclusion

This dissertation proposed and developed an object-oriented distributed quasi-dynamic state estimator for distribution systems. The main contribution of this dissertation include: (1) development of an object-oriented quasi-dynamic domain multi-phase multi-physics detailed device modeling approach so that all the devices in the distribution system are expressed in a unified syntax; (2) development of an object-oriented network-level measurement model creation procedure, given device models and measurements; (3) development of an object-oriented quasi-dynamic state estimation, given network-level measurement model.

The proposed DS-DQDSE performs state estimation for distribution systems in a distributed manner. Specifically, a distribution system is partitioned into several sections with each section installing a local state estimator that only collects section-wise measurements and perform state estimation for the local section. The estimated states and validated model output from each local state estimator are then streamed to a master state estimator where the estimated states and the validated model of the whole distribution system are synthesized. Such architecture accelerates the speed of state estimation, and dramatically reduces the data traffic between IEDs and the DMS.

The infrastructure of the DS-DQDSE is based on the object-oriented high-fidelity modeling approach, which describes the physical properties of a power device model in detail incorporating slow dynamic such as electromechanical transients in the rotor and

controls in DERs. By adopting such modeling approach, all the devices in distribution systems are expressed in a unified syntax. An example of this modeling approach is illustrated in Appendix A (synchronous generator model). To achieve observability and increase redundancy, the measurement set is augmented with derived measurements (type I derived measurements and type II derived measurements), virtual measurements, and pseudo measurements. Given the augmented measurement set and all the device models in a selected network, DS-DQDSE creates the network-level measurement model and the QDSE is executed. The QDSE provides the best estimate of the states, the differences (residuals) between measurements and estimated measurements, and a quantitative probabilistic consistency between the network measurement model and the network model. If an inconsistency occurs, a bad date detection and identification process is performed. The bad data are then removed and QDSE is rerun using the remaining measurements. Finally, the output of each DS-DQDSE for each section is sent to the DMS where the states and the model of the entire distribution system is constructed from the states and model of each section at a specific time stamp, which is referred to as real-time operating conditions and model.

As the conventional state estimator adopts SSE instead of QDSE, a comparison study between QDSE and SSE has been performed and presented in Chapter 7. This example compares the performance between QDSE and SSE on an example power system with several generators. The generators are modeled with turbine, governor, and exciter, which capture the slow dynamics in the generators. Since QDSE considers the full model of the generator incorporating all the slow dynamics in power systems while SSE utilizes simplified frequency domain models without dynamics, QDSE is able to provide more

accurate information (e.g., dynamics in the rotating rotor, etc.) of the monitored power system compared with SSE with the aid of high-sampling rate PMUs.

To illustrate the effectiveness of the proposed DS-DQDSE, a real feeder model provided by a utility company is selected for demonstration in Chapter 8. The proposed DS-DQDSE is first applied on the reduced feeder with 15 buses. Then it is applied on the full feeder model with over 200 buses. The state estimation results show that the proposed DS-DQDSE is able to monitor the operating states of the system including those dynamic states such as rotor position of distributed generators in a fast rate (60 state estimators per second). In addition, DS-DQDSE is able to operate on both GPS-synchronized data and non-synchronized data.

9.2 Future Work Direction

The operating state and validated model of the monitored system enable the optimal control platform to issue a more economic and reliable control command to the distribution system. By leveraging the developed DS-DQDSE, a closed loop can be formed starting from the sensors across the distribution system and ending with the optimal control command issued by the distribution system optimal control platform using the operating states and the validated model provided by the DS-DQDSE.

In addition, DS-DQDSE offers alternative ways of protecting critical components in the distribution system such as distributed generators by properly using the estimated states provided by DS-DQDSE. As a matter of fact, an out-of-step protection algorithm has been proposed in a substation level distributed quasi-dynamic state estimator in [78], [79]. The basic idea of this protection algorithm is to obtain the internal states (rotor angle, etc.)

of the monitored generator and compute the total energy of this generator after a disturbance occurs. The total energy is then compared with the stability barrier. If the total energy is higher than the barrier, it indicates the monitored generator will not be stable anymore, and a trip decision is issued. The protection algorithm could be further applied in protection of distributed generators.

PUBLICATIONS

1. B. Xie, A. P. S. Meliopoulos, D. Zhao, J. Xie, C. Zhong, O. Vasios and K. Liu, "A Performance Comparison Study of Quasi-Dynamic State Estimation and Static State Estimation," *2020 IEEE Power & Energy Society General Meeting (PESGM)*, Montreal, 2020, pp. 1-5.

2. K. Liu, A. P. S. Meliopoulos, B. Xie, C. Zhong and J. Xie, "Dynamic State Estimation-Based Protection of Distribution Systems with High Penetration of DERs," *2020 IEEE Power & Energy Society General Meeting (PESGM)*, Montreal, 2020, pp. 1-5.

3. J. Xie, A. P. S. Meliopoulos, B. Xie, C. Zhong and K. Liu, "A Reliable Dynamic State Estimation Based Protection during Geomagnetic Disturbances," *2020 IEEE Power & Energy Society General Meeting (PESGM)*, Montreal, 2020, pp. 1-5.

4. D. Lu, Y. Liu, B. Xie, R. Fan and L. Sun, "An Improved Phasor Domain Parameter-Free Fault Location Algorithm on Untransposed Lines," *2020 Transmission and Distribution Conference and Exposition (T&D)*, Chicago, IL, 2020, pp. 1-5.

5. B. Xie, D. Zhao, and T. Hong, “Transformer Monitoring and Protection in Dynamic Power Systems – A Review,” *Front. Energy Res.*, vol. 8, p. 150, Jul. 2020.

6. J. Johnson, A. Summers, R. Darbali-Zamora, C. Hansen, M. J. Reno, A. Castillo, S. Gonzalez, J. Hernandez-Alvidrez, N. S. Gurule, B. Xie, C. Zhong, A. P. Meliopoulos, C. Showalter, T. Rohrer, M. Rupnik, J. Anandan, N. Heine, M. E. Hernandez F., D. Montenegro, T. Tansy, B. Fox, A. Pochiraju, S. Martinez, H. Smith, S. Arafa, J. Woodard, J. Hawkins, P. Rothblum, M. Bintz, P. Chapman, “Optimal distribution system voltage regulation using state estimation and DER grid-support functions,” Sandia Nat. Lab., Albuquerque, NM, USA, SAND2020-2331, Feb. 2020.

7. K. Liu, A. P. S. Meliopoulos, B. Xie, C. Zhong and J. Xie, "Quasi-dynamic domain modeling of line-commutated converters with the analytical approach," *2019 North American Power Symposium (NAPS)*, Wichita, KS, 2019, pp. 1-6.

8. C. Zhong, B. Xie and A. P. S. Meliopoulos, "Distribution network voltage profile optimization via multi-stage flexible optimal power flow," *2019 North American Power Symposium (NAPS)*, Wichita, KS, 2019, pp. 1-6.

9. B. Xie, A. P. S. Meliopoulos, G. Cokkinides, J. Xie, C. Zhong, Y. Liu and T. Prevost, "Dynamic state estimation based unit protection," *2019 IEEE Power & Energy Society General Meeting (PESGM)*, Atlanta, GA, 2019, pp. 1-5.

10. O. Vasios, B. Xie and A. P. S. Meliopoulos, "Estimation based protection of three-phase saturable core transformer for cross-country fault detection," *2019 IEEE Power & Energy Society General Meeting (PESGM)*, Atlanta, GA, 2019, pp. 1-5.

11. J. Xie, A. P. S. Meliopoulos, B. Xie, C. Zhong and K. Liu, "Geoelectric field estimation during geomagnetic disturbances," *2019 IEEE Power & Energy Society General Meeting (PESGM)*, Atlanta, GA, 2019, pp. 1-5.

12. C. Zhong, A. P. S. Meliopoulos, B. Xie, J. Xie, K. Liu and H. Shao, "Detailed Multiphysics Modeling of Air-Conditioned House," *2019 IEEE Power & Energy Society Innovative Smart Grid Technologies Conference (ISGT)*, Washington, DC, USA, 2019, pp. 1-5.

13. S. Meliopoulos, C. Zhong, G. Cokkinides, B. Xie, C. Dalton, P. Myrda and E. Farantatos, "Autonomous multi-stage flexible OPF for active distribution systems with DERs, " *2019 52nd Hawaii International Conference on System Sciences (HICSS)*, Maui, HI, 2019.

14. B. Xie, A. P. S. Meliopoulos, C. Zhong, Y. Liu, L. Sun and J. Xie, "Distributed Quasi-Dynamic State Estimation Incorporating Distributed Energy Resources," *2018 North American Power Symposium (NAPS)*, Fargo, ND, 2018, pp. 1-6.

15. J. Xie, A. P. S. Meliopoulos and B. Xie, "Transmission Line Fault Classification Based on Dynamic State Estimation and Support Vector Machine," *2018 North American Power Symposium (NAPS)*, Fargo, ND, 2018, pp. 1-5.

16. C. Zhong, A. P. Sakis Meliopoulos, J. Sun, M. Saeedifard and B. Xie, "Modeling of Converter Losses with High Fidelity in a Physically Based Object-Oriented Way," *2018 IEEE Power & Energy Society General Meeting (PESGM)*, Portland, OR, 2018, pp. 1-5.

17. C. Zhong, A. P. Sakis Meliopoulos, G. J. Cokkinides and B. Xie, "Object-Oriented Voltage Control for AC-DC Hybrid Distribution Systems," *2018 9th IEEE International Symposium on Power Electronics for Distributed Generation Systems (PEDG)*, Charlotte, NC, 2018, pp. 1-4.

18. G. De Carne, M. Liserre, B. Xie, C. Zhong, S. A. P. Meliopoulos and C. Vournas, "Multiphysics Modelling of Asynchronously-Connected Grids," *2018 Power Systems Computation Conference (PSCC)*, Dublin, 2018, pp. 1-8.

19. J. Johnson, J. Flicker, A. Castillo, C. Hansen, M. El-Khatib, D. Schoenwald, M. A. Smith, R. Graves, J. Henry, T. Hutchins, J. Stamp, D. Hart, A. Chavez, M. Burnett, J. Tabarez, C. Glatter, B. Xie, A. P. Meliopoulos, P. Huynh, H. Zhu, K. Davis, “Design and implementation of a secure virtual power plant,” Sandia Nat. Lab., Albuquerque, NM, USA, SAND2017-10177, Sep. 2017.

20. A.P. Meliopoulos, G. Cokkinides, B. Xie, C. Zhong, and J. Johnson, “Full state feedback control for virtual power plants,” Sandia Nat. Lab., Albuquerque, NM, USA, SAND2017-10178, Sep. 2017.

21. Y. Liu, Y. An and B. Xie, "State estimation based transmission line fault locating with sequence distributed parameter models," *2017 IEEE Conference on Energy Internet and Energy System Integration (EI2)*, Beijing, 2017, pp. 1-6.

22. B. Xie, A. P. S. Meliopoulos, Y. Liu and L. Sun, "Distributed quasi-dynamic state estimation with both GPS-synchronized and non-synchronized data," *2017 North American Power Symposium (NAPS)*, Morgantown, WV, 2017, pp. 1-6.

23. L. Sun, A. P. S. Meliopoulos, Y. Liu and B. Xie, "Dynamic state estimation based synchronous generator model calibration using PMU data," *2017 IEEE Power & Energy Society General Meeting (PESGM)*, Chicago, IL, 2017, pp. 1-5.

24. Y. Liu, S. Meliopoulos, N. Tai, L. Sun and B. Xie, "Protection and fault locating method of series compensated lines by wavelet based energy traveling wave," *2017 IEEE Power & Energy Society General Meeting (PESGM)*, Chicago, IL, 2017, pp. 1-5.

APPENDIX A. QUASI-DYNAMIC DOMAIN MODEL OF GENERATOR

This appendix describes the quasi-dynamic domain model of a synchronous generator with governor, turbine, and exciter. As shown in Figure 9.2.1, a generator model consists of three parts, (1) synchronous generator model, (2) governor and turbine model, and (3) exciter model. The quasi-dynamic domain model of a generator model incorporates all slow dynamics from these components.

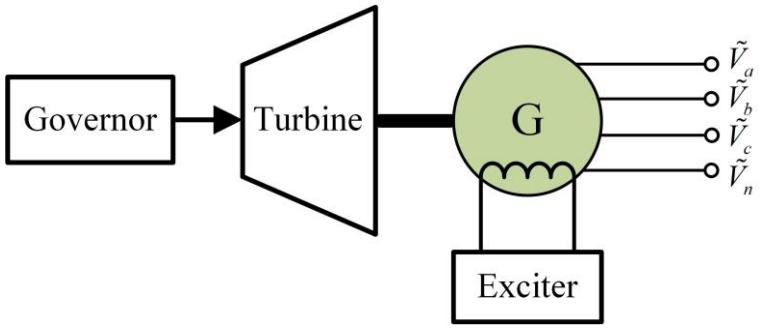

Figure 9.2.1: Generator Model

A.1 Compact Device Model

The quasi-dynamic domain model of a synchronous generator considers the dynamics in the rotor (including its rotating speed and position as shown in equation (A.1.2), power output (A.1.3), and the field winding (A.1.5)) [80]. The compact model equations of the generator part are listed from (A.1.1) to (A.1.5).

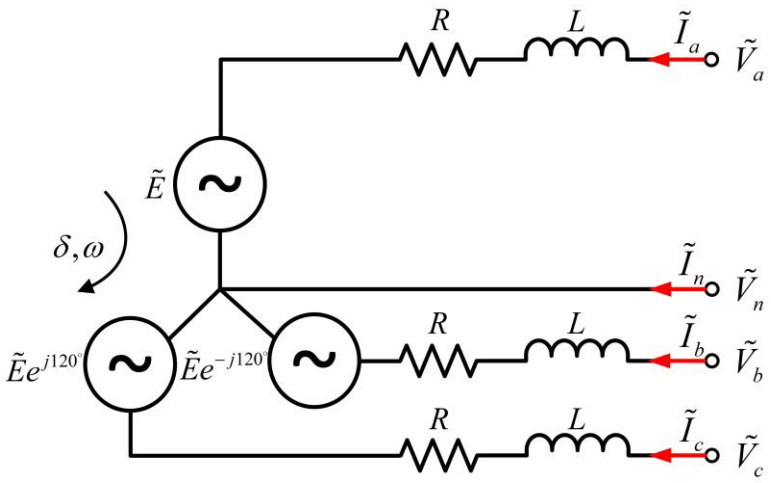

Figure 8.3.3.2: Synchronous Generator Model

$$\begin{bmatrix}\tilde{I}_a\\ \tilde{I}_b\\ \tilde{I}_c\end{bmatrix}=\begin{bmatrix}Y_{aa} & Y_{ab} & Y_{ac}\\ Y_{ba} & Y_{bb} & Y_{bc}\\ Y_{ca} & Y_{cb} & Y_{cc}\end{bmatrix}\begin{bmatrix}\tilde{V}_a-\tilde{V}_n-\tilde{E}_a\\ \tilde{V}_b-\tilde{V}_n-\tilde{E}_b\\ \tilde{V}_c-\tilde{V}_n-\tilde{E}_c\end{bmatrix}=y_{abc}\begin{bmatrix}\tilde{V}_a-\tilde{V}_n-\tilde{E}_a\\ \tilde{V}_b-\tilde{V}_n-\tilde{E}_b\\ \tilde{V}_c-\tilde{V}_n-\tilde{E}_c\end{bmatrix}$$

$$\tilde{I}_n=\begin{bmatrix}-1 & -1 & -1\end{bmatrix}\begin{bmatrix}Y_{aa} & Y_{ab} & Y_{ac}\\ Y_{ba} & Y_{bb} & Y_{bc}\\ Y_{ca} & Y_{cb} & Y_{cc}\end{bmatrix}\begin{bmatrix}\tilde{V}_a-\tilde{V}_n-\tilde{E}_a\\ \tilde{V}_b-\tilde{V}_n-\tilde{E}_b\\ \tilde{V}_c-\tilde{V}_n-\tilde{E}_c\end{bmatrix}=\begin{bmatrix}-1 & -1 & -1\end{bmatrix}y_{abc}\begin{bmatrix}\tilde{V}_a-\tilde{V}_n-\tilde{E}_a\\ \tilde{V}_b-\tilde{V}_n-\tilde{E}_b\\ \tilde{V}_c-\tilde{V}_n-\tilde{E}_c\end{bmatrix} \quad \text{(A.1.1)}$$

$$0=\frac{d\delta}{dt}-\omega+\omega_0 \quad \text{(A.1.2)}$$

$$0=-\frac{2\cdot H\cdot S}{\omega_{m0}^2}\cdot\frac{d\omega_m}{dt}\cdot\omega_m+\mathrm{Re}\left(\tilde{E}_a\tilde{I}_a^*+\tilde{E}_b\tilde{I}_b^*+\tilde{E}_c\tilde{I}_c^*\right)+P_{m,G} \quad \text{(A.1.3)}$$

$$0=i_{fd,G}-\frac{\sqrt{2}E}{\omega M_f} \quad \text{(A.1.4)}$$

$$0=-V_{fd}+L_f\frac{di_{fd,G}}{dt}+R_f i_{fd,G} \quad \text{(A.1.5)}$$

where $\tilde{E}_a=Ee^{j\delta}$, $\tilde{E}_b=\tilde{E}_a e^{j-120^\circ}$, $\tilde{E}_c=\tilde{E}_a e^{j120^\circ}$; $\tilde{V}_a$, $\tilde{V}_b$, $\tilde{V}_c$, $\tilde{V}_n$ are the terminal phase voltages of the generator, $Ee^{j\delta}$ is the internal voltage of the generator, ω is the rotating

speed of the rotor, $P_{m,G}$ is the mechanical power from the turbine to the generator, $i_{fd,G}$ is the field current from the exciter to the generator, ω_m is the rotating speed of the rotor, V_{fd} is the field voltage, y_{abc} is the admittance matrix, ω_0 is the nominal rotating speed, ω_{m0} is the nominal mechanical rotating speed, H is the per unit inertia, S is the power base, R_f, L_f, and M_f are the field resistance, reactance, and mutual reactance.

The quasi-dynamic domain model of a generic governor and turbine considers the dynamics in both the governor and the turbine. The control flow chart of the governor and the turbine is shown in Figure A.1.3, and the equations describing this flow chart are listed from (A.1.6) to (A.1.10). Notice that (A.1.10) is the interface equation between the generator and the turbine.

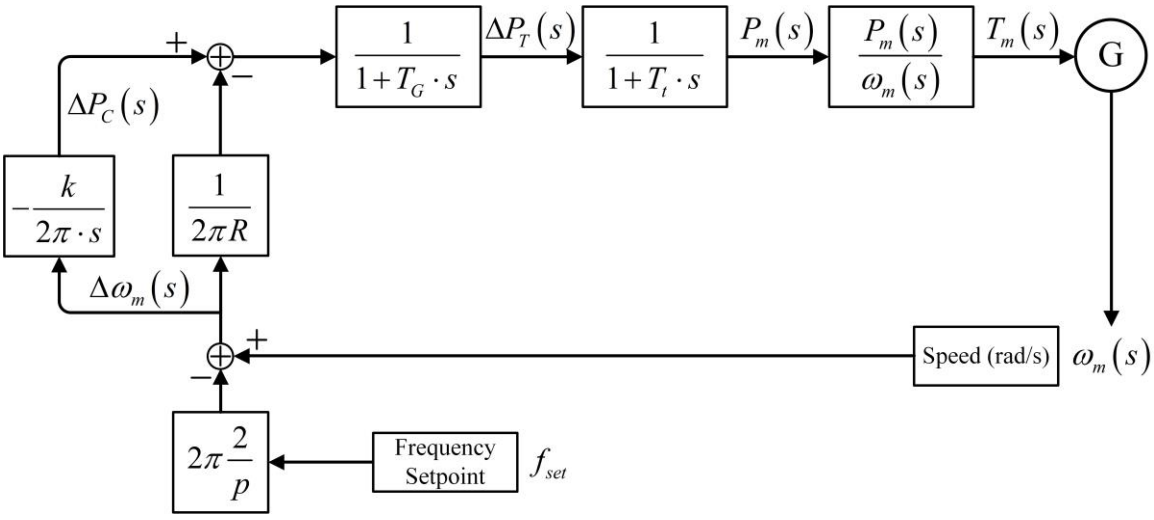

Figure A.1.3: Control Flow Chart of Governor and Turbine

$$0 = \frac{p}{2}\omega_m - \omega \tag{A.1.6}$$

$$0 = T_G \frac{d\Delta P_T}{dt} + \Delta P_T + \left(\frac{1}{2\pi R}\left(\omega_m(t) - \omega_{set}(t)\right) - \Delta P_C \right) \tag{A.1.7}$$

$$0 = \frac{d\Delta P_C}{dt} + \frac{k}{2\pi}\left(\omega_m(t) - \omega_{set}(t)\right) \tag{A.1.8}$$

$$0 = -T_t \frac{dP_{m,T}}{dt} - P_{m,T} - \Delta P_T \tag{A.1.9}$$

$$0 = P_{m,T} + P_{m,G} \tag{A.1.10}$$

where p is the number of poles, T_G, T_t, R, k are the control parameters in the governor and turbine, ω_{set} is the rotating speed setpoint, ΔP_T, ΔP_C are the internal variables in the control loop, $P_{m,T}$ is the mechanical power from the generator to the turbine.

The quasi-dynamic domain model of an exciter considers the dynamics of control on the field current. The control flow chart of an IEEE type I exciter [81] is shown in Figure A.1.4, and the equations describing this flow chart are listed from (A.1.11) to (A.1.16). Notice that (A.1.16) is the interface equation between the generator and the exciter.

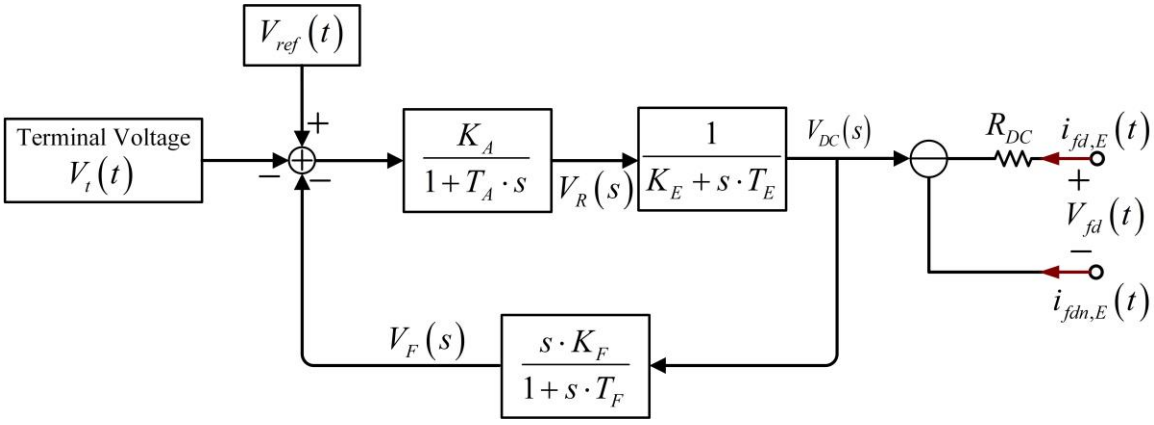

Figure A.1.4: Control Flow Chart of Exciter

$$0 = T_A \frac{dV_R}{dt} + V_R + K_A\left(V_t + V_F - V_{ref}\right) \tag{A.1.11}$$

$$0 = T_E \frac{dV_{DC}}{dt} + K_E \cdot V_{DC} - V_R \tag{A.1.12}$$

$$0 = K_F \frac{dV_{DC}}{dt} - T_F \frac{dV_F}{dt} - V_F \tag{A.1.13}$$

$$0 = V_t - \left|\tilde{V}_a\right| \tag{A.1.14}$$

$$0 = \frac{1}{R_{DC}}\left(V_{fd} - V_{DC}\right) - i_{fd,E} \tag{A.1.15}$$

$$0 = i_{fd,G} + i_{fd,E} \tag{A.1.16}$$

where V_R, V_F are the internal variables in the control loop, V_t is the terminal voltage magnitude, $i_{fd,E}$ is the field current from the generator to the exciter, V_{DC} is the voltage in the armature, T_A, T_E, T_F, K_A, K_E, K_F are the parameters in the exciter, R_{DC} is the armature resistance, and V_{ref} is the voltage reference.

By combining (A.1.1) to (A.1.16), we have the compact device model of the quasi-dynamic domain model of the generator. For this model the through variables are: $\tilde{I}_a$, $\tilde{I}_b$, $\tilde{I}_c$, and $\tilde{I}_n$. The states are: $\tilde{V}_a$, $\tilde{V}_b$, $\tilde{V}_c$, $\tilde{V}_n$, $Ee^{j\delta}$, ω, $P_{m,G}$, $P_{m,T}$, ω_m, ΔP_T, ΔP_C, V_t, V_R, V_F, $i_{fd,G}$, $i_{fd,E}$, V_{DC}, V_{fd}.

A.2 Quasi-Dynamic Domain State and Control Quadratized Device Model

The quasi-dynamic domain state and control quadratrized model of the generator is obtained by introducing eight states so that the highest order is limited to two. Then the quadratized model is expanded into real and imaginary parts to yield the model below. The final result of the quadratized device model is arranged into three equation sets, and it has 30 states and 30 equations.

The states are: V_{ar}, V_{ai}, V_{br}, V_{bi}, V_{cr}, V_{ci}, V_{nr}, V_{ni}, c, s, ω, x_1, y_1, y_2, $P_{m,G}$, $P_{m,T}$, ω_m, ΔP_T, ΔP_C, V_t, V_R, V_F, E, z_1, z_2, z_3, $i_{fd,G}$, $i_{fd,E}$, V_{DC}, V_{fd}.

The equations are listed as follows:

Equation set 1:

$$I_{ar} = Y_{aar}V_{ar} - Y_{aai}V_{ai} + Y_{abr}V_{br} - Y_{abi}V_{bi} + Y_{acr}V_{cr} - Y_{aci}V_{ci} - \left(Y_{aar} + Y_{abr} + Y_{acr}\right)V_{nr} + \left(Y_{aai} + Y_{abi} + Y_{aci}\right)V_{ni} + \left(Y_{aar} - \frac{1}{2}Y_{abr} + \frac{\sqrt{3}}{2}Y_{abi} - \frac{1}{2}Y_{acr} - \frac{\sqrt{3}}{2}Y_{aci}\right)\cdot z_1 + \left(-Y_{aai} + \frac{\sqrt{3}}{2}Y_{abr} + \frac{1}{2}Y_{abi} - \frac{\sqrt{3}}{2}Y_{acr} + \frac{1}{2}Y_{aci}\right)\cdot z_2 \quad \text{(A.2.1)}$$

$$I_{ai} = Y_{aai}V_{ar} + Y_{aar}V_{ai} + Y_{abi}V_{br} + Y_{abr}V_{bi} + Y_{aci}V_{cr} + Y_{acr}V_{ci} - \left(Y_{aai} + Y_{abi} + Y_{aci}\right)V_{nr} - \left(Y_{aar} + Y_{abr} + Y_{acr}\right)V_{ni} + \left(Y_{aai} - \frac{\sqrt{3}}{2}Y_{abr} - \frac{1}{2}Y_{abi} + \frac{\sqrt{3}}{2}Y_{acr} - \frac{1}{2}Y_{aci}\right)\cdot z_1 + \left(Y_{aar} - \frac{1}{2}Y_{abr} + \frac{\sqrt{3}}{2}Y_{abi} - \frac{1}{2}Y_{acr} - \frac{\sqrt{3}}{2}Y_{aci}\right)\cdot z_2 \quad \text{(A.2.2)}$$

$$I_{br} = Y_{bar}V_{ar} - Y_{bai}V_{ai} + Y_{bbr}V_{br} - Y_{bbi}V_{bi} + Y_{bcr}V_{cr} - Y_{bci}V_{ci} - \left(Y_{bar} + Y_{bbr} + Y_{bcr}\right)V_{nr} + \left(Y_{bai} + Y_{bbi} + Y_{bci}\right)V_{ni} + \left(Y_{bar} - \frac{1}{2}Y_{bbr} + \frac{\sqrt{3}}{2}Y_{bbi} - \frac{1}{2}Y_{bcr} - \frac{\sqrt{3}}{2}Y_{bci}\right)\cdot z_1 + \left(-Y_{bai} + \frac{\sqrt{3}}{2}Y_{bbr} + \frac{1}{2}Y_{bbi} - \frac{\sqrt{3}}{2}Y_{bcr} + \frac{1}{2}Y_{bci}\right)\cdot z_2 \quad \text{(A.2.3)}$$

$$I_{bi} = Y_{bai}V_{ar} + Y_{bar}V_{ai} + Y_{bbi}V_{br} + Y_{bbr}V_{bi} + Y_{bci}V_{cr} + Y_{bcr}V_{ci} - \left(Y_{bai} + Y_{bbi} + Y_{bci}\right)V_{nr} - \left(Y_{bar} + Y_{bbr} + Y_{bcr}\right)V_{ni} + \left(Y_{bai} - \frac{\sqrt{3}}{2}Y_{bbr} - \frac{1}{2}Y_{bbi} + \frac{\sqrt{3}}{2}Y_{bcr} - \frac{1}{2}Y_{bci}\right)\cdot z_1 + \left(Y_{bar} - \frac{1}{2}Y_{bbr} + \frac{\sqrt{3}}{2}Y_{bbi} - \frac{1}{2}Y_{bcr} - \frac{\sqrt{3}}{2}Y_{bci}\right)\cdot z_2 \quad \text{(A.2.4)}$$

$$I_{cr} = Y_{car}V_{ar} - Y_{cai}V_{ai} + Y_{cbr}V_{br} - Y_{cbi}V_{bi} + Y_{ccr}V_{cr} - Y_{cci}V_{ci} - \left(Y_{car} + Y_{cbr} + Y_{ccr}\right)V_{nr} + \left(Y_{cai} + Y_{cbi} + Y_{cci}\right)V_{ni}$$
$$+\left(Y_{car} - \frac{1}{2}Y_{cbr} + \frac{\sqrt{3}}{2}Y_{cbi} - \frac{1}{2}Y_{ccr} - \frac{\sqrt{3}}{2}Y_{cci}\right)\cdot z_1 + \left(-Y_{cai} + \frac{\sqrt{3}}{2}Y_{cbr} + \frac{1}{2}Y_{cbi} - \frac{\sqrt{3}}{2}Y_{ccr} + \frac{1}{2}Y_{cci}\right)\cdot z_2$$

(A.2.5)

$$I_{ci} = Y_{cai}V_{ar} + Y_{car}V_{ai} + Y_{cbi}V_{br} + Y_{cbr}V_{bi} + Y_{cci}V_{cr} + Y_{ccr}V_{ci} - \left(Y_{cai} + Y_{cbi} + Y_{cci}\right)V_{nr} - \left(Y_{car} + Y_{cbr} + Y_{ccr}\right)V_{ni}$$
$$+\left(Y_{cai} - \frac{\sqrt{3}}{2}Y_{cbr} - \frac{1}{2}Y_{cbi} + \frac{\sqrt{3}}{2}Y_{ccr} - \frac{1}{2}Y_{cci}\right)\cdot z_1 + \left(Y_{car} - \frac{1}{2}Y_{cbr} + \frac{\sqrt{3}}{2}Y_{cbi} - \frac{1}{2}Y_{ccr} - \frac{\sqrt{3}}{2}Y_{cci}\right)\cdot z_2$$

(A.2.6)

$$I_{nr} = -\left(\begin{array}{l} Y_{aar}V_{ar} - Y_{aai}V_{ai} + Y_{abr}V_{br} - Y_{abi}V_{bi} + Y_{acr}V_{cr} - Y_{aci}V_{ci} - \left(Y_{aar} + Y_{abr} + Y_{acr}\right)V_{nr} + \left(Y_{aai} + Y_{abi} + Y_{aci}\right)V_{ni} \\ +\left(Y_{aar} - \frac{1}{2}Y_{abr} + \frac{\sqrt{3}}{2}Y_{abi} - \frac{1}{2}Y_{acr} - \frac{\sqrt{3}}{2}Y_{aci}\right)\cdot z_1 + \left(-Y_{aai} + \frac{\sqrt{3}}{2}Y_{abr} + \frac{1}{2}Y_{abi} - \frac{\sqrt{3}}{2}Y_{acr} + \frac{1}{2}Y_{aci}\right)\cdot z_2 \end{array}\right)$$
$$-\left(\begin{array}{l} Y_{bar}V_{ar} - Y_{bai}V_{ai} + Y_{bbr}V_{br} - Y_{bbi}V_{bi} + Y_{bcr}V_{cr} - Y_{bci}V_{ci} - \left(Y_{bar} + Y_{bbr} + Y_{bcr}\right)V_{nr} + \left(Y_{bai} + Y_{bbi} + Y_{bci}\right)V_{ni} \\ +\left(Y_{bar} - \frac{1}{2}Y_{bbr} + \frac{\sqrt{3}}{2}Y_{bbi} - \frac{1}{2}Y_{bcr} - \frac{\sqrt{3}}{2}Y_{bci}\right)\cdot z_1 + \left(-Y_{bai} + \frac{\sqrt{3}}{2}Y_{bbr} + \frac{1}{2}Y_{bbi} - \frac{\sqrt{3}}{2}Y_{bcr} + \frac{1}{2}Y_{bci}\right)\cdot z_2 \end{array}\right)$$
$$-\left(\begin{array}{l} Y_{car}V_{ar} - Y_{cai}V_{ai} + Y_{cbr}V_{br} - Y_{cbi}V_{bi} + Y_{ccr}V_{cr} - Y_{cci}V_{ci} - \left(Y_{car} + Y_{cbr} + Y_{ccr}\right)V_{nr} + \left(Y_{cai} + Y_{cbi} + Y_{cci}\right)V_{ni} \\ +\left(Y_{car} - \frac{1}{2}Y_{cbr} + \frac{\sqrt{3}}{2}Y_{cbi} - \frac{1}{2}Y_{ccr} - \frac{\sqrt{3}}{2}Y_{cci}\right)\cdot z_1 + \left(-Y_{cai} + \frac{\sqrt{3}}{2}Y_{cbr} + \frac{1}{2}Y_{cbi} - \frac{\sqrt{3}}{2}Y_{ccr} + \frac{1}{2}Y_{cci}\right)\cdot z_2 \end{array}\right)$$

(A.2.7)

$$I_{ni} = -\left(\begin{array}{l} Y_{aai}V_{ar} + Y_{aar}V_{ai} + Y_{abi}V_{br} + Y_{abr}V_{bi} + Y_{aci}V_{cr} + Y_{acr}V_{ci} - \left(Y_{aai} + Y_{abi} + Y_{aci}\right)V_{nr} - \left(Y_{aar} + Y_{abr} + Y_{acr}\right)V_{ni} \\ + \left(Y_{aai} - \frac{\sqrt{3}}{2}Y_{abr} - \frac{1}{2}Y_{abi} + \frac{\sqrt{3}}{2}Y_{acr} - \frac{1}{2}Y_{aci}\right)\cdot z_1 + \left(Y_{aar} - \frac{1}{2}Y_{abr} + \frac{\sqrt{3}}{2}Y_{abi} - \frac{1}{2}Y_{acr} - \frac{\sqrt{3}}{2}Y_{aci}\right)\cdot z_2 \end{array}\right)$$
$$-\left(\begin{array}{l} Y_{bai}V_{ar} + Y_{bar}V_{ai} + Y_{bbi}V_{br} + Y_{bbr}V_{bi} + Y_{bci}V_{cr} + Y_{bcr}V_{ci} - \left(Y_{bai} + Y_{bbi} + Y_{bci}\right)V_{nr} - \left(Y_{bar} + Y_{bbr} + Y_{bcr}\right)V_{ni} \\ + \left(Y_{bai} - \frac{\sqrt{3}}{2}Y_{bbr} - \frac{1}{2}Y_{bbi} + \frac{\sqrt{3}}{2}Y_{bcr} - \frac{1}{2}Y_{bci}\right)\cdot z_1 + \left(Y_{bar} - \frac{1}{2}Y_{bbr} + \frac{\sqrt{3}}{2}Y_{bbi} - \frac{1}{2}Y_{bcr} - \frac{\sqrt{3}}{2}Y_{bci}\right)\cdot z_2 \end{array}\right)$$
$$-\left(\begin{array}{l} Y_{cai}V_{ar} + Y_{car}V_{ai} + Y_{cbi}V_{br} + Y_{cbr}V_{bi} + Y_{cci}V_{cr} + Y_{ccr}V_{ci} - \left(Y_{cai} + Y_{cbi} + Y_{cci}\right)V_{nr} - \left(Y_{car} + Y_{cbr} + Y_{ccr}\right)V_{ni} \\ + \left(Y_{cai} - \frac{\sqrt{3}}{2}Y_{cbr} - \frac{1}{2}Y_{cbi} + \frac{\sqrt{3}}{2}Y_{ccr} - \frac{1}{2}Y_{cci}\right)\cdot z_1 + \left(Y_{car} - \frac{1}{2}Y_{cbr} + \frac{\sqrt{3}}{2}Y_{cbi} - \frac{1}{2}Y_{ccr} - \frac{\sqrt{3}}{2}Y_{cci}\right)\cdot z_2 \end{array}\right)$$

(A.2.8)

<u>Equation set 2:</u>

$$0 = \frac{dc}{dt} + y_1 \tag{A.2.9}$$

$$0 = \frac{ds}{dt} + y_2 \tag{A.2.10}$$

$$0 = \frac{d\omega}{dt} + x_1 \tag{A.2.11}$$

$$0 = T_G \frac{d\Delta P_T}{dt} + \Delta P_T + \frac{1}{2\pi R}\omega_m(t) - \Delta P_C - \frac{1}{2\pi R}\omega_{set}(t) \tag{A.2.12}$$

$$0 = \frac{d\Delta P_C}{dt} + \frac{k}{2\pi}\omega_m(t) - \frac{k}{2\pi}\omega_{set}(t) \tag{A.2.13}$$

$$0 = -T_t \frac{dP_{m,T}}{dt} - P_{m,T} - \Delta P_T \tag{A.2.14}$$

$$0 = T_A \frac{dV_R}{dt} + V_R + K_A V_t + K_A V_F - K_A V_{ref} \tag{A.2.15}$$

$$0 = T_E \frac{dV_{DC}}{dt} + K_E \cdot V_{DC} - V_R \tag{A.2.16}$$

$$0 = K_F \frac{dV_{DC}}{dt} - T_F \frac{dV_F}{dt} - V_F \tag{A.2.17}$$

$$0 = -V_{fd} + L_f \frac{di_{fd,G}}{dt} + R_f \cdot i_{fd,G} \tag{A.2.18}$$

Equation set 3:

$$0 = \frac{2 \cdot H \cdot S}{\omega_{m0}^2} \cdot \omega_m \cdot \frac{2}{p} \cdot x_1 - z_1 \cdot I_{ar} - z_2 \cdot I_{ai} + \frac{1}{2} z_1 \cdot I_{br} - \frac{\sqrt{3}}{2} z_2 \cdot I_{br} + \frac{\sqrt{3}}{2} z_1 \cdot I_{bi} + \frac{1}{2} z_2 \cdot I_{bi} + \frac{1}{2} z_1 \cdot I_{cr} + \frac{\sqrt{3}}{2} z_2 \cdot I_{cr} - \frac{\sqrt{3}}{2} z_1 \cdot I_{ci} + \frac{1}{2} z_2 \cdot I_{ci} + P_{m,G} \tag{A.2.19}$$

$$0 = \frac{p}{2} \omega_m - \omega \tag{A.2.20}$$

$$0 = \omega_0 \cdot s + y_1 - \omega \cdot s \tag{A.2.21}$$

$$0 = -\omega_0 \cdot c + y_2 + \omega \cdot c \tag{A.2.22}$$

$$0 = V_t^2 - V_{ar}^2 - V_{ai}^2 \tag{A.2.23}$$

$$0 = z_1 + E \cdot c \tag{A.2.24}$$

$$0 = z_2 + E \cdot s \tag{A.2.25}$$

$$0 = E - \omega \cdot z_3 \tag{A.2.26}$$

$$0 = i_{fd,G} - \frac{\sqrt{2}}{M_f} \cdot z_3 \tag{A.2.27}$$

$$0 = \frac{1}{R_{DC}} V_{fd} - \frac{1}{R_{DC}} V_{DC} - i_{fd,E} \tag{A.2.28}$$

$$0 = P_{m,T} + P_{m,G} \tag{A.2.29}$$

$$0 = i_{fd,G} + i_{fd,E} \tag{A.2.30}$$

Above equations are cast in the standard SCQDM syntax. The syntax of the SCQDM is:

Model Description: *Type*, *Code*, *ID*, *Title*

$$\mathbf{i}(t) = Y_{eqx1}\mathbf{x}(t) + Y_{equ1}\mathbf{u}(t) + D_{eqxd1}\frac{d\mathbf{x}(t)}{dt} + C_{eqc1}$$

$$0 = Y_{eqx2}\mathbf{x}(t) + Y_{equ2}\mathbf{u}(t) + D_{eqxd2}\frac{d\mathbf{x}(t)}{dt} + C_{eqc2}$$

$$0 = Y_{eqx3}\mathbf{x}(t) + Y_{equ3}\mathbf{u}(t) + \left\{\begin{array}{c}\vdots\\ \mathbf{x}(t)^T\left\langle F^i_{eqxx3}\right\rangle\mathbf{x}(t)\\ \vdots\end{array}\right\} + \left\{\begin{array}{c}\vdots\\ \mathbf{u}(t)^T\left\langle F^i_{equu3}\right\rangle\mathbf{u}(t)\\ \vdots\end{array}\right\} + \left\{\begin{array}{c}\vdots\\ \mathbf{u}(t)^T\left\langle F^i_{equx3}\right\rangle\mathbf{x}(t)\\ \vdots\end{array}\right\} + C_{eqc3}$$

$$\mathbf{h}(\mathbf{x},\mathbf{u}) = Y_{hfeqx}\mathbf{x}(t) + Y_{hfequ}\mathbf{u}(t) + \left\{\begin{array}{c}\vdots\\ \mathbf{x}(t)^T F^i_{hfeqxx}\mathbf{x}(t)\\ \vdots\end{array}\right\} + \left\{\begin{array}{c}\vdots\\ \mathbf{u}(t)^T F^i_{hfequu}\mathbf{u}(t)\\ \vdots\end{array}\right\} + \left\{\begin{array}{c}\vdots\\ \mathbf{u}(t)^T F^i_{hfequx}\mathbf{x}(t)\\ \vdots\end{array}\right\} + C_{hfeqc}$$

Constraints : $\mathbf{h}(\mathbf{x},\mathbf{u}) \le \mathbf{0},\ \mathbf{u_{hmin}} \le \mathbf{u} \le \mathbf{u_{hmax}},\ \left|\mathbf{du}\right| \le \mathbf{u_{hllim}}$

Model Dimensions : $\mathrm{n}_{equ1}, n_{equ2}, n_{equ3}, n_{state}, n_{control}, n_{Feqxx}, n_{Fequu}, n_{Fequx}, n_{fconst}, n_{Ffeqxx}, n_{Ffequu}, n_{Ffequx}$

Connectivity : $nn_t, ivn, inn, onn, S_{st}$

Normalization Factors: $x_{NF}, e_{NF}, u_{NF}, h_{NF}$

Units: $xUnit, eUnit, uUnit, hUnit$

A.3 Quasi-Dynamic Domain SCAQCF Device Model

Quasi-dynamic domain SCAQCF model of the generator is derived from applying the quadratic integration to SCQDM with a time step *h*. This model is generated by the computer program automatically. Here we just provide the general expressions. The SCAQCF device model is:

Model Description: *Type*, *Code*, *ID*, *Title*

$$\begin{Bmatrix} \mathbf{i}(t) \\ 0 \\ 0 \\ \mathbf{i}(t_m) \\ 0 \\ 0 \end{Bmatrix} = \mathbf{e}_{\mathbf{lhs}} = Y_{eqx}\mathbf{x} + \begin{Bmatrix} \vdots \\ \mathbf{x}^T \left\langle F^i_{eqxx} \right\rangle \mathbf{x} \\ \vdots \end{Bmatrix} + Y_{equ}\mathbf{u} + \begin{Bmatrix} \vdots \\ \mathbf{u}^T \left\langle F^i_{equu} \right\rangle \mathbf{u} \\ \vdots \end{Bmatrix} + \begin{Bmatrix} \vdots \\ \mathbf{u}^T \left\langle F^i_{equx} \right\rangle \mathbf{x} \\ \vdots \end{Bmatrix} - B_{eq}$$

$$B_{eq} = -N_{eqx}\mathbf{x}(t-h) - N_{equ}\mathbf{u}(t-h) - M_{eq}\mathbf{i}(t-h) - K_{eq}$$

$$\mathbf{h}(\mathbf{x},\mathbf{u}) = Y_{feqx}\mathbf{x} + Y_{fequ}\mathbf{u} + \begin{Bmatrix} \vdots \\ \mathbf{x}^T \left\langle F^i_{feqxx} \right\rangle \mathbf{x} \\ \vdots \end{Bmatrix} + \begin{Bmatrix} \vdots \\ \mathbf{u}^T \left\langle F^i_{fequu} \right\rangle \mathbf{u} \\ \vdots \end{Bmatrix} + \begin{Bmatrix} \vdots \\ \mathbf{u}^T \left\langle F^i_{fequx} \right\rangle \mathbf{x} \\ \vdots \end{Bmatrix} + C_{feqc}$$

Constraints : $\mathbf{h}(\mathbf{x},\mathbf{u}) \le \mathbf{0}, \mathbf{u}_{\mathbf{min}} \le \mathbf{u} \le \mathbf{u}_{\mathbf{max}}, \ |\mathbf{du}| \le \mathbf{u}_{\mathbf{llim}}$

Model Dimensions: n_{equ}, n_{state}, $n_{control}$, n_{Feqxx}, n_{Fequu}, n_{Fequx}, n_{fconst}, n_{Ffeqxx}, n_{Ffequu}, n_{Ffequx}

Connectivity: nn_t, *ivn*, *inn*, *onn*, S_{st}

Normalization Factor: x_{NF}, e_{NF}, u_{NF}, h_{NF}

Units: *xUnit*, *eUnit*, *uUnit*, *hUnit*

where all the matrices constructed from SCQDM are shown below:

$$Y_{eqx} = \begin{bmatrix} \frac{4}{t_h}D_{eqxd1} + Y_{eqx1} & -\frac{8}{t_h}D_{eqxd1} \\ \frac{4}{t_h}D_{eqxd2} + Y_{eqx2} & -\frac{8}{t_h}D_{eqxd2} \\ Y_{eqx3} & 0 \\ \frac{1}{2t_h}D_{eqxd1} & \frac{2}{t_h}D_{eqxd1} + Y_{eqx1} \\ \frac{1}{2t_h}D_{eqxd2} & \frac{2}{t_h}D_{eqxd1} + Y_{eqx2} \\ 0 & Y_{eqx3} \end{bmatrix}, Y_{equ} = \begin{bmatrix} Y_{equ1} & 0 \\ Y_{equ2} & 0 \\ Y_{equ3} & 0 \\ 0 & Y_{equ1} \\ 0 & Y_{equ2} \\ 0 & Y_{equ3} \end{bmatrix}, F_{eqx} = \begin{bmatrix} 0 & 0 \\ 0 & 0 \\ F_{eqxx3} & 0 \\ 0 & 0 \\ 0 & 0 \\ 0 & F_{eqxx3} \end{bmatrix},$$

$$F_{equ}=\begin{bmatrix}0 & 0\\ 0 & 0\\ F_{equu3} & 0\\ 0 & 0\\ 0 & 0\\ 0 & F_{equu3}\end{bmatrix},\ F_{equx}=\begin{bmatrix}0 & 0\\ 0 & 0\\ F_{equx3} & 0\\ 0 & 0\\ 0 & 0\\ 0 & F_{equx3}\end{bmatrix},\ N_{eqx}=\begin{bmatrix}-Y_{eqx1}+\frac{4}{t_h}D_{eqxd1}\\ -Y_{eqx2}+\frac{4}{t_h}D_{eqxd2}\\ 0\\ \frac{1}{2}Y_{eqx1}-\frac{5}{2t_h}D_{eqxd1}\\ \frac{1}{2}Y_{eqx2}-\frac{5}{2t_h}D_{eqxd2}\\ 0\end{bmatrix},$$

$$N_{equ}=\begin{bmatrix}-Y_{equ1}\\ -Y_{equ2}\\ 0\\ \frac{1}{2}Y_{equ1}\\ \frac{1}{2}Y_{equ2}\\ 0\end{bmatrix},\ M_{eq}=\begin{bmatrix}I_{size(i(t))}\\ 0\\ 0\\ -\frac{1}{2}I_{size(i(t))}\\ 0\\ 0\end{bmatrix},\ K_{eq}=\begin{bmatrix}0\\ 0\\ C_{eqc3}\\ \frac{3}{2}C_{eqc1}\\ \frac{3}{2}C_{eqc2}\\ C_{eqc3}\end{bmatrix}$$

$$Y_{feqx}=\begin{bmatrix}Y_{hfeqx} & 0\\ 0 & Y_{hfeqx}\end{bmatrix}\qquad Y_{fequ}=\begin{bmatrix}Y_{hfequ} & 0\\ 0 & Y_{hfeqx}\end{bmatrix}\qquad C_{feqc}=\begin{bmatrix}C_{hfeqc}\\ C_{hfeqc}\end{bmatrix}$$

$$F_{feqxx}=\begin{bmatrix}F_{hfeqxx} & 0\\ 0 & F_{hfeqxx}\end{bmatrix}F_{fequu}=\begin{bmatrix}F_{hfequu} & 0\\ 0 & F_{hfequu}\end{bmatrix}\qquad F_{fequx}=\begin{bmatrix}F_{hfequx} & 0\\ 0 & F_{hfequx}\end{bmatrix}$$

$$\mathbf{u}_{min}=\begin{bmatrix}\mathbf{u}_{hmin}\\ \mathbf{u}_{hmin}\end{bmatrix}\qquad \mathbf{u}_{max}=\begin{bmatrix}\mathbf{u}_{hmax}\\ \mathbf{u}_{hmax}\end{bmatrix}\qquad \mathbf{u}_{llim}=\begin{bmatrix}\mathbf{u}_{hllim}\\ \mathbf{u}_{hllim}\end{bmatrix}$$

REFERENCES

[1] "Distributed Energy Resources Technical Cosiderations for the Bulk Power System," FERC, Feb. 2018.

[2] NYISO, "A Review of Distributed Energy Resources," Sep. 2014.

[3] H. Jiayi, J. Chuanwen, and X. Rong, "A review on distributed energy resources and MicroGrid," *Renewable and Sustainable Energy Reviews*, vol. 12, no. 9, pp. 2472–2483, Dec. 2008.

[4] B. Xie, D. Zhao, and T. Hong, "Transformer Monitoring and Protection in Dynamic Power Systems – A Review," *Front. Energy Res.*, vol. 8, p. 150, Jul. 2020.

[5] J. Driesen and R. Belmans, "Distributed generation: challenges and possible solutions," in *2006 IEEE Power Engineering Society General Meeting*, Montreal, Que., Canada, 2006, p. 8 pp.

[6] N. D. Hatziargyriou and A. P. Sakis Meliopoulos, "Distributed energy sources: technical challenges," in *2002 IEEE Power Engineering Society Winter Meeting. Conference Proceedings (Cat. No.02CH37309)*, New York, NY, USA, 2002, vol. 2, pp. 1017–1022.

[7] A. Abur and A. G. Exposito, *Power System State Estimation: Theory and Implementation*. CRC press, 2004.

[8] F. Schweppe and J. Wildes, "Power System Static-State Estimation, Part I: Exact Model," *IEEE Trans. on Power Apparatus and Syst.*, vol. PAS-89, no. 1, pp. 120–125, Jan. 1970.

[9] F. Schweppe and D. Rom, "Power System Static-State Estimation, Part II: Approximate Model," *IEEE Trans. on Power Apparatus and Syst.*, vol. PAS-89, no. 1, pp. 125–130, Jan. 1970.

[10] A. P. Sakis Meliopoulos and Fan Zhang, "Multiphase power flow and state estimation for power distribution systems," *IEEE Trans. Power Syst.*, vol. 11, no. 2, pp. 939–946, May 1996.

[11] Zhenyu Huang *et al.*, "Performance evaluation of phasor measurement systems," in *2008 IEEE Power and Energy Society General Meeting - Conversion and Delivery of Electrical Energy in the 21st Century*, Pittsburgh, PA, USA, 2008, pp. 1–7.

[12] J. De La Ree, V. Centeno, J. S. Thorp, and A. G. Phadke, "Synchronized Phasor Measurement Applications in Power Systems," *IEEE Trans. Smart Grid*, vol. 1, no. 1, pp. 20–27, Jun. 2010.

[13] V. Terzija *et al.*, "Wide-Area Monitoring, Protection, and Control of Future Electric Power Networks," *Proc. IEEE*, vol. 99, no. 1, pp. 80–93, Jan. 2011.

[14] E. Farantatos, G. K. Stefopoulos, G. J. Cokkinides, and A. P. Meliopoulos, "PMU-based dynamic state estimation for electric power systems," in *2009 IEEE Power & Energy Society General Meeting*, Calgary, Canada, 2009, pp. 1–8.

[15] S. Meliopoulos, G. Cokkinides, R. Huang, E. Farantatos, S. Choi, and Y. Lee, "Wide area dynamic monitoring and stability controls," in *2010 IREP Symposium Bulk Power System Dynamics and Control - VIII (IREP)*, Rio de Janeiro, Brazil, 2010, pp. 1–8.

[16] R. Huang, E. Farantatos, G. J. Cokkinides, and A. P. Meliopoulos, "Substation based dynamic state estimator - numerical experiment," in *IEEE PES T&D 2010*, New Orleans, LA, USA, 2010, pp. 1–8.

[17] S. A. P. Meliopoulos, "Legacy SE to distributed dynamic state estimators: Evolution and experience," in *2015 IEEE Power & Energy Society General Meeting*, Denver, CO, USA, 2015, pp. 1–5.

[18] A. P. S. Meliopoulos, E. Polymeneas, Z. Tan, R. Huang, and D. Zhao, "Advanced Distribution Management System," *IEEE Trans. Smart Grid*, vol. 4, no. 4, pp. 2109–2117, Dec. 2013.

[19] R. Huang, G. Cokkinides, C. Hedrington, and S. A. P. Meliopoulos, "Distribution System Distributed Quasi-Dynamic State Estimator," *IEEE Trans. Smart Grid*, vol. 7, no. 6, pp. 2761–2770, Nov. 2016.

[20] B. Xie *et al.*, "A Performance Comparison Study of Quasi-Dynamic State Estimation and Static State Estimation," in *2020 IEEE Power & Energy Society General Meeting (PESGM)*, Montreal, Canada, 2020, pp. 1–5.

[21] B. Xie, A. P. S. Meliopoulos, C. Zhong, Y. Liu, L. Sun, and J. Xie, "Distributed Quasi-Dynamic State Estimation Incorporating Distributed Energy Resources," in *2018 North American Power Symposium (NAPS)*, Fargo, ND, 2018, pp. 1–6.

[22] R. Seguin, J. Woyak, D. Costyk, J. Hambrick, and B. Mather, "High-Penetration PV Integration Handbook for Distribution Engineers," NREL/TP--5D00-63114, 1235905, Jan. 2016.

[23] B. F. Wollenberg, "In my view - from blackout to blackout - 1965 to 2003: how far have we come with reliability?," *IEEE Power and Energy Mag.*, vol. 2, no. 1, pp. 88–86, Jan. 2004.

[24] I. Dzafic, M. Gilles, R. A. Jabr, B. C. Pal, and S. Henselmeyer, "Real Time Estimation of Loads in Radial and Unsymmetrical Three-Phase Distribution Networks," *IEEE Trans. Power Syst.*, vol. 28, no. 4, pp. 4839–4848, Nov. 2013.

[25] A. P. S. Meliopoulos and G. K. Stefopoulos, “Characterization of State Estimation Biases,” *Probability in the Engineering and Informational Sciences*, vol. 20, no. 01, Jan. 2006.

[26] S. Meliopoulos, R. Huang, E. Polymeneas, and G. Cokkinides, “Distributed dynamic state estimation: Fundamental building block for the smart grid,” in *2015 IEEE Power & Energy Society General Meeting*, Denver, CO, USA, 2015, pp. 1–6.

[27] S. Meliopoulos, G. Cokkinides, R. Fan, L. Sun, and B. Cui, “Command authentication via faster than real time simulation,” in *2016 IEEE Power and Energy Society General Meeting (PESGM)*, Boston, MA, USA, 2016, pp. 1–5.

[28] A. P. S. Meliopoulos, G. Cokkinides, R. Fan, and L. Sun, “Data Attack Detection and Command Authentication via Cyber-Physical Comodeling,” *IEEE Des. Test*, vol. 34, no. 4, pp. 34–43, Aug. 2017.

[29] S. Meliopoulos *et al.*, “Integration & automation: From protection to advanced energy management systems,” in *2013 IREP Symposium Bulk Power System Dynamics and Control - IX Optimization, Security and Control of the Emerging Power Grid*, Rethymno, 2013, pp. 1–11.

[30] A. P. S. Meliopoulos, G. J. Cokkinides, Renke Huang, E. Polymeneas, and P. Myrda, “Grid Modernization: Seamless Integration of Protection, Optimization and Control,” in *2014 47th Hawaii International Conference on System Sciences*, Waikoloa, HI, 2014, pp. 2463–2474.

[31] A. Monticelli, *State estimation in electric power systems: a generalized approach*. Springer Science & Business Media, 2012.

[32] A. Monticelli, “Electric power system state estimation,” *Proc. IEEE*, vol. 88, no. 2, pp. 262–282, Feb. 2000.

[33] R. D. Martin, V. J. Yohai, and R. H. Zamar, “Min-Max Bias Robust Regression,” *Ann. Statist.*, vol. 17, no. 4, pp. 1608–1630, Dec. 1989.

[34] S. J. Julier and J. K. Uhlmann, “Unscented Filtering and Nonlinear Estimation,” *Proc. IEEE*, vol. 92, no. 3, pp. 401–422, Mar. 2004.

[35] L. Fan and Y. Wehbe, “Extended Kalman filtering based real-time dynamic state and parameter estimation using PMU data,” *Electric Power Systems Research*, vol. 103, pp. 168–177, Oct. 2013.

[36] Z. Huang, K. Schneider, and J. Nieplocha, “Feasibility studies of applying Kalman filter techniques to power system dynamic state estimation,” in *Power Engineering Conference, 2007. IPEC 2007. International*, 2007, pp. 376–382.

[37] N. Zhou, D. Meng, Z. Huang, and G. Welch, “Dynamic State Estimation of a Synchronous Machine Using PMU Data: A Comparative Study,” *IEEE Trans. Smart Grid*, vol. 6, no. 1, pp. 450–460, Jan. 2015.

[38] E. Ghahremani and I. Kamwa, “Dynamic State Estimation in Power System by Applying the Extended Kalman Filter With Unknown Inputs to Phasor Measurements,” *IEEE Trans. Power Syst.*, vol. 26, no. 4, pp. 2556–2566, Nov. 2011.

[39] J. Zhao, M. Netto, and L. Mili, “A Robust Iterated Extended Kalman Filter for Power System Dynamic State Estimation,” *IEEE Trans. Power Syst.*, vol. 32, no. 4, pp. 3205–3216, Jul. 2017.

[40] A. Jain, Y. Kawazoe, R. Balasubramanian, and S. C. Tripathy, “Network observability: A solution technique using neural networks,” in *TENCON 2003. Conference on Convergent Technologies for Asia-Pacific Region*, Bangalore, India, 2003, vol. 3, pp. 1007–1011.

[41] D. Singh, J. P. Pandey, and D. S. Chauhan, “Radial basis neural network state estimation of electric power networks,” in *2004 IEEE International Conference on Electric Utility Deregulation, Restructuring and Power Technologies. Proceedings*, Hong Kong, China, 2004, pp. 90–95.

[42] M. Biserica, Y. Besanger, R. Caire, O. Chilard, and P. Deschamps, “Neural Networks to Improve Distribution State Estimation—Volt Var Control Performances,” *IEEE Trans. Smart Grid*, vol. 3, no. 3, pp. 1137–1144, Sep. 2012.

[43] L. Ramesh, S. Chowdhury, S. P. Chowdhury, A. A. Natarajan, G. A. Taylor, and Y. H. Song, “Intelligent Approach for Distribution System Load Estimation,” in *2007 IEEE Power Engineering Society General Meeting*, Tampa, FL, USA, 2007, pp. 1–7.

[44] E. Manitsas, R. Singh, B. C. Pal, and G. Strbac, “Distribution System State Estimation Using an Artificial Neural Network Approach for Pseudo Measurement Modeling,” *IEEE Trans. Power Syst.*, vol. 27, no. 4, pp. 1888–1896, Nov. 2012.

[45] J. Wu, Y. He, and N. Jenkins, “A robust state estimator for medium voltage distribution networks,” *IEEE Trans. Power Syst.*, vol. 28, no. 2, pp. 1008–1016, May 2013.

[46] B. Xie, A. P. Sakis Meliopoulos, Y. Liu, and L. Sun, “Distributed quasi-dynamic state estimation with both GPS-synchronized and non-synchronized data,” in *2017 North American Power Symposium (NAPS)*, Morgantown, WV, 2017, pp. 1–6.

[47] G. De Carne, M. Liserre, B. Xie, C. Zhong, and C. Vournas, “Multiphysics Modelling of Asynchronously-Connected Grids,” in *2018 Power Systems Computation Conference (PSCC)*, Dublin, Ireland, 2018, pp. 1–8.

[48] C. Zhong, A. P. Sakis Meliopoulos, J. Sun, M. Saeedifard, and B. Xie, “Modeling of Converter Losses with High Fidelity in a Physically Based Object-Oriented Way,” in

2018 IEEE Power & Energy Society General Meeting (PESGM), Portland, OR, 2018, pp. 1–5.

[49] C. Zhong, A. P. S. Meliopoulos, B. Xie, J. Xie, K. Liu, and H. Shao, "Detailed Multiphysics Modeling of Air-Conditioned House," in *2019 IEEE Power & Energy Society Innovative Smart Grid Technologies Conference (ISGT)*, Washington, DC, USA, 2019, pp. 1–5.

[50] A. Meliopoulos, G. J. Cokkinides, and G. K. Stefopoulos, "Quadratic integration method," in *Proceedings of the 2005 International Power System Transients Conference (IPST 2005)*, 2005, pp. 19–23.

[51] Y. Liu, Y. An, and B. Xie, "State Estimation Based Transmission Line Fault Locating with Sequence Distributed Parameter Models," in *2017 IEEE Conference on Energy Internet and Energy System Integration (EI2)*, Beijing, 2017, pp. 1–6.

[52] A. P. S. Meliopoulos, G. Cokkinides, B. Xie, C. Zhong, and J. Johnson, "Full State Feedback Control for Virtual Power Plants," Sandia Nat. Lab., Albuquerque, NM, USA, SAND2017-10178, Sep. 2017.

[53] S. Meliopoulos *et al.*, "Autonomous Multi-Stage Flexible OPF for Active Distribution Systems with DERs," p. 10.

[54] A. P. Sakis Meliopoulos *et al.*, "Smart Grid Technologies for Autonomous Operation and Control," *IEEE Trans. Smart Grid*, vol. 2, no. 1, pp. 1–10, Mar. 2011.

[55] C. Zhong, A. P. Sakis Meliopoulos, G. J. Cokkinides, and B. Xie, "Object-Oriented Voltage Control for AC-DC Hybrid Distribution Systems," in *2018 9th IEEE International Symposium on Power Electronics for Distributed Generation Systems (PEDG)*, Charlotte, NC, USA, 2018, pp. 1–4.

[56] C. Zhong, B. Xie, and A. P. S. Meliopoulos, "Distribution Network Voltage Profile Optimization via Multi-Stage Flexible Optimal Power Flow," in *2019 North American Power Symposium (NAPS)*, Wichita, KS, USA, 2019, pp. 1–6.

[57] J. Johnson *et al.*, "Design and Implementation of a Secure Virtual Power Plant," Sandia Nat. Lab., Albuquerque, NM, USA, SAND2017-10177, Sep. 2017.

[58] O. Vasios, B. Xie, and A. P. Meliopoulos, "Estimation Based Protection of Three-Phase Saturable Core Transformer for Cross-Country Fault Detection," in *2019 IEEE Power & Energy Society General Meeting (PESGM)*, Atlanta, GA, USA, 2019, pp. 1–5.

[59] S. Meliopoulos, J. Xie, and G. Cokkinides, "Power system harmonic analysis under geomagnetic disturbances," in *2018 18th International Conference on Harmonics and Quality of Power (ICHQP)*, Ljubljana, 2018, pp. 1–6.

[60] J. Xie, A. P. Meliopoulos, and Y. Liu, "Low Broadband Transmission Line Model for Geomagnetically Induced Current Analysis," in *2018 IEEE Power & Energy Society General Meeting (PESGM)*, Portland, OR, 2018, pp. 1–5.

[61] K. Liu, A. P. S. Meliopoulos, B. Xie, C. Zhong, and J. Xie, "Quasi-Dynamic Domain Modeling of Line-Commutated Converters with the Analytical Approach," in *2019 North American Power Symposium (NAPS)*, Wichita, KS, USA, 2019, pp. 1–6.

[62] B. Xie *et al.*, "Dynamic State Estimation Based Unit Protection," in *2019 IEEE Power & Energy Society General Meeting (PESGM)*, Atlanta, GA, USA, 2019, pp. 1–5.

[63] K. Liu, A. P. S. Meliopoulos, B. Xie, C. Zhong, and J. Xie, "Dynamic State Estimation-Based Protection of Distribution Systems with High Penetration of DERs," in *2020 IEEE Power & Energy Society General Meeting (PESGM)*, Montreal, Canada, 2020, pp. 1–5.

[64] Y. Liu, S. Meliopoulos, N. Tai, L. Sun, and B. Xie, "Protection and fault locating method of series compensated lines by wavelet based energy traveling wave," in *2017 IEEE Power & Energy Society General Meeting*, Chicago, IL, 2017, pp. 1–5.

[65] D. Lu, Y. Liu, B. Xie, R. Fan, and L. Sun, "An Improved Phasor Domain Parameter Free Fault Location Algorithm on Untransposed Lines," in *2020 IEEE Power & Energy Society Transmission & Distribution Conference and Exposition (PES T&D)*, Chicago, IL, USA, 2020, pp. 1–5.

[66] J. Xie, A. P. S. Meliopoulos, and B. Xie, "Transmission Line Fault Classification Based on Dynamic State Estimation and Support Vector Machine," in *2018 North American Power Symposium (NAPS)*, Fargo, ND, 2018, pp. 1–5.

[67] J. Xie, A. P. S. Meliopoulos, B. Xie, C. Zhong, and K. Liu, "Geoelectric Field Estimation during Geomagnetic Disturbances," in *2019 IEEE Power & Energy Society General Meeting (PESGM)*, Atlanta, GA, USA, 2019, pp. 1–5.

[68] J. Xie, A. P. S. Meliopoulos, B. Xie, C. Zhong, and K. Liu, "A Reliable Dynamic State Estimation Based Protection during Geomagnetic Disturbances," in *2020 IEEE Power & Energy Society General Meeting (PESGM)*, Montreal, Canada, 2020, pp. 1–5.

[69] Y. Liu, Z. Tan, and J. Xie, "Phasor Domain Transmission Line Fault Locating with Three Phase Distributed Parameter Modeling," in *2018 IEEE Power & Energy Society General Meeting (PESGM)*, Portland, OR, 2018, pp. 1–5.

[70] J. Xie and A. P. S. Meliopoulos, "Detection of GPS Spoofing Attack via Quasi-Dynamic State Estimation," *Computer*, vol. 53, no. 5, 2020.

[71] L. Sun, R. Fan, A. P. S. Meliopoulos, Y. Liu, and Z. Tan, "Capacitor bank protection via constraint WLS dynamic state estimation method (CWLS-DSE)," in *2016 North American Power Symposium (NAPS)*, Denver, CO, USA, 2016, pp. 1–6.

[72] H. F. Albinali and A. P. S. Meliopoulos, "Resilient Protection System Through Centralized Substation Protection," *IEEE Trans. Power Delivery*, vol. 33, no. 3, pp. 1418–1427, Jun. 2018.

[73] J. Johnson *et al.*, "Optimal Distribution System Voltage Regulation using State Estimation and DER Grid-Support Functions," Sandia Nat. Lab., Albuquerque, NM, USA, SAND2020-2331, Feb. 2020.

[74] C. Zhong, A. P. S. Meliopoulos, M. AlOwaifeer, J. Xie, and G. Ilunga, "Object-oriented security constrained quadratic optimal power flow," in *2020 IEEE Power & Energy Society General Meeting (PESGM)*, Montreal, Canada, 2020, pp. 1–5.

[75] C. Zhong, "Autonomous Multi-Stage Flexible Optimal Power Flow," Georgia Institute of Technology, Atlanta, GA, USA, 2019.

[76] C. Zhong and J. L. Mathieu, "Relation between overheating of distribution transformers and switching frequency of electric loads used for demand response," in *2015 North American Power Symposium (NAPS)*, Charlotte, NC, USA, 2015, pp. 1–6.

[77] J. Zhao *et al.*, "Power System Dynamic State Estimation: Motivations, Definitions, Methodologies, and Future Work," *IEEE Trans. Power Syst.*, vol. 34, no. 4, pp. 3188–3198, Jul. 2019.

[78] E. Farantatos, R. Huang, G. J. Cokkinides, and A. P. Meliopoulos, "A predictive out of step protection scheme based on PMU enabled dynamic state estimation," in *2011 IEEE Power and Energy Society General Meeting*, San Diego, CA, 2011, pp. 1–8.

[79] E. Farantatos, R. Huang, G. J. Cokkinides, and A. P. Meliopoulos, "A Predictive Generator Out-of-Step Protection and Transient Stability Monitoring Scheme Enabled by a Distributed Dynamic State Estimator," *IEEE Trans. Power Delivery*, vol. 31, no. 4, pp. 1826–1835, Aug. 2016.

[80] L. Sun, A. P. Sakis Meliopoulos, Y. Liu, and B. Xie, "Dynamic state estimation based synchronous generator model calibration using PMU data," in *2017 IEEE Power & Energy Society General Meeting*, Chicago, IL, 2017, pp. 1–5.

[81] "IEEE Recommended Practice for Excitation System Models for Power System Stability Studies," IEEE.